HOKKAIDO UNIVERSITY

Title	Development of Microfluidic Paper-based Devices for Food Analysis
Author(s)	Busa, Lori Shayne Alamo
Degree Grantor	北海道大学
Degree Name	博士(総合化学)
Dissertation Number	甲第12470号
Issue Date	2016-09-26
DOI	https://doi.org/10.14943/doctoral.k12470
Doc URL	https://hdl.handle.net/2115/67169
Type	doctoral thesis
File Information	Lori_Shayne_Alamo_Busa.pdf

Hokkaido University Collection of Scholarly and Academic Papers : HUSCAP

Development of Microfluidic Paper-Based Devices for Food Analysis

LORI SHAYNE ALAMO BUSA

Doctor of Philosophy

Graduate School of Chemical Sciences and Engineering

Hokkaido University

2016

Development of Microfluidic Paper-Based Devices for Food Analysis

by

LORI SHAYNE ALAMO BUSA

Submitted to

Hokkaido University

In partial fulfillment of the requirements

For the degree of

Doctor of Philosophy

In Chemical Sciences and Engineering

Supervisor: Professor Dr. Manabu Tokeshi

Graduate School of Chemical Sciences and Engineering

Hokkaido University

September 2016

Title	DEVELOPMENT OF MICROFLUIDIC PAPER-BASED DEVICES FOR FOOD ANALYSIS
Author	Lori Shayne Alamo Busa
Degree	Doctor of Philosophy (Chemical Sciences and Engineering)
Thesis Supervisor	Professor Manabu Tokeshi

Abstract

Food and water contamination cause safety and health concerns to both animals and humans. Conventional methods for monitoring food and water contamination are often laborious and require highly skilled technicians to perform the measurements, making the quest for developing simpler and cost-effective techniques for rapid monitoring incessant. Since the pioneering works of Whitesides' group from 2007, interest has been strong in the development and application of microfluidic paper-based analytical devices (μPADs) for food and water analysis, which allow easy, rapid and cost-effective point-of-need screening of the targets. Several methods of detection using μPADs have been developed so far including colorimetric, electrochemical, fluorescence, chemiluminescence, and electrochemiluminescence techniques for food and water analysis. In this research, we have developed μPADs for the detection of aflatoxin B_1 (AFB_1), a highly toxic and carcinogenic foodborne substance and the most toxic aflatoxin produced by *Aspergillus* fungi, via a simple colorimetric competitive immunoassay. AFB_1 is a common contaminant in a variety of agricultural as well as processed food products including peanuts, corn and other grains, cottonseed meal, as well as animal feeds. The maximum permissible levels set by several food agencies are 5 μg kg^{-1} for AFB_1 and 20 μg kg^{-1} for total aflatoxins. However, more rigorous regulations for AFB_1 and total aflatoxins in groundnuts, nuts, dried fruits and cereals have been set to 2 μg kg^{-1} and 4 μg kg^{-1}, respectively, by the European Union. Hence, it is highly necessary to device a practical method to detect AFB_1 for food safety and monitoring.

In this context, the general introduction including the research theme and objectives are described in Chapter 1.

In chapter 2, the development of a simple, portable assay system using μPADs coupled with colorimetric detection for rapid measurements is described. The properties of different paper substrates are investigated first to determine which type of paper would be the most suitable for the fabrication of the μPADs. Simultaneous detection of horseradish peroxidase (HRP) is demonstrated using a single μPAD, which is fabricated through photolithography. The test regions are immobilized with 3,3',5,5'-tetramethylbenzidine for

HRP assay. The detection range obtained with the proposed system covers HRP concentrations from 0.37 to 124 fmol (or 3 to 1000 ng mL^{-1}). The detection limit (blank + 3σ) for HRP is calculated to be 0.69 fmol (or 5.58 ng mL^{-1}) through a 4-parameter logistic nonlinear regression. The findings obtained using the developed system suggest that μPAD assay systems for simple but highly sensitive measurements can be designed to give on-site determinations of target compounds using peroxidase-conjugated molecules.

Chapter 3 describes the development of a competitive immunoassay system on a μPAD platform. The photolithography-fabricated μPADs consist of a sample introduction zone, control and test zones located at the other end of the μPAD and are opposite to the sample introduction zone, and a capture zone wherein a capture reagent is immobilized allowing competition during immunoassay. The colorimetric detection similarly involves TMB-H_2O_2 reaction to produce the blue colored TMB/dimiine complex in the presence of peroxidase enzyme conjugated to antibody. The color intensity generated at the test zone after TMB oxidation increases with increasing target concentration introduced at the sample zone, but remains constant at the control zone. The developed competitive immunoassay system using μPADs is tested first using biotin as the model compound. In the present work, the detection limit for the competitive immunoassay of biotin on μPADs is 0.10 μg mL^{-1}. To demonstrate the versatility of the developed competitive immunoassay system further for the detection of target compounds on μPADs for practical applications, AFB_1 has been detected as well. The detection limit obtained for AFB_1 using the developed μPAD immunoassay system is 1.31 ng mL^{-1}.

In chapter 4, two competitive immunoassay (CI) systems are described for the detection of AFB_1. Using a different μPAD platform from the one used in the previous chapter, the μPAD immunoassay system similarly consists of a reaction zone, a sample introduction zone, and a capture zone. In both CI systems, detection is performed at the reaction zone via TMB oxidation by hydrogen peroxide in the presence of peroxidase conjugate. However, in the first CI system (CI-S1), competition occurs at the capture zone and signal intensities at the reaction zone increases with increasing target AFB_1 concentration. In CI system 2 (CI-S2), on the other hand, competition takes place prior to sample introduction. Similarly, signal intensity increases with increasing target AFB_1 concentration. In all sections of the manuscript, images of the μPADs are captured and colorimetrically analyzed via ImageJ software for quantification.

The final chapter is the summary of the findings in the present research. In addition, several prospects on μPAD analysis for future research are described in this chapter.

Table of Contents

Page

Title Page i

Abstract iii

Table of Contents v

Abbreviations ix

CHAPTER 1 General Introduction **1**

1.1 Introduction 1

1.2 Paper-based Microfluidics 2

1.3 Applications to Food and Water Contamination 5

1.3.1 Detection of Foodborne and Waterborne Pathogens 5

1.3.2 Detection of Pesticides and Herbicides 9

1.3.3 Detection of Food Additives 12

1.3.4 Detection of Heavy Metals 16

1.3.5 Detection of Food and Other Water Contaminants 20

1.4 Present Perspective 24

1.5 Objectives of the Present Research 25

References 32

CHAPTER 2 Simple and Sensitive Colorimetric Assay System for Horseradish Peroxidase Using Microfluidic Paper-based Devices **41**

2.1 Introduction 41

2.2 Research Methodology 43

2.2.1 Chemicals 43

2.2.2 Fabrication of μPADs 44
2.2.3 SEM Observations and Wicking Rate Evaluation of the Substrates and μPADs 45
2.2.4 Simple HRP Assay using Different μPADs 47
2.2.5 Optimization of HRP Assay System 48
2.2.6 HRP Determination 49
2.2.7 TMB Oxidation on Photolithography-fabricated vs. Wax-printed μPADs 49
2.3 Results and Discussion 50
2.3.1 SEM observations and wicking rate evaluation of the substrates and μPADs 50
2.3.2 Simple HRP Reaction on the μPADs 52
2.3.3 Optimization of HRP Assay System 53
2.3.4 HRP Determination 58
2.3.5 Effect of Photoresist and Solvent Exposure of the μPADs on TMB Oxidation 60
2.4 Conclusion 64
2.5 Additional Information 65
2.5.1 Preparation of Buffer and Blocking Solutions 65
2.5.2 Image Processing Using ImageJ Software 65
2.5.3 Wicking Rate Evaluation of the μPADs 66
2.5.4 Comparison of Results With and Without Blocking in the Assay Procedure 72
2.5.4.1 Microfluidic Paper-based Assay of HRP 72
2.5.4.2 Microfluidic Paper-based Assay of Anti-biotin IgG-peroxidase 74
References 76

CHAPTER 3 Novel Competitive Immunoassay System for Microfluidic Paper-based Analytical Detection **83**

3.1 Introduction 83

3.2 Research Methodology 84

3.2.1 Chemicals 84

3.2.2 Fabrication of μPADs 85

3.2.3 Preparation of μPADs for Competitive Immunoassay 85

3.2.4 Competitive Immunoassay of Biotin on μPADs 86

3.2.5 Competitive Immunoassay of Aflatoxin B_1 on μPADs 87

3.2.6 Image Analysis for Colorimetric Measurements 87

3.3 Results and Discussion 88

3.3.1 Competitive Immunoassay on μPAD 88

3.3.2 Data Evaluation for Colorimetric Measurements 90

3.3.3 Method Application for Specific Target Detection 92

3.3.3.1 Biotin Immunoassay 92

3.3.3.2 Aflatoxin B_1 Immunoassay 93

3.4 Conclusion 95

References 96

CHAPTER 4 Microfluidic Paper-based Analytical Devices for Aflatoxin B_1 Immunoassay in Food **99**

4.1 Introduction 99

4.2 Research Methodology 100

4.2.1 Chemicals 100

4.2.2 Preparation of μPADs 101

4.2.2.1 μPADs for AFB_1 Measurements via Competitive Immunoassay

System 1 (CI-S1) 101

4.2.2.2 μPADs for AFB_1 Measurements via Competitive Immunoassay System 2 (CI-S2) 102

4.2.3 AFB_1 Detection using ELISA kit 103

4.3 Results and Discussion 103

4.3.1 Competitive Immunoassay Systems on μPADs 103

4.3.1.1 AFB_1 Competitive Immunoassay System 1 (CI-S1) 104

4.3.1.2 AFB_1 Competitive Immunoassay System 2 (CI-S2) 106

4.3.2 Comparison of the μPAD CI Methods with the Conventional Method for AFB_1 Detection 107

4.3.3 pH Evaluation on μPAD CI Systems 109

4.4 Conclusion 110

References 112

CHAPTER 5 Conclusion and Future Prospects 114

5.1 Conclusive Remarks in the Present Research 114

5.2 Future Prospects 116

5.2.1 Innovation of Novel Microfluidic Paper-based Analytical Detection Methods for Food and Water Monitoring 117

5.2.2 μPAD Analysis of Target Analytes in Food and Water via Enhanced Detection Methods 118

References 119

Curriculum Vitae 120

Acknowledgement 125

Abbreviations

The following abbreviations are used in this manuscript:

2,4-D	2,4-dichlorophenoxyacetic acid
A319	Ahlstrom grade 319
Ach	acetylcholinesterase
AFB_1	Aflatoxin B_1
AgNP	silver nanoparticle
AgNPl	silver nanoplate
ATP	adenosine triphosphate
B[a]P	benzo[a]pyrene
B-GAL	β-galactosidase
BPA	bisphenol A
BSA	bovine serum albumin
CFU	colony-forming unit
CI	competitive immunoassay
CI-S1	competitive immunoassay system 1
CI-S2	competitive immunoassay system 2
CL	chemiluminescence
CMYK	cyan-magenta-yellow-key
CP	chromatography paper
CPRG	chlorophenol red β-galactopyranoside
DDV	dichlorvos
E. coli	*Escherichia coli*
ECL	electrochemiluminescence

ELISA	Enzyme-linked immunosorbent assay
FL	fluorescence
FP	filter paper
GO	graphene oxide
HRP	horseradish peroxidase
L. monocytogenes	*Listeria monocytogenes*
LOD	limit of detection
MCE	mixed cellulose esters
MC-LR	microcystin-LR
MIP	molecularly imprinted polymer
NC	nitrocellulose membrane
NEO	neomycin
PBST	phosphate-buffered saline Tween® 20
PCP	pentachlorophenol
PDMS	poly(dimethylsiloxane)
PEC	photoelectrochemical detection
PIM	polymer inclusion membrane
Ppy	polypyrrole
PS-MS	paper spray mass spectrometry
Qdots	quantum dots
RGB	red-green-blue
ROI	region of interest
S. aureus	*Staphylococcus aureus*
S. enterica	*Salmonella enterica*
S. Typhimurium	*Salmonella* Typhimurium

SERS	surface-enhanced Raman spectroscopy
SEM	scanning electron microscope
SWASV	square wave anodic stripping voltammetry
TBST	tris-buffered saline Tween® 20
TMB	3,3’,5,5’-tetramethylbenzidine
μPAD	microfluidic paper-based analytical device

CHAPTER 1 General Introduction

1.1 Introduction

Ensuring the safety and quality of food is an incessant concern. Hamburg's editorial in *Science* entitled "Advancing regulatory science" [1] states the relevance of this matter, and indeed, one of the key points of food analysis is to ensure food safety [2]. In order to meet this goal, there is a constant search for new and more practical methods for food monitoring. Food is after all the source of nutrition and energy of every human. Similarly, water safety and quality is of great importance. With water being the major constituent of the human body, it is natural that enough water must be consumed to regulate bodily functions [3]. However, failure to warrant the safety and quality of food and water brings risks that often lead to illnesses and sometimes fatalities.

The safety of food and water is often affected by several factors, including the presence of pathogens, pesticides and herbicides, metals and other toxic materials generally borne to the food and water through agricultural and industrial processes. Another influencing factor is the amount of food additives used to provide food preservation, coloring and sweetening [4]. Such food additives have to be controlled due to the potential risks that these substances pose to human health. Some have even become prohibited due to their toxicity such as furylfuramide (AF-2), which was used as food preservative in Japan from 1965 or earlier; it was later banned due to its carcinogenicity in experimental animals [5].

This review discusses the recent progress in microfluidic paper-based analytical device (μPAD) technology for food and water safety monitoring, specifically μPAD applications to the detection of different target compounds and pathogens that are either borne naturally to food and water, or caused by unmonitored industrial and agricultural processing and

waste contamination to both. Lateral-flow immunoassays (also known as immunochromatographic assays) are excluded as they have been reviewed elsewhere [6,7]. This review also covers the types of paper substrates that have been utilized in the μPAD fabrication and the detection methods that were incorporated into the μPAD for specific target detection for food and water analysis.

1.2 Paper-based Microfluidics

Microfluidics as defined by Whitesides [8] in his article published in *Nature* in 2006 is the science and technology of systems that process and manipulate small amounts of fluid up to 10^{-9} to 10^{-18} L using fluidic channels with dimensions ranging from tens to hundreds of micrometers. Microfluidics has undergone rapid growth with notable impacts to the analytical chemistry community due to a number of capabilities including its ability to utilize small amounts of samples and reagents and to perform separation and detection with high resolution and sensitivity, at low cost and rapidly [9]. Some of the early reports on microfluidic fabrication involved the use of glass [10,11], silicon [12,13], and polymers such as poly(dimethylsiloxane) (PDMS) [14,15] as substrates. Though these microfluidic devices miniaturize the conventional methods for specific target separation and detection, they have some drawbacks such as the expense of the substrate materials, and the need for power supply and fluid transport instruments.

Paper is a very promising substrate material for microfluidic device fabrication for a number of reasons. The properties of paper and the many advantages that it provides as a low-cost platform for diagnostics have been well-discussed [16–18]: It is easily printed, coated and impregnated; its cellulose composition is particularly compatible with proteins and biomolecules; it is environment-compatible as it is easily disposed of by incineration; and it is accessible almost everywhere. With paper as its main substrate, the cellulose

membrane network of the microfluidic paper-based analytical devices (μPADs) provide instrument-free liquid transport by capillary action, a high surface area to volume ratio that enhances detection limits for colorimetric assays, and the ability to store chemical components in their active form within the paper fiber network [19]. Although μPADs lack the high resolution and sensitivity that the silicon, glass or plastic-based devices offer, the application of μPADs is highly suitable to point-of-need monitoring that requires inexpensive analysis for constant testing especially in less industrialized countries where complex instrumentation and analytical laboratories and experts are limited. Hence, μPADs have emerged as an attractive alternative to highly sophisticated instrumentation in analytical research applications particularly in food and water monitoring and safety.

To date, much analytical research has focused on the development and application of μPADs for food and water safety and quality monitoring; including fabrication procedures of the μPADs and suitable methods of detection for qualitative or quantitative interpretation of measurements. Fabrication usually entails the selection of a type of paper substrate before subjecting it to fabrication techniques such as cutting [20–25], inkjet printing [26,27], wax patterning [28,29], wax pencil drawing [30], wax printing [31–40], screen printing [29,41,42], contact stamping [43–45], and photolithography [46–48]. Examples of μPADs fabricated using various methods and paper substrates are shown in Figure 1-1. Among the various cellulose-based paper substrates that have been used, Whatman chromatography paper grade 1 was the first type to be utilized in 2007 [17] and it has been subsequently used in many reported μPAD fabrication and detection methods [28,29,33,37,38,47,49,50]. Whatman filter paper grade 1, on the other hand, has been the most commonly used paper substrate for μPAD fabrication in food and water analysis [25,30,32,34–36,41,45,51–54]. Paper substrates that have been similarly utilized include Whatman chromatography paper 3 MM Chr [20,21], Whatman filter paper grade 4 [42,55], Whatman RC60 regenerated

cellulose membrane filter [56], Millipore MCE membrane filter [57], Canson paper [58], Fisherbrand P5 filter paper [59], JProLab JP 40 filter paper [44], Advantec 51B chromatography paper [48], and Ahlstrom 319 paper [39]. Although comparing the capabilities of each paper substrate is inappropriate when different fabrication methods and detection methods are employed among the studies, some comparisons of substrates have been made. Liu *et al.* [20], for instance, investigated paper substrates including nitrocellulose membrane, filter paper, quantitative filter paper, qualified filter paper and Whatman 3 mm chromatography paper for the μPAD chemiluminescence (CL) detection of dichlorvos (DDV) in vegetables. With the filter paper, quantitative filter paper and qualified filter paper, a high CL signal of the blank sample and poor repeatability for sample detection were observed due to the non-uniform thickness of the substrates (from 10 to 250 μm) affecting the optical path length, scattering, assay sensitivity, and volume of fluid required for an assay. However, Whatman 3mm chromatography paper, which has high quality, purity and consistency, provided good repeatability.

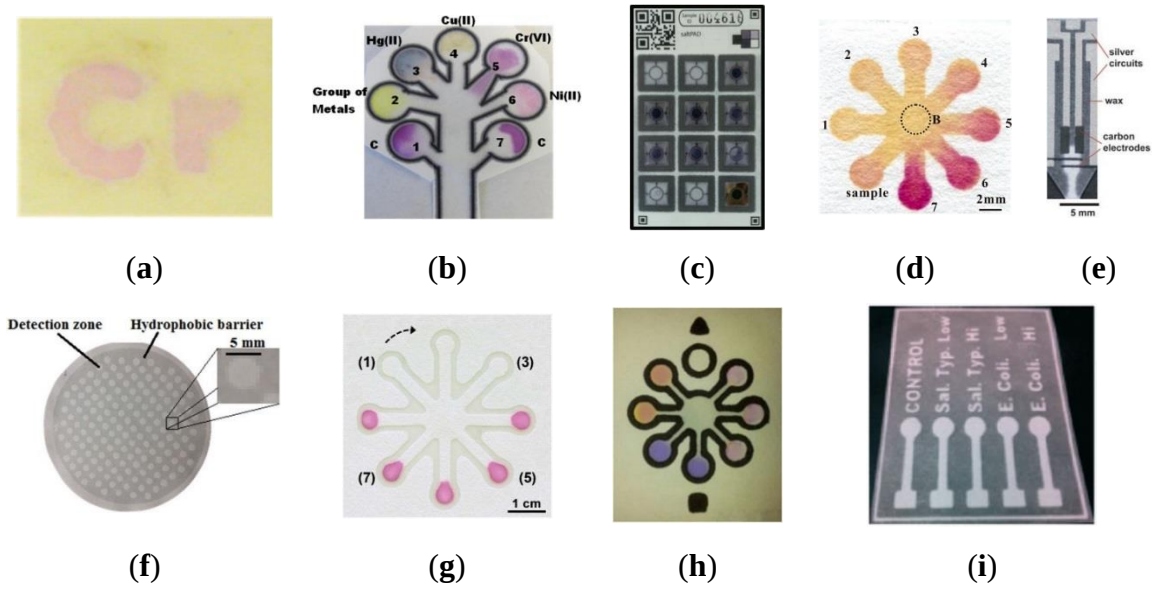

Figure 1-1 Examples of μPADs fabricated using different methods and paper substrates: (**a**) Wax patterning, WCP1. Reprinted with permission from

reference [28]. Copyright 2015 American Chemical Society. (**b**) Wax printing, WP1. Reprinted with permission from reference [31]. Copyright 2011 American Chemical Society. (**c**) Wax printing, AP319. Reprinted with permission from reference [39]. Copyright 2015 American Chemical Society. (**d**) Alkylsilane self-assembling and UV/O_3-patterning, WFP1. Reprinted with permission from reference [52]. Copyright 2013 American Chemical Society. (**e**) Wax printing with screen-printed electrodes, WCP1. Reprinted with permission from reference [38]. Copyright 2010 The Royal Society of Chemistry. (**f**) Polymer screen printing, WFP4. Reprinted with permission from reference [42]. Copyright 2016 The Royal Society of Chemistry. (**g**) Contact stamping, JPFP40. Reprinted with permission from reference [44]. Copyright 2015 The Royal Society of Chemistry. (**h**) Contact stamping, WFP1. Reprinted with permission from reference [45]. Copyright 2014 American Chemical Society. (**i**) Photolithography, CP. Reprinted with permission from reference [46]. Copyright 2013 The Royal Society of Chemistry. WFP1, Whatman No. 1 filter paper; WCP1, Whatman No. chromatography paper; WP1, Whatman No. 1 paper; AP310, Ahlstrom 319 paper; WFP4, Whatman No. 4 filter paper; JPFP40, JProLab JP 40 filter paper; CP, chromatography paper.

1.3 Applications to Food and Water Contamination

1.3.1 Detection of Foodborne and Waterborne Pathogens

Paper-based approaches for food safety monitoring are attractive because simple, low-cost, and on-site detection of foodborne contaminants is achievable and they are also applicable as preventive measures. μPADs developed for pathogen detection in food have relied

primarily on enzymatic assay-based optical methods where results are either confirmed visually by the naked eye or digitally converted and measured using image analysis software. Two of the most commonly used programs are ImageJ and Adobe Photoshop where RGB (red-green-blue) image intensities are measured relative to the image pixels or are first converted into CMYK (cyan-magenta-yellow-key) scale before intensity measurement. In a study reported by Jokerst *et al.* [32], a μPAD was developed for the microspot assay of *Escherichia coli* (*E. coli*) O157:H7, *Listeria monocytogenes* (*L. monocytogenes*) and *Salmonella* Typhimurium in ready-to-eat meat samples. The pathogens were collected from foods by a swab sampling technique and then cultured in media before adding to a chromogen-impregnated paper-based well device. A color change is observed indicating the presence of an enzyme associated with the pathogen of interest and detection is achieved. Although the detection limits determined for each of the live bacterial assays after ImageJ analysis were high (10^6 colony-forming unit (CFU) mL^{-1} for *E. coli*, 10^4 CFU mL^{-1} for *Salmonella* Typhimurium, and 10^8 CFU mL^{-1} for *L. monocytogenes*), the developed μPAD was capable of detecting pathogenic bacteria in ready-to-eat meat (bologna) at a concentration of as low as 10^1 CFU mL^{-1} within 12 h or less, which is significantly less time than the gold standard method (requires several days) for bacterial detection and enumeration. Another method presented by Jin *et al.* [33] was based on CL detection of *Salmonella* via adenosine triphosphate (ATP) quantification on μPAD. *Salmonella* was cultured and then lysed after harvesting by the boiling method. Color change is observed in the μPAD only when ATP is present as an indication of the presence of *Salmonella* in the sample. In the presence of ATP, the HRP-tagged DNA that is initially associated with the ATP aptamer attached to the chemically modified surface of the paper is released and later it allows the catalytic oxidation of 3-amino-9-ethylcarbazole by HRP/H_2O_2. The detection limit for *Salmonella* was determined to be 2×10^7 CFU mL^{-1}.

While no real samples were tested, the developed μPAD could be applied for food and water monitoring. Park *et al.* [46] presented another optical-based technique using a highly angle-dependent and less wavelength-dependent method of detection through a Mie scattering strategy for *Salmonella* Typhimurium. *Salmonella* samples were pre-mixed with anti-*Salmonella* conjugated particles to allow immunoagglutination before loading into the μPAD. At the optimized Mie scatter angle, scatter intensities were analyzed using a smartphone for quantification. An illustration of the μPAD and the smartphone application used for the pathogen quantification are shown in Figure 1-2a,b, respectively. The detection limit of the smartphone-based μPAD assay was 10^2 CFU mL^{-1}. A one-step multiplexed fluorescence (FL) strategy for detecting pathogens was also developed by Zuo *et al.* [60] using a μPAD that was a hybrid of PDMS and glass. The paper substrate enabled the integration of the fluorescent aptamer-functionalized graphene oxide biosensor on the microfluidic device (Figure 1-2c). While the aptamer is adsorbed on the surface of the graphene oxide, the FL of the aptamer is quenched. In the presence of the target pathogen, the pathogen induced the liberation of the aptamer from the graphene oxide layer and thereby restored the FL of the aptamer for detection. The detection limits for the simultaneous detection of *S. aureus* and *S. enterica* were 800.0 CFU mL^{-1} and 61.0 CFU mL^{-1}, respectively. Other works on *E. coli* detection in water were reported by Burnham *et al.* [57] and Ma *et al.* [30]. Burnham *et al.* specifically demonstrated the use of bacteriophages as capture and sensing elements for the paper-based detection of the pathogen. The method was based on the detection of β-galactosidase released from the pathogenic cells following bacteriophage-mediated lysis. Colorimetric and bioluminescence methods were performed for *E. coli* detection using red-β-D-galactopyranoside chromogenic substrate and Beta-Glo® reagent (Promega Corporation, Madison, WI, USA) to produce the color and bioluminescence, respectively, for

measurement with a detection limit of 4 CFU mL^{-1} for both methods. Ma *et al.*, on the other hand, presented a μPAD for the colorimetric determination of *E. coli* using AuNP-labeled detection antibodies via sandwich immunoassay with a silver enhancing step for signal amplification. The detection limit was 57 CFU mL^{-1}.

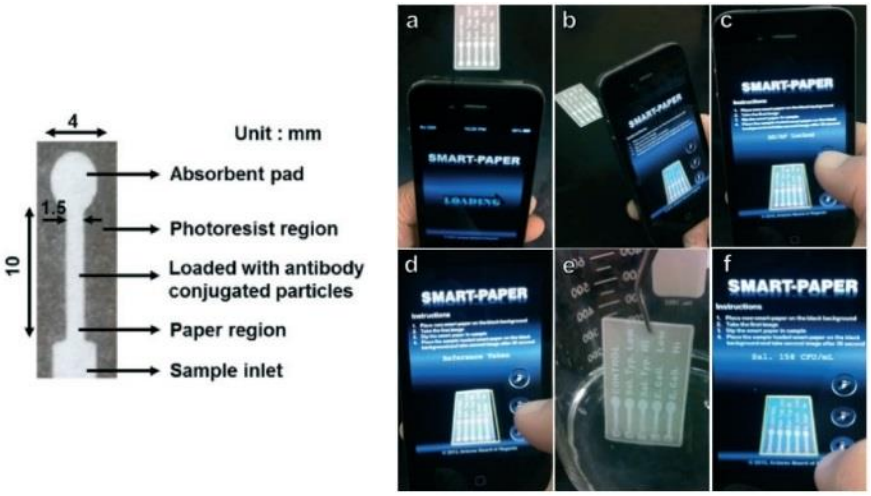

(**a**) (**b**)

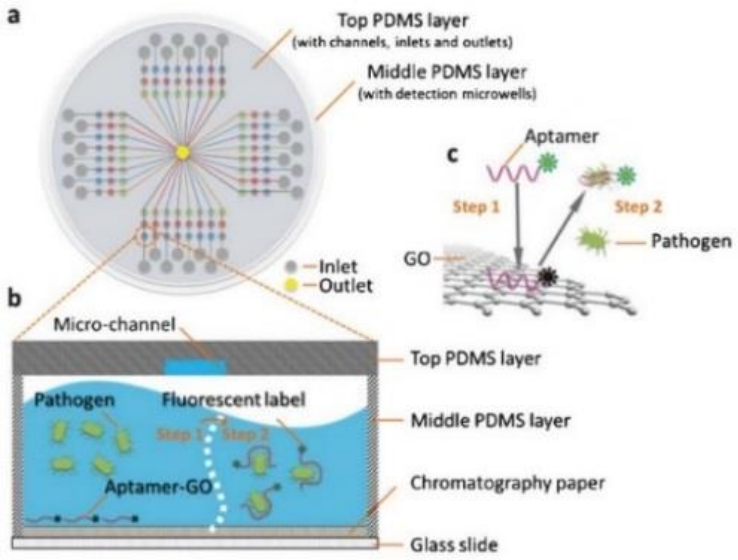

(**c**)

Figure 1-2 Detection methods for pathogens. (**a**) An image of a single-channel μPAD and (**b**) the smartphone application for *Salmonella* detection on a multi-channel μPAD. Reprinted with permission from reference [46]. Copyright 2013 The Royal Society of Chemistry. (**c**) Schematic layout of the

PDMS/paper hybrid μPAD system and illustration of the one-step multiplexed FL detection principle on the μPAD during aptamer adsorption (Step 1) and liberation (Step 2) from the GO surface and the restoration of the FL for detection in the presence of the target pathogen. Reprinted with permission from reference [60]. Copyright 2013 The Royal Society of Chemistry.

1.3.2 Detection of Pesticides and Herbicides

Pesticides have been used for many years in agriculture and have significantly contributed to maintaining food quality and production. Simultaneously, however, these materials bring harmful effects on human health [61,62]. Wang *et al.* [49] developed a paper-based molecular imprinted polymer-grafted multi-disk micro-disk plate for CL detection of 2,4-dichlorophenoxyacetic acid (2,4-D). The MIP approach was proposed as an alternative to immunoassays, which rely on antibodies and have fundamental drawbacks such as the possible denaturation and instability of the antibodies during manufacture and transport. An indirect competitive assay was made with tobacco peroxidase (TOP)-labeled 2,4-D that was molecularly imprinted on the polymer-grafted device. An enzyme catalyzed CL emission was achieved from the luminol-TOP-H_2O_2 CL system with a detection limit of 1.0 pM. A simple paper-based luminol-H_2O_2 CL detection of DDV was reported by Liu *et al.* [20]. Paper chromatography was combined in the μPAD CL assay of DDV in fruits and vegetables and the separation was achievable in 12 min utilizing 100 μL of developing reagent. The method was successfully applied to the trace DDV detection on cucumber, tomato and cabbage by a spiking method with a detection limit of 3.6 $ng \cdot mL^{-1}$. Liu *et al.* [21] also presented another MIP-based approach using a paper-based device with a molecularly imprinted polymer for the CL detection of DDV. The detection limit was 0.8

ng·mL^{-1} and the method was successfully applied to cucumber and tomato. A paper-based colorimetric approach has also been demonstrated for the detection of organophosphate and carbamate pesticides. Badawy *et al.* [58] developed a method that was based on the inhibition of acetylcholinesterase (AChE) on the degradation of acetylcholine molecules into choline and acetic acid by organophosphate (methomyl) and carbamate (profenos) pesticides. The degree of inhibition of the AChE indicates the toxicity of the pesticides; this makes the AChE a standard bioevaluator for the presence of organophosphates and carbamates [63]. While the method was not tested on real samples, the method could detect AChE inhibitors within 5 min response time.

With the goal to devise portable and easy measuring techniques and considering the increasing use of smartphones, the number of μPAD strategies that incorporate mobile or smartphones for target measurements is increasing. A μPAD sensor and novel smartphone application was developed by Sicard *et al.* [34] for the on-site colorimetric detection of organophosphate pesticides (paraoxon and malathion) based on the inhibition of immobilized AChE by the pesticides. AChE hydrolyzes the colorless indoxyl acetate substrate and converts it to an indigo-colored product in the absence of pesticides. The color intensity is reduced with increasing pesticide concentration owing to inhibition of AChE. The color produced is processed by the image analysis algorithm using a smartphone, allowing real time monitoring and mapping of water quality. The method is capable of detecting pesticide concentration of around 10 nM as evidenced by a color change in the μPAD. Another colorimetric approach was reported by Nouanthavong *et al.* [42] on the use of nanoceria-coated μPAD for colorimetric organophosphate pesticide detection via enzyme-inhibition assay with AChE and choline oxidase. In the presence of the pesticides, AChE activity is inhibited leading to no or less production of H_2O_2 and hence less yellow color development of the nanoceria (the color production mechanism is shown in Figure 1-

3). The assay was able to analyze methyl-paraoxon and chlorpyrifos-oxon with detection limits of 18 ng·mL^{-1} and 5.3 ng·mL^{-1}, respectively. The method was successfully applied for methyl-paraoxon detection on spiked cabbage and dried green mussel, with ~95% recovery values for both samples.

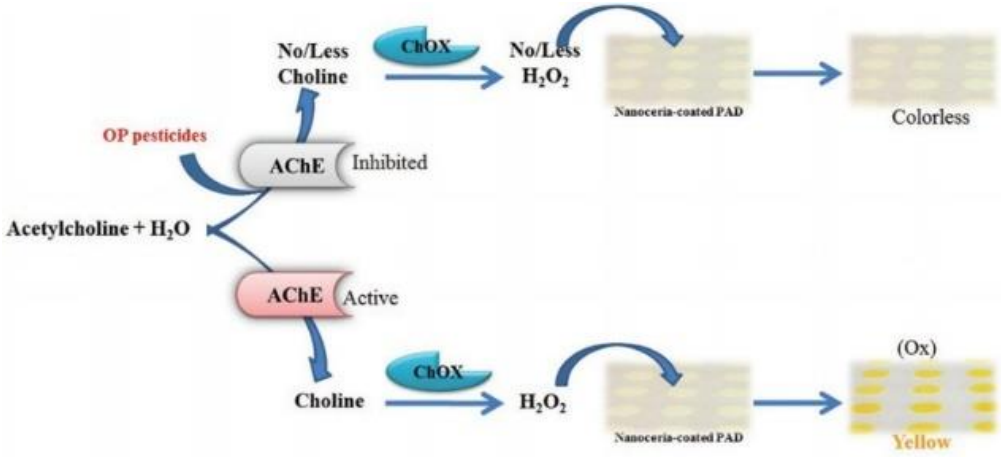

Figure 1-3 Colorimetric detection of pesticides based on the enzyme inhibition properties of the pesticide on nanoceria substrate. Reprinted with permission from reference [42]. Copyright 2016 The Royal Society of Chemistry.

Another pesticide causing a health concern is pentachlorophenol (PCP) [64–66]. PCP is a xenobiotic that accumulates in the body with carcinogenic and acute toxic effects. Sun *et al.* [50] developed a photoelectrochemical (PEC) sensor that utilized the MIP technique on a μPAD to detect PCP. The paper working electrode of the μPAD was covered with a layer of gold nanoparticles (AuNPs) and a layer of polypyrrole (Ppy)-functionalized ZnO nanoparticles. The photoelectrochemical mechanism involves the excitation of electrons from Ppy from its highest occupied molecular orbital to the lowest unoccupied molecular orbital of ZnO after being irradiated with visible light. Since the lowest unoccupied molecular orbital of ZnO and Ppy matched well, the transfer of the excited electrons to ZnO was allowed

and the electrons subsequently reached the gold-paper working electrode (Au-PWE) surface, where photocurrent generation efficiency was improved leading to a sharp increase of the photocurrent. However, in the presence of the PCP, the steric hindrance toward the diffusion of the quencher molecules and/or photogenerated holes on the interface of the electrode increased, thereby leading to a decrease in generated photocurrent. The device was capable of measuring PCP down to a limit of 4 $pg \cdot mL^{-1}$.

The only paper-based approach applied to herbicide detection that has utilized FL as a method of detection for methyl viologen is presented by Su *et al.* [67]. The method was based on the integration of CdTe Qdots on the paper device and the CdTe quenching effect in the presence of the target methyl viologen. Presence of a higher methyl viologen concentration in the system gave a darker area on the μPAD as a result of the quenching of the methyl viologen on the CdTe Qdots. The detection limit of the CdTe-paper-based visual sensor was 0.16 $\mu mol \cdot L^{-1}$.

1.3.3 Detection of Food Additives

In food and beverage industries, wide use is made of food additives such as glucose, fructose and sucrose, which are specifically used as sweeteners, and other food additives, which are used to improve or enhance the flavor or color of the food or beverage. Though most of these food additives are essentially nontoxic, large intakes of them may promote unhealthy nutrition, and some become toxic above a certain amount. Hence, there is a strong demand for fast, highly sensitive and economical methods of analysis that can be provided by the easily accessible and portable point-of-need testing of μPAD technology. Kuek Lawrence *et al.* [51] reported on an amperometric detection of glucose on a screen-printed electrode μPAD. The assay involved the use of ferrocene monocarboxylic acid as a mediator for the catalytic oxidation of glucose on the μPAD by the immobilized glucose

oxidase on the paper. The method was successfully applied to glucose detection in commercially marketed carbonated beverages with a limit of 0.18 mM. Adkins *et al.* [35] presented a μPAD that utilized microwire electrodes as an alternative to screen-printed electrodes for the non-enzymatic electrochemical detection of glucose, fructose and sucrose in beverage samples. A copper working electrode was used and the copper electrocatalytically reacted with glucose in the alkaline media, allowing the non-enzymatic electrochemical detection of the carbohydrates. A variety of commercial beverages were tested including Coca-Cola™, Orange Powerade™, Strawberry Lemonade Powerade™, Red Bull™ and Vitamin Water™. The detection limits were 270 nM, 340 nM and 430 nM for glucose, fructose and sucrose, respectively.

Colletes *et al.* [43] presented a study that utilized a paraffin-stamped paper substrate for the detection of glucose in hydrolysis of liquors (detection limit 2.77 $mmol \cdot L^{-1}$) by paper spray mass spectrometry (PS-MS). PS-MS is a fast, precise, accurate and cost-effective ionization method introduced by Crooks and co-workers in 2010 that provides complex analyses in a simple and economical way by mass spectrometry [68]. Although the paraffin-stamped paper substrate is not a μPAD *per se,* Colletes *et al.* explained the potential of the paper substrate for the combination of a microfluidic paper-based analytical device with mass spectrometry that used paper spray as the ionization method.

Nitrites are food additives used to prevent the growth of microorganisms as well as to inhibit lipid oxidation that causes rancidity [69]. Nitrite monitoring in food and water is essential due to the ability of nitrite to readily react with secondary and tertiary amines and produce carcinogenic nitrosamine compounds [70]. Several works on nitrite detection have involved the use of the Griess-color reaction mechanism to visually detect the presence of nitrite in food. For instance, He *et al.* [52] described a μPAD using the Griess-color nitrite

assay, where, upon reaction of nitrite with the Griess reagent in the μPAD, a color developed with intensities depending on the amount of nitrite in the sample. Image processing was done for quantification showing a dynamic range of 0.156–2.50 mM, and a successful application to nitrite detection in red cubilose (a traditional nutritious food and medicine in China) was achieved. Other works presented by Lopez-Ruiz *et al.* [45], Cardoso *et al.* [44] and Jayawardane *et al.* [53] similarly focused on the colorimetric detection of nitrite in water and food using the Griess method in μPADs. Lopez-Ruiz *et al.* presented a strategy using a mobile phone with a customized algorithm for image analysis and detection. As depicted in Figure 1-4a, the method allowed a multidetection of the μPAD sensing areas specific for pH detection simultaneously with nitrite detection in water samples. The strategy involved capturing the μPAD image upon sample detection with the smartphone camera, and processing of the image in order to extract the colorimetric information for measurement, wherein, hue (H) and saturation (S) of the HSV color space were used for the determination of pH and nitrite concentration, respectively. The colorimetric assay for pH determination was based on the use of two pH indicators, phenol red and chlorophenol red. A color transition of chlorophenol red from yellow to purple indicated a pH from 4 to 6, while a color transition of phenol red from yellow to pink indicated a pH from 6 to 9. The nitrite assay, on the other hand, involved a Griess-color reaction in which the color formation was quantitatively interpreted showing a detection limit of 0.52 $mg \cdot L^{-1}$. Cardoso *et al.* similarly reported a μPAD strategy for nitrite detection in ham, sausage and the preservative water from a bottle of Vienna sausage using the Griess-color assay with a detection limit of 5.6 μM. The colorimetric analysis was performed by first taking the image of the detection device using a scanner, and later processing the magenta scale of the image after conversion to the CMYK using Corel Photo-Paint™ software. Finally, Jayawardane *et al.* presented their work for nitrite and

nitrate determination in different water samples using two μPADs, each specific for nitrate and nitrite, respectively. The image of the 2D and 3D μPADs used for detection are shown in Figure 1-4b. The nitrite detection simply employed the Griess method for colorimetric measurements after image scanning and processing using ImageJ software. In the nitrate detection however, a conversion of the colorimetrically undetected species was first performed to the colorimetrically detected nitrite using a Zn reduction channel incorporated in the μPAD for nitrate detection. After conversion, the Griess method was employed and image quantification was performed. The method was successfully applied to actual analysis of different water samples (tap water, mineral water, and pond water) with detection limits of 1.0 μM and 19 μM for nitrite and nitrate, respectively.

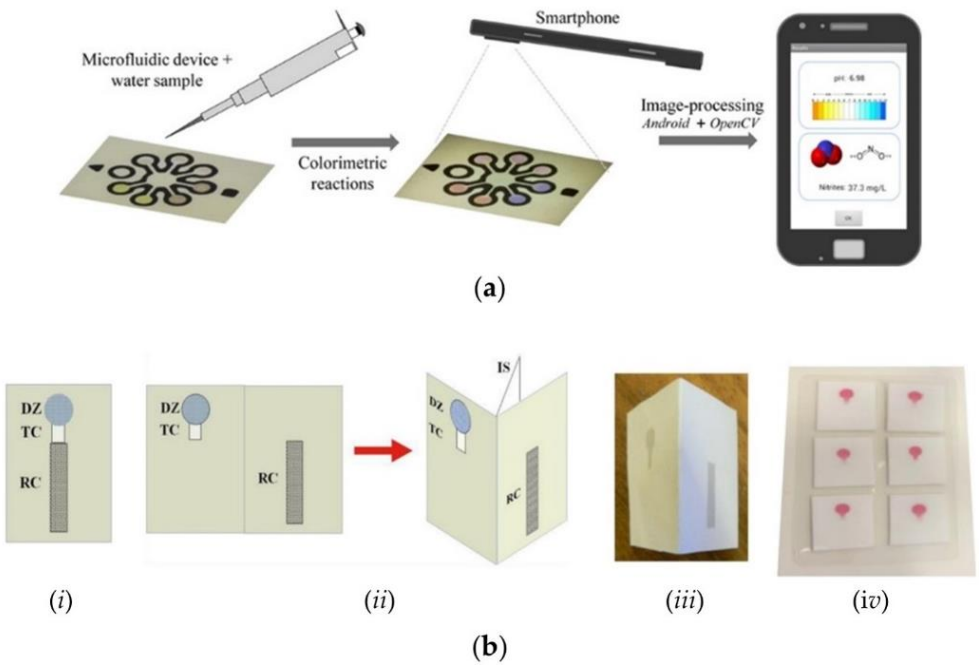

Figure 1-4 (**a**) Griess-color reaction assay-based detection methods for nitrite using a smartphone for image processing. Reprinted with permission from reference [45]. Copyright 2014 American Chemical Society. (**b**) Griess-color reaction assay-based detection methods for nitrite and nitrate using

2D (*i*) and 3D (*ii–iv*) μPADs. Reprinted with permission from reference [53]. Copyright 2014 American Chemical Society.

The addition of colorants to food has become a normal practice to enhance or change food color and make it more attractive to consumers. However, most of these colorants are potentially harmful to human health especially after excessive consumption. One μPAD design that has been developed for detecting colorants was presented in the work of Zhu *et al.* [22] where a poly(sodium 4-styrenesulfonate)-functionalized paper substrate was used for the rapid separation, preconcentration and detection of colorants in drinks with complex components via a surface-enhanced Raman spectroscopy (SERS) method. Sunset yellow and lemon yellow were both detected in grape juice and orange juice with detection limits of 10^{-5} M and 10^{-4} M, respectively.

1.3.4 Detection of Heavy Metals

Several μPADs have been developed for the detection of heavy metals in both food and water. The most common methods of detection integrated with the μPADs were colorimetric-based using silver or gold nanoparticles and nanoplates, but electrochemical and FL based methods were used as well. Nie *et al.* [47] developed a μPAD for the versatile and quantitative electrochemical detection of biological and inorganic analytes in aqueous solutions. Specifically, for water analysis, lead was investigated via square wave anodic stripping voltammetry using a μPAD with screen-printed electrodes as shown in Figure 1-5a. The measurements relied on the simultaneous plating of bismuth and lead onto the screen-printed carbon electrodes of the μPAD, which formed alloys, followed by anodic stripping of the metals from the electrode. The method showed a detection limit of 1.0 ppb in water medium. Similarly, Shi *et al.* [54] developed an electrochemical μPAD for Pb(II) and Cd(II) detection based on square wave anodic stripping voltammetry (SWASV) relying

on *in situ* plating of bismuth film. The method was capable of detecting lead and cadmium ions simultaneously in carbonated electrolyte drink (salty soda water as described by the authors) samples with detection limits of 2.0 ppb and 2.3 ppb for Pb(II) and Cd(II), respectively.

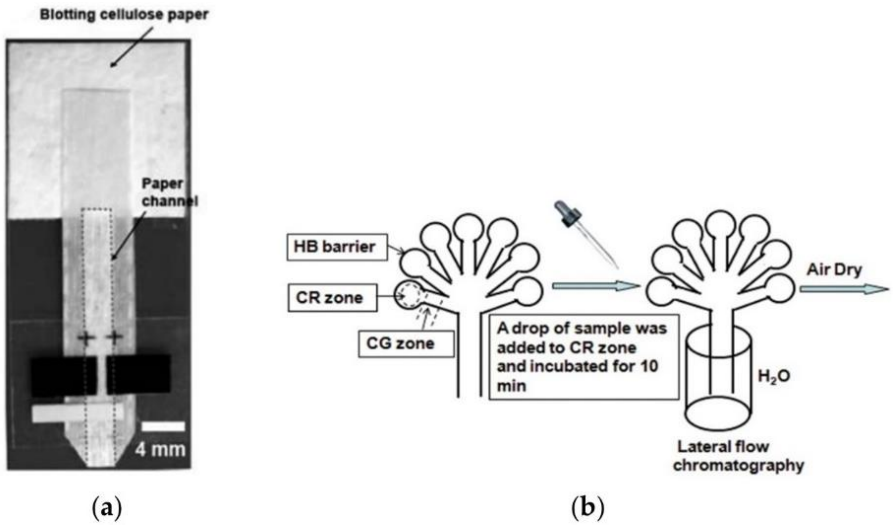

Figure 1-5 Detection methods for metals. (**a**) Electrochemical device for SWASV analysis of lead in water with screen-printed carbon working and counter electrodes and Ag/AgCl pseudo-reference electrode. Reprinted with permission from reference [47]. Copyright 2009 The Royal Society of Chemistry. (**b**) Multiplexed colorimetric detection of metals based on B-GAL and CPRG interaction in the presence of Hg^{2+}, Cu^{2+}, Cr^{6+} and Ni^{2+} mixture. Reprinted with permission from reference [31]. Copyright 2011 American Chemical Society.

Using silver nanoparticles (AgNP) self-assembled with aminothiol compounds on μPADs, Ratnarathorn *et al.* [25] reported on the colorimetric detection of copper in drinking water samples. In the presence of Cu^{2+}, the modified AgNP solution changed from yellow to orange and then green-brown due to nanoparticle aggregation. The method was tested

on tap water and pond water samples with a detection limit of 7.8 nM or 0.5 $\mu g \cdot L^{-1}$. Two other applications of μPAD with colorimetric detection for Cu(II) were reported by Jayawardane *et al.* [55] and Chaiyo et al [36]. In the former work, a polymer inclusion membrane (PIM) containing the chromophore (1-(2′-pyridylazo)-2-naphthol (PAN)) reactive to Cu(II) was incorporated in the μPAD and was used as the sensing element selective to the metal ion. The original yellow color of the membrane changed to red/purple as the Cu(II) formed a complex with PAN. The device was applied to Cu(II) determination in hot tap water samples with a detection limit of 0.6 $mg \cdot L^{-1}$. The latter work by Chaiyo *et al.* on the other hand used silver nanoplates (AgNPls) modified with hexadecyltrimethyl-ammonium bromide (CTAB) for the colorimetric detection of Cu(II) based on the catalytic etching of the AgNPls with thiosulfate ($S_2O_3^{2-}$). The violet-red $S_2O_3^{2-}$/CTAB/AgNPl on the detection zone lost its color with increasing Cu^{2+} concentration. The method was applied for determination of Cu^{2+} in drinking water, ground water, tomato and rice with a detection limit of 1.0 $ng \cdot mL^{-1}$ by visual detection. Nath *et al.* [23] presented a sensing system that could detect As^{3+} ions using gold nanoparticles chemically conjugated with thioctic acid (TA) and thioguanine (TG) molecules on paper. During detection, a visible bluish-black color appeared on the paper due to nanoparticle aggregation through transverse diffusive mixing of the Au–TA–TG with As^{3+} ions. While no real water sample testing was performed, the detection limit (1.0 ppb) was lower than the reference standard of World Health Organization (WHO) for arsenic in drinking water, hence there would be method applicability to real water sample analysis. Another work presented by the same group used a similar approach for the detection of Pb^{2+} and Cu^{2+} using AuNP that was chemically conjugated with TA and dansylhydrazine [24]. The detection limit was ≤0.0 ppb for both metal ions. Apilux *et al.* [41] developed a colorimetric method using AgNPls for the detection of Hg(II) ion levels. A change in color from pinkish violet to pinkish

yellow occurred with the Hg(II) ion detection, a phenomenon that can be attributed to a change in the surface plasmon resonance of the AgNPls, which is related to the AgNPl apparent color. At Hg(II) concentration levels above 25 ppm, the color of the AgNPls fades as observed by the naked eye. With digital imaging and software processing though, the quantitative capability of the system was improved and showed a detection limit of 0.12 ppm with successful applications to real sample analysis of drinking water and tap water. Another method via FL detection for the determination of Hg(II), Ag(I) and neomycin (NEO) for food analysis was presented by Zhang *et al.* [37]. The method used a Cy5-labeled single-stranded DNA (ssDNA)-functionalized graphene oxide (GO) sensor that generated FL in the presence of the target analytes, otherwise, the Cy5 was quenched while adsorbed on the GO surface. The detection limits were 121 nM, 47 nM and 153 nM for Hg(II), Ag(I) and NEO, respectively.

Hossain *et al.* [31] presented a multiplexed μPAD that is capable of detecting heavy metals simultaneously in a single μPAD. As shown in Figure 1-5b, the μPAD is composed of seven reaction zones, two of which are for control experiments, one for testing the mixture of metal ions via β-galactosidase (B-GAL) assay, and four using colorimetric reagents specific for Hg(II), Cu(II), Cr(VI) and Ni(II), respectively. In the B-GAL assay, the chromogenic substrate, chlorophenol red β-galactopyranoside (CPRG), which is printed on a region upstream to the B-GAL zone, is transported into the detection zone by the sample solution through capillary action and it is hydrolyzed by the B-GAL enzyme to form the red-magenta product. In the presence of the metal ions, the red-magenta color produced upon CPRG hydrolysis is lost to a degree dependent on the concentration of the metal ions in the sample. For the assays specific for each metal ion, color appearance is observed in the presence of each metal ion on their respective detection zones, while the absence of any of the metal ions results in no color change on the respective zones. The detection limit of

the device is ~0.5–1.0 ppm. Li *et al.* [28] demonstrated the use of a μPAD that enables easy detection of trace metals via text-reporting of results. Using the color-generating periodic table symbols of the specific trace metals fabricated on the μPAD as markers, even nonprofessional users can carry out handy detection and monitoring. The Cu(II) assay was based on the formation of an orange to brown complex by bathocuproine as the indicator with Cu(II). For the Cr(VI) assay, a magenta to purple complex formed in the presence of the metal ion with the indicator 1,5-diphenylcarbazide in acidic medium, while for the Ni(II) assay, a stable pink-magenta colored complex formed between dimethylglyoxime and Ni(II). The device was capable of colorimetric detection of Cu(II), Cr(VI) and Ni(II) in tap water with concentrations of ≥0.8 $mg \cdot L^{-1}$, >0.5 $mg \cdot L^{-1}$ and ≥0.5 $mg \cdot L^{-1}$, respectively. Finally, for μPAD detection of heavy metals, a colorimetric approach for image processing and quantification based on an iron-phenanthroline (Fe-phen) assay that has colored response with increasing concentration of iron was incorporated for the investigation of iron in water samples by Asano *et al.* [48]. The developed method allowed a direct analysis of tap and river water samples without pretreatment with a detection limit of 3.96 μM.

1.3.5 Detection of Other Food and Water Contaminants

Several methods have also been demonstrated for detecting other food and water contaminants using μPAD technology. Nie *et al.* [38] presented an electrochemical technique for ethanol detection in water for possible food quality control purposes. Electrochemical μPADs and a glucometer (Figure 1-6a) were used to amperometrically measure ethanol (LOD 0.1 mM) using ferricyanide as an electron-transfer mediator and alcohol dehydrogenase/β-NAD^+ as detecting components in the device. An electrochemical μPAD for halide detection in food supplement and water samples via cyclic voltammetry

was also developed by Cuartero *et al.* [56]. The device utilizes silver elements as working and counter/reference electrodes as illustrated in Figure 1-6b. The oxidation of the silver foil working electrode is induced by an anodic potential scan resulting in a current that is related to the plating rate of the target halides in the sample as silver halides precipitate. This process is complemented by the reduction of the silver/silver halide element in the reference/counter electrode upon ion exchange movement of the Na^+ ion (halide counterion) through the permselective membrane to maintain the neutrality of charges in each paper compartment, and that leads to the release of halide ions into the solution. The two silver elements are regenerated to their previous states through the application of a backward potential sweep after the forward scan. The device was found capable of detecting bromide, iodide and chloride mixtures in food supplement, seawater, mineral water, tap water and river water samples with a detection limit of around 10^{-5} M of halide mixtures. Myers *et al.* [39] developed a multiplexed μPAD (called a saltPAD) that is capable of making an iodometric titration in a single printed card. Multiple reagents are stored on every compartment of each detection zone of the saltPAD and they are allowed to recombine and undergo surface-tension-enabled mixing upon introduction of the iodized salt sample solution for determination. During the iodometric titration process, triiodide is formed as excess iodide that reacts with iodate in the presence of acid. The triiodide is then titrated with thiosulfate that was previously stored in the saltPAD. Using starch as an indicator, the detection zone produces a blue color if the amount of triiodide exceeds the reducing capacity of the thiosulfate. The indicator remains uncolored if the amount of triiodide is smaller than the reducing capacity of the thiosulfate. The detection limit of the device expressed as mg iodine/kg salt was 0.8 ppm.

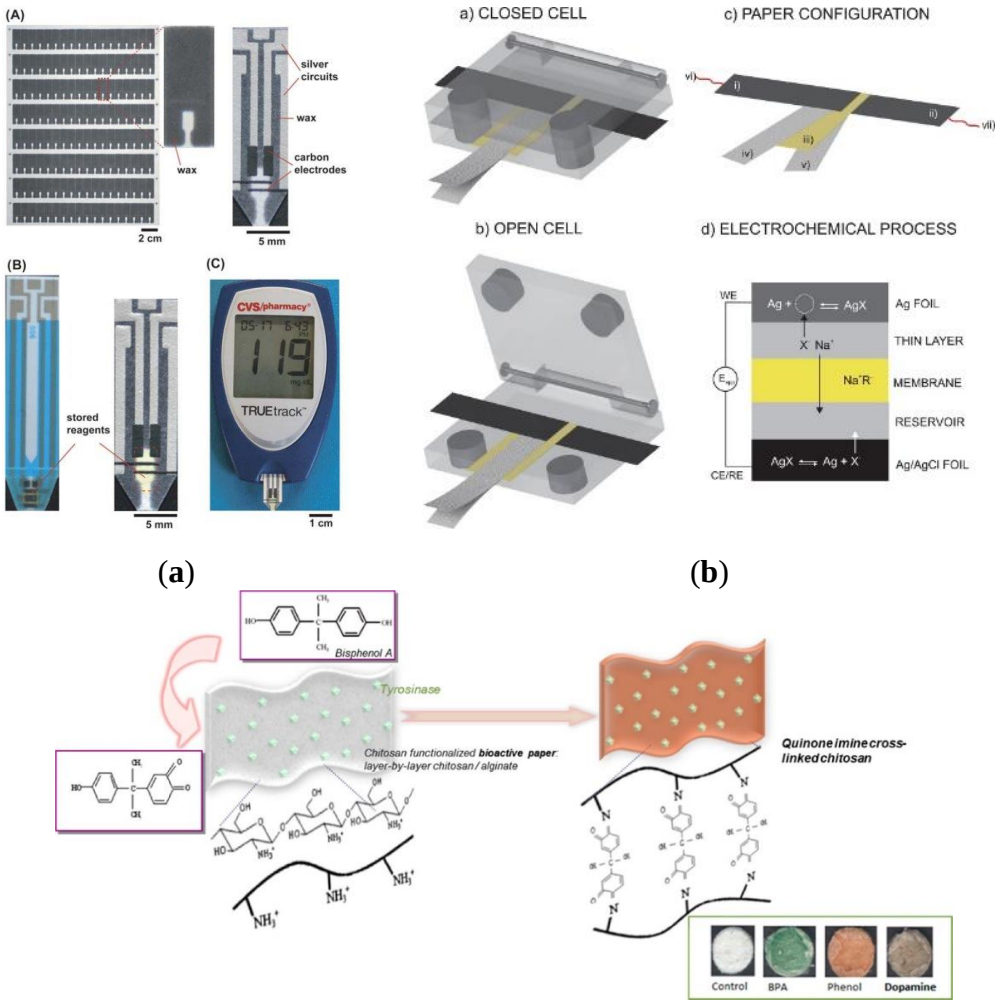

Figure 1-6 Detection methods for other food and water contaminants. (**a**) Components of the electrochemical detection system for ethanol using a glucometer as a readout device. Reprinted with permission from reference [38]. Copyright 2010 The Royal Society of Chemistry. (**b**) The configuration of the electrochemical cell for the analysis of halides utilizing silver components as electrodes on paper-assisted electrochemical detection. Reprinted with permission from reference [56]. Copyright 2015 American Chemical Society. (**c**) A representative paper-based colorimetric bioassay of BSA based on the enzymatically generated quinone from tyrosinase and chitosan interaction in the presence of the phenolic compound. Reprinted with permission from ref [59]. Copyright 2012 American Chemical Society.

Cyanobacteria in drinking water pose a great threat to public health due to the cyanotoxins produced and released into water supplies. The most toxic of the cyanotoxins is microcystin-LR (MC-LR) [71,72]. Ge *et al.* [40] focused on the development of a method that specifically detects MC-LR in water using a gold-paper working electrode (Au-PWE) for electrochemical immunoassay. Differential pulse voltammetric measurements were performed by monitoring the oxidation process of thionine in the system for the quantification of MC-LR under the catalysis of HRP and peroxidase mimetics (Fe_3O_4). The sandwich immunoreaction produced a current proportional to the logarithm of MC-LR and gave a detection limit of 0.004 $\mu g \cdot mL^{-1}$. Phenolic compounds are generally produced as byproducts from industrial processes that present health risks to humans after consumption of contaminated food and water. For detection of phenolic compounds, Alkasir *et al.* [59] developed a paper sensor that produces different color responses for phenol (reddish-brown), bisphenol A (blue-green), dopamine (dark-brown), cathecol (orange), and m-cresol (orange) and p-cresol (orange) resulting from the specific binding of enzymatically generated quinone to chitosan immobilized in multiple layers on the paper. Figure 1-6c illustrates an example of the layer-by-layer paper-based bioassay for bisphenol A. The paper sensor was successfully applied to the analysis of tap and river water samples with a detection limit of 0.86 ($\pm$0.102) $\mu g \cdot L^{-1}$ for each of the phenolic compounds.

Finally, the only μPAD detection strategy based on electrochemiluminescence (ECL) detection for the specific analysis of food has been reported by Mani *et al.* [29]. The work described a device that specifically measures the genotoxic activity of a certain compound (benzo[a]-pyrene (B[a]P)) whose metabolite reacts with DNA and the responses are measured via ECL detection. The measurement essentially involves two steps, the first of which involves the conversion of the test compound B[a]P to a metabolite by a microsomal enzyme from rat liver microsomes. The second step is a DNA damage detection that

involves the liberation of ECL light upon oxidation of the guanine in the damaged DNA by the (bis-2,2′-bipyridyl) ruthenium polyvinylpyridine ([Ru(bpy)2(PVP)10]2+ or RuPVP) polymer of the electrochemical device. The technique was specifically tested on grilled chicken, and the detection limit was ~150 nM.

1.4 Present Perspective

A review on microfluidic paper-based devices for food and water analysis has been discussed and recently published in *Micromachines*. Table 1-1 summarizes the uses of microfluidic paper-based devices for detection of different pathogens, additives and contaminants in food and water that have been reported to date. μPADs in food and water safety and analysis represent a burgeoning technology that provides fast, economic, easy-to-use advantages and is highly applicable for point-of-need testing especially in resource limited environments. While the field of microfluidic paper-based sensors has expanded rapidly, food and water safety remains an area with many issues still to be addressed. One specific challenge in food analysis for example is the method of handling and pretreatment of the samples before μPAD detection. While fluid samples such as water and beverage usually do not require any pretreatment to the sample before introducing into the device for μPAD detection [22,28,38,48,49,51,53–56,59], food specimens could be in solid form, and therefore, a suitable pretreatment step is necessary for target sample collection before introducing into the μPAD for detection. In treating fruits, vegetables and meat samples for instance, most groups employ an extraction method to collect the target of interest [29,42], although an elution process [20,21], or boiling method [44], with the use of distilled water, followed by filtration are simple steps that are possibly performed to collect the target for μPAD detection. For pathogen collection, the swab sampling technique has also been performed which requires a significantly reduced enrichment times compared to the gold

standard culture method before sample introduction and colorimetric paper-based detection [32]. While successful, the enzymatic assay systems point to the potential for exploring the use of specific inducers to enhance enzyme production as well as using selective enrichment media to inhibit the growth of competing microorganisms. Despite the current limitations on selectivity and sensitivity using paper as substrates for detection, the ability of μPADs to detect specific targets such as pathogenic bacteria, food additives and contaminants has been demonstrated in real food and water samples at levels that are vital to the safety and health of both animals and humans, therefore demonstrating its significant impact to the community for food and water safety and quality monitoring. Based on the number of references reporting the development of μPADs specifically directed to food and water safety and quality monitoring in the last six years, μPAD technology is still in its early stage and there are wide opportunities for developments and applications. Particularly exciting is the potential for application of μPADs for regular monitoring of food crops and drinking water sources, where, contamination is a risk from mining and industrial processes, and analytical measurements have traditionally been a cost limiting factor. From the detection of foodborne and waterborne infectious pathogens to different organic and inorganic analytes in general, μPADs offer the means to detect different targets using an inexpensive material like paper as their main substrate for qualitative as well as quantitative on-site food and water monitoring.

1.5 Objectives of the Present Research

The main objective of the present research is to develop novel microfluidic paper-based analytical devices with the incorporation of suitable detection methods for the analysis of food that would be suitable for rapid onsite food testing. This dissertation then describes the experimental procedures and results obtained during the time of research.

A simple, portable assay system using μPADs coupled with colorimetric detection for rapid measurements is developed and described in chapter 2. The properties of different paper substrates are first investigated to determine which type of paper would be the most suitable for the fabrication of the μPADs. Simultaneous detection of horseradish peroxidase (HRP) is demonstrated using a single μPAD, which is fabricated via photolithography. This work suggests that μPAD assay systems for simple but highly sensitive measurements can be designed to give on-site determinations of target compounds using peroxidase-conjugated molecules.

In chapter 3, a competitive immunoassay system on a μPAD platform is developed. The colorimetric detection similarly involves TMB-H_2O_2 reaction to produce the blue colored TMB dimiine product in the presence of an antigen-bound peroxidase enzyme conjugated to the antibody. Biotin is first used as the model compound to test the developed competitive immunoassay system using μPADs. Then, in order to demonstrate the versatility of the developed competitive immunoassay system for target compound detection on μPADs for practical applications, AFB_1 has been detected as well. The work proposes an alternative low-cost and portable immunoassay device that offers good sensitivity and selectivity with rapid analysis of the target.

Finally, two competitive immunoassay (CI) systems are developed for the detection of AFB_1 in food. Using a different μPAD platform compared to the one used in the previous chapter, both the μPAD CI systems similarly involve colorimetric detection of the target based on peroxidase-catalyzed TMB oxidation. The results obtained for the proposed CI systems are described in chapter 4.

In all sections of the manuscript, images of the μPADs have been captured and colorimetrically analyzed through ImageJ software for quantification. The overall findings of the present research are summarized in chapter 5.

Table 1-1 Summary of foodborne pathogens, toxins, pesticides and insecticides, heavy metals and food additives for food and water analyses on paper-based platforms.

Target	μPAD Wall Fabrication Method	Paper Substrate	Detection Method	Linear Detection Range	LOD	Real Sample Application	Reference
Pathogens							
E. coli O157:H7, *Salmonella* Typhimurium, *L. monocytogenes*	Wax printing	Whatman No. 1 filter paper	Colorimetric	-	10^6 CFU mL^{-1}, 10^4 CFU mL^{-1}, 10^8 CFU mL^{-1}	Bologna	[32]
Salmonella	Wax printing	Whatman No. 1 chromatography paper	CL	-	2.6×10^7 CFU mL^{-1}	-	[33]
S. Typhimurium	Photolithography	Chromatography paper	Optical (Mie scattering)	10^2–10^5 CFU mL^{-1}*	10^2 CFU mL^{-1}	-	[46]
S. aureus, *S. enterica*	Cutting by punching (PDMS/paper/glass hybrid)	Whatman chromatography paper	FL	10^4–10^6 CFU mL^{-1}, 42.2–675.0 CFU mL^{-1}	800.0 CFU mL^{-1}, 61.0 CFU mL^{-1}	-	[60]
E. coli	-	Millipore MCE membrane filter	Colorimetric and bioluminescence	-	4 CFU mL^{-1}	-	[57]
E. coli	Wax pencil drawing and PDMS screen printing	Whatman No. 1 filter paper	Colorimetric	-	57 CFU mL^{-1}	Drinking water	[30]
Pesticides and Herbicides							
2,4-D	-	Whatman No. 1 chromatography paper	CL	-	1.0 pM	Tap water, lake water	[49]
Paraoxon, Malathion	Wax printing	Whatman No. 1 filter paper	Colorimetric	1×10^{-8}–ca. 1×10^{-6} M	10 nM	-	[34]
Methyl-paraoxon, Chlorpyrifos-oxon	Polymer screen-printing	Whatman No. 4 filter paper	Colorimetric	0–0.1 μg·mL^{-1}, 0–60 ng·mL^{-1}	18 ng·mL^{-1}, 5.3 ng·mL^{-1}	For methyl-paraoxon: cabbage, dried green mussel	[42]

Table 1-1 Continued…

Target	μPAD Wall Fabrication Method	Paper Substrate	Detection Method	Linear Detection Range	LOD	Real Sample Application	Reference
Dichlorvos	Cutting	Whatman 3MM Chr chromatography paper	CL	10 ng·mL^{-1}–1.0 μg·mL^{-1}	3.6 ng·mL^{-1}	Cucumber, tomato, cabbage	[20]
Dichlorvos	Cutting	Whatman 3MM Chr chromatography paper	CL	3.0 ng·mL^{-1}–1.0 μg·mL^{-1}	0.8 ng·mL^{-1}	Cabbage, tomato	[21]
Methomyl, Profenofos	Cutting	Canson paper	Colorimetric	-	6.16 × 10^{-4} mM, 0.27 mM	-	[58]
PCP	Wax screen-printing	Whatman No. 1 chromatography paper	PEC	0.01–100 ng·mL^{-1}	4 pg·mL^{-1}	-	[50]
Methyl viologen (paraquat)	Cutting	Whatman filter paper	FL	0.39–3.89 μmol·L^{-1}	0.16 μmol·L^{-1}	-	[67]
Food Additives							
Glucose	Cutting by punching	Whatman No. 1 filter paper	Electrochemical	1–5 mM	0.18 mM	Commercial soda beverages	[51]
Glucose, Fructose, Sucrose	Wax printing	Whatman No. 1 filter paper	Electrochemical	-	270 nM, 340 nM, 430 nM	Coca-Cola™, Orange Powerade™, Strawberry Lemonade Powerade™, Red Bull™, Vitamin Water™	[35]
Glucose	Paraffin stamping	Whatman grade 1 paper	PS-MS	1–500 μmol·L^{-1}	2.77 μmol·L^{-1}	Liquors	[43]
Sunset yellow, Lemon yellow	Cutting	Filter paper	SERS	-	10^{-5} M, 10^{-4} M	Grape juice, orange juice	[22]
Nitrite	Paraffin stamping	JProLab JP 40 filter paper	Colorimetric	0–100 μM	5.6 μM	Ham, sausage, preservative water	[44]

Table 1-1 Continued…

Target	μPAD Wall Fabrication Method	Paper Substrate	Detection Method	Linear Detection Range	LOD	Real Sample Application	Reference
Nitrite	Alkylsilane assembling and UV-lithography	Whatman No. 1 filter paper	Colorimetric	0.156–2.50 mM	-	Processed red cubilose	[52]
Nitrite	Indelible ink contact stamping	Whatman No. 1 filter paper	Colorimetric	-	0.52 $mg \cdot L^{-1}$	-	[45]
Nitrite, Nitrate	Inkjet printing	Whatman No. 1 and no.4 filter papers	Colorimetric	10–150 μM, 50–1000 μM	1.0 μM, 19 μM	Tap water, mineral water, pond water	[53]
Metals							
Pb(II)	Photolithography	Whatman No. 1 chromatography paper	Electrochemical	0–100 ppb	1.0 ppb	-	[47]
Hg(II), Cu(II), Cr(VI), Ni(II)	Wax printing	Whatman No. 1 paper	Colorimetric	-	~0.5–1 ppm	-	[31]
Pb(II), Cd(II)	Cutting	Whatman No. 1 filter paper	Electrochemical	10–100 ppb	2.0 ppb, 2.3 ppb	Carbonated electrolyte drinks	[54]
As(III)	Cutting	Whatman filter paper	Colorimetric	-	1.0 ppb	-	[23]
Pb(II), Cu(II)	Cutting	Whatman filter paper	Colorimetric	-	≤10.0 ppb for both	-	[24]
Cu(II)	Cutting	Whatman No. 1 filter paper	Colorimetric	7.8–62.8 μM	7.8 nM or 0.5 $\mu g \cdot L^{-1}$	Drinking water	[25]
Cu(II)	Wax printing	Whatman No. 1 filter paper	Colorimetric	0.5–200 $ng \cdot mL^{-1}$	0.3 $ng \cdot mL^{-1}$	Drinking water, ground water, tomato, rice	[36]
Cu(II)	Inkjet printing	Whatman No. 4 filter paper	Colorimetric	0.1–30.0 $mg \cdot L^{-1}$	0.6 $mg \cdot L^{-1}$	Hot tap water	[55]
Hg(II)	Wax screen printing	Whatman No. 1 filter paper	Colorimetric	5–75 ppm	0.12 ppm	Commercial bottled drinking water, tap water	[41]

Table 1-1 Continued…

Target	μPAD Wall Fabrication Method	Paper Substrate	Detection Method	Linear Detection Range	LOD	Real Sample Application	Reference
Hg(II), Ag(I), NEO	Wax printing	Whatman No. 1 chromatography paper	FL	0–3 μM, 0–1.75 μM, 0–2 μM	121 nM, 47 nM, 153 nM	-	[37]
Cu(II), Cr(VI), Ni(II)	Wax patterning	Whatman No. 1 chromatography paper	Colorimetric	-	≥0.8 $mg \cdot L^{-1}$, >0.5 $mg \cdot L^{-1}$, ≥0.5 $mg \cdot L^{-1}$	Tap water	[28]
Fe	Photolithography	Advantec No. 51B chromatography paper	Colorimetric	8.9–89 μM	3.96 μM	Tap water, river water	[48]
Others							
Ethanol	Wax printing	Whatman No. 1 chromatography paper	Electrochemical	0.1–3 mM	0.1 mM	Water	[38]
Phenol, Bisphenol A, Dopamine, Catechol, m-Cresol p-Cresol	Cutting by hole punching	Fisherbrand P5 filter paper	Colorimetric	1–400 $\mu g \cdot L^{-1}$, 1–200 $\mu g \cdot L^{-1}$, 1–300 $\mu g \cdot L^{-1}$, 1–300 $\mu g \cdot L^{-1}$, 1–500 $\mu g \cdot L^{-1}$, 1–200 $\mu g \cdot L^{-1}$	0.86 (±0.102) $\mu g \cdot L^{-1}$ for each of the phenolic compounds	Tap water, river water	[59]
Bromide, Iodide, Chloride	-	Whatman RC60 regenerated cellulose membrane filter	Electrochemical	$10^{-4.8}$–0.1 M for bromide and iodide, $10^{-4.8}$–0.6 M for chloride	10^{-5} M	Food supplement, seawater, mineral water, tap water, river water	[56]
Iodate	Wax printing	Ahlstrom 319 paper	Colorimetric	0.8–15 ppm iodine atoms from iodate	0.8 ppm iodine atoms	Iodized salt	[39]
MC-LR	Wax printing	Whatman No. 1 chromatography paper	Electrochemical	0.01–200 $\mu g \cdot mL^{-1}$	0.004 $\mu g \cdot mL^{-1}$	-	[40]
B[a]P	Wax patterning and screen printing	Whatman No. 1 filter paper	ECL	0.15–12.5 μM	~150 nM	Chicken skin	[29]

References

[1] M. A. Hamburg, Advancing regulatory science, *Science*, 2011, **331**, 987.

[2] A. Escarpa, Lights and shadows on food microfluidics, *Lab Chip*, 2014, **14**, 3213–3224.

[3] E. Jéquier and F. Constant, Water as an essential nutrient: The physiological basis of hydration, *Eur. J. Clin. Nutr.*, 2010, **64**, 115–123.

[4] Y. F. Sasaki, S. Kawaguchi, A. Kamaya, M. Ohshita, K. Kabasawa, K. Iwama, K. Taniguchi and S. Tsuda, The comet assay with 8 mouse organs: Results with 39 currently used food additives, *Mutat. Res. Toxicol. Environ. Mutagen.*, 2002, **519**, 103–119.

[5] International Agency for Research in Cancer (IARC). 2-(2-Furyl)-3-(5-nitro-2-fyryl)acrylamide (AF-2). In *IARC Monographs on the Evaluation of the Carcinogenic Risk of Chemicals to Humans: Some Food Additives, Feed Additives and Naturally Occurring Substances*; World Health Organization: Lyon, France, 1983; Volume 31, p. 41.

[6] M. Sajid, A. -N. Kawde and M. Daud, Designs, formats and applications of lateral flow assay: A literature review, *J. Saudi Chem. Soc.*, 2014, **19**, 689–705.

[7] G. A. Posthuma-Trumpie, J. Korf and A. van Amerongen, Lateral flow (immuno)assay: Its strengths, weaknesses, opportunities and threats. A literature survey, *Anal. Bioanal. Chem.*, 2009, **393**, 569–582.

[8] G. M. Whitesides, The origins and the future of microfluidics, *Nature*, 2006, **442**, 368–373.

[9] A. Manz, D. J. Harrison, E. M. J. Verpoorte, J. C. Fettinger, A. Paulus, H. Lüdi and H. M. Widmer, Planar chips technology for miniaturization and integration of

separation techniques into monitoring systems, *J. Chromatogr. A*, 1992, **593**, 253–258.

[10] J. M. Ruano, V. Benoit, J. S. Aitchison and J. M. Cooper, Flame hydrolysis deposition of glass on silicon for the integration of optical and microfluidic devices, *Anal. Chem.*, 2000, **72**, 1093–1097.

[11] S. Queste, R. Salut, S. Clatot, J. -Y. Rauch and C. G. Khan Malek, Manufacture of microfluidic glass chips by deep plasma etching, femtosecond laser ablation, and anodic bonding, *Microsyst. Technol.*, 2010, **16**, 1485–1493.

[12] N. R. Harris, M. Hill, S. Beeby, Y. Shen, N. M. White, J. J. Hawkes and W. T. Coakley, A silicon microfluidic ultrasonic separator, *Sens. Actuators B Chem.*, 2003, **95**, 425–434.

[13] A. Sanjoh and T. Tsukihara, Spatiotemporal protein crystal growth studies using microfluidic silicon devices, *J. Cryst. Growth*, 1999, **196**, 691–702.

[14] J. C. McDonald and G. M. Whitesides, Poly(dimethylsiloxane) as a material for fabricating microfluidic devices, *Acc. Chem. Res.*, 2002, **35**, 491–499.

[15] E. Leclerc, Y. Sakai and T. Fujii, Microfluidic PDMS (polydimethylsiloxane) bioreactor for large-scale culture of hepatocytes, *Biotechnol. Prog.*, 2004, **20**, 750–755.

[16] R. Pelton, Bioactive paper provides a low-cost platform for diagnostics. *TrAC Trends Anal. Chem.*, 2009, **28**, 925–942.

[17] A. W. Martinez, S. T. Phillips, M. J. Butte and G. M. Whitesides, Patterned paper as a platform for inexpensive, low-volume, portable bioassays, *Angew. Chem. Int. Ed.*, 2007, **46**, 1318–1320.

[18] S. Mohammadi, M. Maeki, R. M. Mohamadi, A. Ishida, H. Tani and M. Tokeshi, An instrument-free, screen-printed paper microfluidic device that enables bio and chemical sensing, *Analyst*, 2015, **140**, 6493–6499.

[19] D. M. Cate, J. A. Adkins, J. Mettakoonpitak and C. S. Henry, Recent developments in paper-based microfluidic devices, *Anal. Chem.*, 2015, **87**, 19–41.

[20] W. Liu, J. Kou, H. Xing and B. Li, Paper-based chromatographic chemiluminescence chip for the detection of dichlorvos in vegetables, *Biosens. Bioelectron.*, 2014, **52**, 76–81.

[21] W. Liu, Y. Guo, J. Luo, J. Kou, H. Zheng, B. Li and Z. Zhang, A molecularly imprinted polymer based a lab-on-paper chemiluminescence device for the detection of dichlorvos, *Spectrochim. Acta. A Mol. Biomol. Spectrosc.*, 2015, **141**, 51–57.

[22] Y. Zhu, L. Zhang and L. Yang, Designing of the functional paper-based surface-enhanced Raman spectroscopy substrates for colorants detection, *Mater. Res. Bull.*, 2015, **63**, 199–204.

[23] P. Nath, R. K. Arun and N. Chanda, A paper based microfluidic device for the detection of arsenic using a gold nanosensor, *RSC Adv.*, 2014, **4**, 59558–59561.

[24] P. Nath, R. K. Arun and N. Chanda, Smart gold nanosensor for easy sensing of lead and copper ions in solution and using paper strips, *RSC Adv.*, 2015, **5**, 69024–69031.

[25] N. Ratnarathorn, O. Chailapakul, C. S. Henry and W. Dungchai, Simple silver nanoparticle colorimetric sensing for copper by paper-based devices, *Talanta*, 2012, **99**, 552–557.

[26] S. M. Z. Hossain, R. E. Luckham, A. M. Smith, J. M. Lebert, L. M. Davies, R. H. Pelton, C. D. M. Filipe and J. D. Brennan, Development of a bioactive paper sensor for detection of neurotoxins using piezoelectric inkjet printing of sol-gel-derived bioinks, *Anal. Chem.*, 2009, **81**, 5474–5483.

[27] S. M. Z. Hossain, R. E. Luckham, M. J. McFadden and J. D. Brennan, Reagentless bidirectional lateral flow bioactive paper sensors for detection of pesticides in beverage and food samples, *Anal. Chem.*, 2009, **81**, 9055–9064.

[28] M. Li, R. Cao, A. Nilghaz, L. Guan, X. Zhang and W. Shen, "Periodic-table-style" paper device for monitoring heavy metals in water, *Anal. Chem.*, 2015, **87**, 2555–2559.

[29] V. Mani, K. Kadimisetty, S. Malla, A. A. Joshi and J. F. Rusling, Paper-based electrochemiluminescent screening for genotoxic activity in the environment, *Environ. Sci. Technol.*, 2013, **47**, 1937–1944.

[30] S. Ma, Y. Tang, J. Liu and J. Wu, Visible paper chip immunoassay for rapid determination of bacteria in water distribution system, *Talanta*, 2014, **120**, 135–140.

[31] S. M. Z. Hossain and J. D. Brennan, β-Galactosidase-based colorimetric paper sensor for determination of heavy metals, *Anal. Chem.*, 2011, **83**, 8772–8778.

[32] J. C. Jokerst, J. A. Adkins, B. Bisha, M. M. Mentele, L. D. Goodridge and C. S. Henry, Development of a paper-based analytical device for colorimetric detection of select foodborne pathogens, *Anal. Chem.*, 2012, **84**, 2900–2907.

[33] S. -Q. Jin, S. -M. Guo, P. Zuo and B. -C. Ye, A cost-effective Z-folding controlled liquid handling microfluidic paper analysis device for pathogen detection via ATP quantification, *Biosens. Bioelectron.*, 2014, **63**, 379–383.

[34] C. Sicard, C. Glen, B. Aubie, D. Wallace, S. Jahanshahi-Anbuhi, K. Pennings, G. T. Daigger, R. Pelton, J. D. Brennan and C. D. M. Filipe, Tools for water quality monitoring and mapping using paper-based sensors and cell phones, *Water Res.*, 2015, **70**, 360–369.

[35] J. A. Adkins and C. S. Henry, Electrochemical detection in paper-based analytical devices using microwire electrodes, *Anal. Chim. Acta*, 2015, **891**, 247–254.

[36] S. Chaiyo, W. Siangproh, A. Apilux and O. Chailapakul, Highly selective and sensitive paper-based colorimetric sensor using thiosulfate catalytic etching of silver nanoplates for trace determination of copper ions, *Anal. Chim. Acta*, 2015, **866**, 75–83.

[37] Y. Zhang, P. Zuo and B. -C. Ye, A low-cost and simple paper-based microfluidic device for simultaneous multiplex determination of different types of chemical contaminants in food, *Biosens. Bioelectron.*, 2015, **68**, 14–19.

[38] Z. Nie, F. Deiss, X. Liu, O. Akbulut and G. M. Whitesides, Integration of paper-based microfluidic devices with commercial electrochemical readers, *Lab Chip*, 2010, **10**, 3163–3169.

[39] N. M. Myers, E. N. Kernisan and M. Lieberman, Lab on paper: Iodometric titration on a printed card, *Anal. Chem.*, 2015, **87**, 3764–3770.

[40] S. Ge, W. Liu, L. Ge, M. Yan, J. Yan, J. Huang and J. Yu, *In situ* assembly of porous Au-paper electrode and functionalization of magnetic silica nanoparticles with HRP via click chemistry for Microcystin-LR immunoassay, *Biosens. Bioelectron.*, 2013, **49**, 111–117.

[41] A. Apilux, W. Siangproh, N. Praphairaksit and O. Chailapakul, Simple and rapid colorimetric detection of Hg(II) by a paper-based device using silver nanoplates, *Talanta*, 2012, **97**, 388–394.

[42] S. Nouanthavong, D. Nacapricha, C. Henry and Y. Sameenoi, Pesticide analysis using nanoceria-coated paper-based devices as a detection platform, *Analyst*, 2016, **141**, 1837–1846.

[43] T. C. Colletes, P. T. Garcia, R. B. Campanha, P. V. Abdelnur, W. Romão, W. K. T. Coltro and B. G. Vaz, A new insert sample approach to paper spray mass spectrometry: Paper substrate with paraffin barriers, *Analyst*, 2016, **141**, 1707–1713.

[44] T. M. G. Cardoso, P. T. Garcia and W. K. T. Coltro, Colorimetric determination of nitrite in clinical, food and environmental samples using microfluidic devices stamped in paper platforms, *Anal. Methods*, 2015, **7**, 7311–7317.

[45] N. Lopez-Ruiz, V. F. Curto, M. M. Erenas, F. Benito-Lopez, D. Diamond, A. J. Palma and L. F. Capitan-Vallvey, Smartphone-based simultaneous pH and nitrite colorimetric determination for paper microfluidic devices, *Anal. Chem.*, 2014, **86**, 9554–9562.

[46] T. S. Park, W. Li, K. E. McCracken and J. -Y. Yoon, Smartphone quantifies Salmonella from paper microfluidics, *Lab Chip*, 2013, **13**, 4832–4840.

[47] Z. Nie, C. A. Nijhuis, J. Gong, X. Chen, A. Kumachev, A. W. Martinez, M. Narovlyansky and G. M. Whitesides, Electrochemical sensing in paper-based microfluidic devices, *Lab Chip*, 2010, **10**, 477–483.

[48] H. Asano and Y. Shiraishi, Development of paper-based microfluidic analytical device for iron assay using photomask printed with 3D printer for fabrication of hydrophilic and hydrophobic zones on paper by photolithography, *Anal. Chim. Acta*, 2015, **883**, 55–60.

[49] S. Wang, L. Ge, L. Li, M. Yan, S. Ge and J. Yu, Molecularly imprinted polymer grafted paper-based multi-disk micro-disk plate for chemiluminescence detection of pesticide, *Biosens. Bioelectron.*, 2013, **50**, 262–268.

[50] G. Sun, P. Wang, S. Ge, L. Ge, J. Yu and M. Yan, Photoelectrochemical sensor for pentachlorophenol on microfluidic paper-based analytical device based on the molecular imprinting technique, *Biosens. Bioelectron.*, 2014, **56**, 97–103.

[51] C. S. Kuek Lawrence, S. N. Tan and C. Z. Floresca, A “green” cellulose paper based glucose amperometric biosensor, *Sens. Actuators B Chem.*, 2014, **193**, 536–541.

[52] Q. He, C. Ma, X. Hu and H. Chen, Method for fabrication of paper-based microfluidic devices by alkylsilane self-assembling and UV/O3-patterning, *Anal. Chem.*, 2013, **85**, 1327–1331.

[53] B. M. Jayawardane, S. Wei, I. D. McKelvie and S. D. Kolev, Microfluidic paper-based analytical device for the determination of nitrite and nitrate, *Anal. Chem.*, 2014, **86**, 7274–7279.

[54] J. Shi, F. Tang, H. Xing, H. Zheng, B. Lianhua and W. Wei, Electrochemical detection of Pb and Cd in paper-based microfluidic devices, *J. Braz. Chem. Soc.*, 2012, **23**, 1124–1130.

[55] B. M. Jayawardane, L. dlC. Coo, R. W. Cattrall and S. D. Kolev, The use of a polymer inclusion membrane in a paper-based sensor for the selective determination of Cu(II), *Anal. Chim. Acta*, 2013, **803**, 106–112.

[56] M. Cuartero, G. A. Crespo and E. Bakker, Paper-based thin-layer coulometric sensor for halide determination, *Anal. Chem.*, 2015, **87**, 1981–1990.

[57] S. Burnham, J. Hu, H. Anany, L. Brovko, F. Deiss, R. Derda and M. W. Griffiths, Towards rapid on-site phage-mediated detection of generic Escherichia coli in water using luminescent and visual readout, *Anal. Bioanal. Chem.*, 2014, **406**, 5685–5693.

[58] M. E. I. Badawy and A. F. El-Aswad, Bioactive paper sensor based on the acetylcholinesterase for the rapid detection of organophosphate and carbamate pesticides, *Int. J. Anal. Chem.*, 2014, **2014**, Article ID 536823, 8 pages, doi:10.1155/2014/536823.

[59] R. S. J. Alkasir, M. Ornatska and S. Andreescu, Colorimetric paper bioassay for the detection of phenolic compounds, *Anal. Chem.*, 2012, **84**, 9729–9737.

[60] P. Zuo, X. Li, D. C. Dominguez and B. -C. Ye, A PDMS/paper/glass hybrid microfluidic biochip integrated with aptamer-functionalized graphene oxide nano-

biosensors for one-step multiplexed pathogen detection, *Lab Chip*, 2013, **13**, 3921–3928.

[61] B. Gilbert-López, J. F. García-Reyes and A. Molina-Díaz, Sample treatment and determination of pesticide residues in fatty vegetable matrices: A review, *Talanta*, 2009, **79**, 109–128.

[62] C. Wilson and C. Tisdell, Why farmers continue to use pesticides despite environmental, health and sustainability costs, *Ecol. Econ.*, 2001, **39**, 449–462.

[63] C. S. Pundir and N. Chauhan, Acetylcholinesterase inhibition-based biosensors for pesticide determination: A review, *Anal. Biochem.*, 2012, **429**, 19–31.

[64] M. Dai and S. D. Copley, Genome shuffling improves degradation of the anthropogenic pesticide pentachlorophenol by sphingobium chlorophenolicum ATCC 39723, *Appl. Environ. Microbiol.*, 2004, **70**, 2391–2397.

[65] M. S. Fuentes, G. E. Briceño, J. M. Saez, C. S. Benimeli, M. C. Diez and M. J. Amoroso, Enhanced removal of a pesticides mixture by single cultures and consortia of free and immobilized streptomyces strains, *BioMed Res. Int.*, 2013, **2013**, 392573, doi:10.1155/2013/392573.

[66] N. Nesakumar, B. L. Ramachandra, S. Sethuraman, U. M. Krishnan and J. B. B. Rayappan, Evaluation of inhibition efficiency for the detection of captan, 2,3,7,8-Tetrachlorodibenzodioxin, pentachlorophenol and carbosulfan in water: An electrochemical approach, *Bull. Environ. Contam. Toxicol.*, 2016, **96**, 217–223.

[67] Y. Su, S. Ma, K. Jiang and X. Han, CdTe-paper-based visual sensor for detecting methyl viologen, *Chin. J. Chem.*, 2015, **33**, 446–450.

[68] J. Liu, H. Wang, N. E. Manicke, J. -M. Lin, R. G. Cooks and Z. Ouyang, Development, characterization, and application of paper spray ionization, *Anal. Chem.*, 2010, **82**, 2463–2471.

[69] K. -O. Honikel, The use and control of nitrate and nitrite for the processing of meat products, *Meat Sci.*, 2008, **78**, 68–76.

[70] H. Zhang, S. Qi, Y. Dong, X. Chen, Y. Xu, Y. Ma and X. Chen, A sensitive colorimetric method for the determination of nitrite in water supplies, meat and dairy products using ionic liquid-modified methyl red as a colour reagent, *Food Chem.*, 2014, **151**, 429–434.

[71] T. P. J. Kull, P. H. Backlund, K. M. Karlsson and J. A. O. Meriluoto, Oxidation of the cyanobacterial hepatotoxin microcystin-LR by chlorine dioxide: Reaction kinetics, characterization, and toxicity of reaction products, *Environ. Sci. Technol.*, 2004, **38**, 6025–6031.

[72] Y. Ding and R. Mutharasan, Highly sensitive and rapid detection of microcystin-LR in source and finished water samples using cantilever sensors, *Environ. Sci. Technol.*, 2011, **45**, 1490–1496.

CHAPTER 2 Simple and Sensitive Colorimetric Assay System for Horseradish Peroxidase Using Microfluidic Paper-Based Devices

2.1 Introduction

Applications of paper substrates as porous media for the development and fabrication of microfluidic devices have been widely realized in such fields as clinical diagnostics [1–4], environmental monitoring [5–8], and food and nutrition safety [9–12]. Microfluidic paper-based analytical devices (μPADs) are being exploited in various fields of analytical research mainly due to the inexpensive materials and cost-effective manufacturing processes required [13–15]. Consequently, these analytical devices are seen as a tool that can be mass produced for point-of-need applications.

Paper as a substrate material for fabricating μPADs has many advantages including its abilities to provide instrument-free liquid transport through capillary action, to store chemical components in their active form within the fiber network of the paper, and to provide a high surface area to volume ratio that improves sensitivity for colorimetric techniques [16]. These advantages have led to paper being applied in μPAD fabrication for specific target compound detection ranging from simple spot tests for metals [5,17] and salts [18], to bioassays for proteins [19,20] and other biomolecules [21,22]. Though paper has long been utilized in analytical research studies, for example, in 1812 John Davy reported a use of litmus paper [23], Whitesides and his co-workers [24] have sparked the resurgence of the application of paper to microfluidic analytical and clinical research. Whitesides' group presented the fabrication of a microfluidic paper device by structuring a hydrophobic region using photoresist on paper to direct the flow of reagents within the

hydrophilic flow region of the device. This led to what is now an emerging technology for easy target detection and screening, most applicably in resource-limited environments, where access to expensive equipment and the availability of highly skilled technicians are a challenge such as in the developing countries.

When subjected to certain fabrication procedures to assemble the μPADs, however, the properties of the paper substrates, such as porosity and wicking, are often altered. With cellulose-based types of paper, including filter paper and chromatography paper, when photolithography is used, the wicking ability and hydrophilicity of each paper substrate is reduced depending on the type of the paper, and hence, an extra step such as plasma oxidation is necessary to increase the hydrophilicity of the fabricated μPADs [24,25]. In order to meet the desired requirements for the fabrication of μPADs – *i.e.*, ease of fabrication, simple to no instrumentation required, less pretreatment of the paper and/or μPAD – the most suitable paper substrate to undergo a specific fabrication procedure should be investigated.

In this report, we use photolithography as the fabrication method due to the availability of the equipment. Photolithography was the first reported fabrication method for μPADs with the main advantage of producing clearly defined hydrophilic channels of up to 186 ± 13 μm width and hydrophobic barriers formed after polymerization of the photoresist [26]. We describe which paper substrate is the most suitable to undergo the photolithographic fabrication that does not necessitate any further treatments to increase its hydrophilicity and at the same time does not lower the detection performance of the μPADs. We developed an assay system for horseradish peroxidase (HRP) using the μPADs. HRP is a widely used enzyme conjugate in bioanalytical studies due to its high stability and its ability to intensify a weak detection signal, hence, increasing the detectability of the target compound [27–30].

HRP is used in immunoassays [29,31] including enzyme-linked immunosorbent assays (ELISA) [32,33] due to its monomeric characteristic and its quick reactive response through the generation of a colored product with a chromogenic substrate such as 3,3',5,5'-tetratmethylbenzidine (TMB) [34] in the presence of an oxidant such as H_2O_2, which is the most commonly produced substance from optical enzymatic reactions [35]. Although several groups have reported on the HRP-TMB-H_2O_2 ELISA method for target compound detection [36,37], detailed basic information for the HRP-TMB-H_2O_2 assay on μPADs including its protocol is still elusive. Hence, we present a simple HRP assay system that can be applied to a variety of target molecules for point-of-need testing using portable microfluidic paper-based analytical devices. By appropriately designing a μPAD assay system using HRP-labeled molecules, the developed HRP-TMB-H_2O_2 assay system can be applied to the determination of specific target compounds. The wicking rates of the paper devices are investigated after subjecting each to photolithography and SEM observations are made of each paper before and after the photolithography. The most suitable paper substrate is identified as Whatman filter paper grade 41 and it is used for the HRP assay system. Then, we investigated the effect of the photoresist and solvent exposure of the hydrophilic areas of the photolithography-fabricated paper-based analytical devices to detection signals produced as compared to the un-exposed hydrophilic areas that were fabricated via wax-printing. Finally, we discuss assay results obtained for the system.

2.2 Research Methodology

2.2.1 Chemicals

All reagents were of analytical grade and all solutions were prepared using deionized water (Millipore, France). 10 mM of 3,3',5,5'-tetramethylbenzidine (Dojindo Laboratories, Kumamoto, Japan) was dissolved in acetonitrile (Wako Pure Chemical Industries, Ltd.,

Japan). Horseradish peroxidase (Wako Pure Chemical Industries, Ltd.) standards were prepared with 1x phosphate-buffered saline Tween® 20 (PBST), pH 7.5 (Thermo Fisher Scientific Inc., IL, USA). The blocker stock solutions including bovine serum albumin in phosphate-buffered saline (BSA-PBS), casein in PBS (casein-PBS), BSA in Tris-buffered saline (BSA-TBS) and casein in TBS (casein-TBS) were obtained from Thermo Fisher Scientific Inc. Working solutions of 1x BSA-PBS and 1x casein-PBS were diluted with PBST while working solutions of 1x BSA-TBS and 1x casein-TBS were diluted with 1x Tris-buffered saline Tween®-20 (TBST), pH 7.5 (Thermo Fisher Scientific Inc.). A 0.001% (v/v) hydrogen peroxide solution (Wako Pure Chemical Industries, Ltd.) was added into each HRP standard solution for the HRP assay.

2.2.2 Fabrication of µPADs

The µPADs were fabricated by photolithography, with slight modification of the reported method [24]. Figure 2-1 illustrates the steps in the µPAD fabrication. In brief, each paper substrate was impregnated with SU-8 2010 photoresist (Microchem, MA, USA) for about 30 s, spun for 5 s at 500 rpm then for 30 s at 2000 rpm with a spin coater (Mikasa MS-A100, Japan) to remove excess photoresist, prebaked for 5 min at 95^{o}C, cooled to room temperature for 30 s, aligned under a photomask using a mask aligner (Mikasa M-1S, Japan) before being exposed to UV radiation for 18 s, post-baked for another 5 min at 95^{o}C, developed (SU-8 developer, Microchem) for 6 min, washed 3 times with 2-propanol (Wako Pure Chemical Industries, Ltd.), then finally dried with high pressurized air before storing for future use. The dried µPADs were stored in a sealed plastic bag until the time of use. The patterns of the photomasks were designed using AutoCAD 2015 (Autodesk, Inc., USA), and then ordered from Unno Giken Co., Ltd. (Tokyo, Japan) for printing with resolutions of 12700 dpi each.

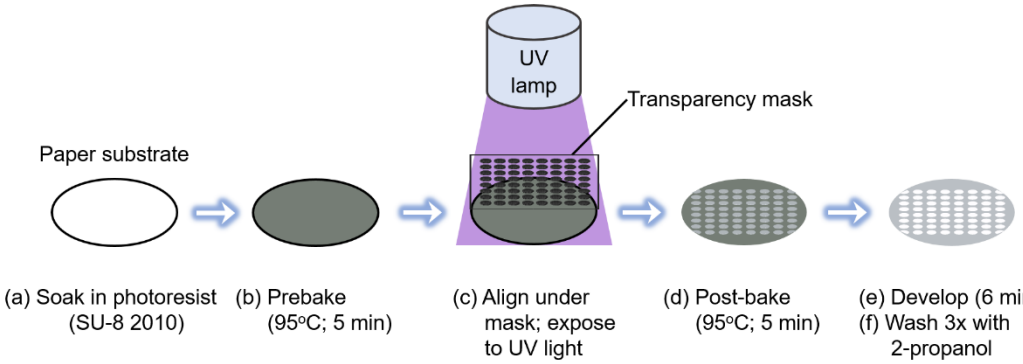

Figure 2-1 Schematic diagram of the photolithographic procedure used for fabricating the μPADs.

2.2.3 SEM Observation and Wicking Rate Evaluation of the Substrates and μPADs

The paper substrates (GE Healthcare Life Sciences, UK) selected for study are listed in Table 2-1 along with some of their properties. One had a nitrocellulose (NC) membrane and the other six had a cellulose membrane.

For observation with the SEM (JEOL JSM-639OLVS, Japan), specimens were prepared: each fabricated μPAD and its respective untreated paper substrate were sputtered with platinum using a magnetron sputtering device (JEOL JUC-5000) for 2-3 min at a pressure of 4 Pa and a current of 10 mA. The SEM images of the μPADs and untreated paper substrates were compared.

The wicking rates of the μPADs were evaluated. Figure 2-2 shows the set-up for the deionized water wicking rate evaluation and the structure and dimensions of the μPADs studied. A microtiter plate was used and 200 μL of deionized water was wicked through each μPAD.

Table 2-1 Relevant properties and the evaluated wicking rates of the paper substrates and their μPADs.

Paper type[*a]	**Material**	**Typical thickness**[*b] **(μm)**	**Filtration speed**[*b] **(Herzberg) (s per 100 mL)**	**Wicking rate before photolithography (s mm^{-1})**[*c]	**Wicking rate after photolithography (s mm^{-1})**[*c]
FP41	Cellulose	220	54	2.5 ± 0.1	2.8 ± 0.1
FP4	Cellulose	205	ca. 37	2.4 ± 0.1	21 ± 23
FP541	Cellulose	155	34	1.8 ± 0.1	40 ± 9
CP1	Cellulose	180	---	5.9 ± 0.1	86 ± 8
FP40	Cellulose	210	340	4.0 ± 0.2	120 ± 16
FP1	Cellulose	180	ca. 150	6.2 ± 0.2	183 ± 60
NC	Cellulose nitrate[*d]	200[*e]	---	2.4 ± 0.1	N/A

*[a] FP – filter paper; CP – chromatography paper; NC – Nitrocellulose membrane (FF120HP)

*[b] Data obtained from GE Healthcare Life Sciences

*[c] 4 mm × 20 mm (n=3)

*[d] Cellulose nitrate with polyester backing

*[e] 200 μm including 100 μm backing

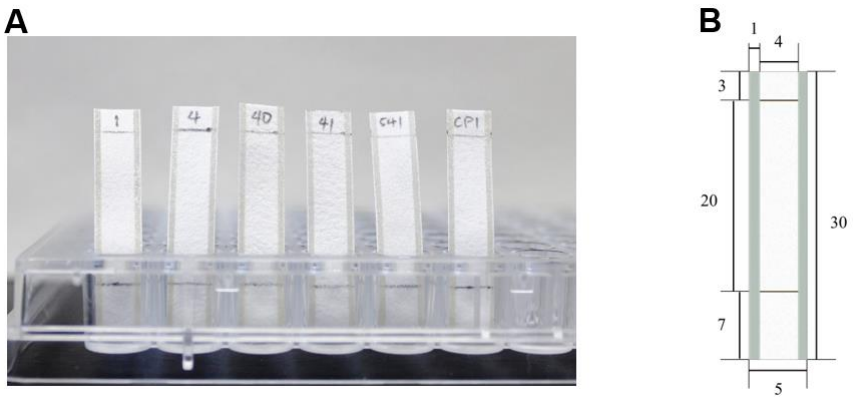

Figure 2-2 (A) Setup using a microtiter plate for the wicking rate evaluation of the μPADs with hydrophobic vertical boundaries and center hydrophilic regions. (B) An illustration of the μPAD showing the dimensions in mm.

2.2.4 Simple HRP Assay using Different μPADs

The reaction of TMB with H_2O_2 in the presence of HRP was done on the μPADs fabricated with different paper substrates. First, the μPADs were bonded onto an aluminum foil backing using an acrylic double adhesive tape (Figure 2-3) to limit the reagents on the test regions and avoid leakage. A 10 mM TMB solution was then added onto the test regions of the μPADs. After at least 2 min of air-drying each test region, the TMB-immobilized devices were then blocked with BSA-PBS for 20 min by adding 10 μL of the blocking solution to each hydrophilic test regions. Then, the blocked hydrophilic test regions of the μPADs were washed three times by adding 5 μL of PBST (pH 7.5) to each and then sequentially wiped by simply pressing a cellulose absorbent sheet on top of the μPADs with the washing solution. Finally, the washed μPADs were air-dried for 15 min. Next, 5 μL of 100 ng mL^{-1} of HRP in PBST containing 0.001% (v/v) H_2O_2 was reacted with the immobilized TMB on the test regions. The blue color intensities were then captured using a digital camera (EOS Kiss X6i Canon, Japan), and analyzed using ImageJ software.

(Please refer to Section 2.5.2 for more details regarding the image acquisition and processing.)

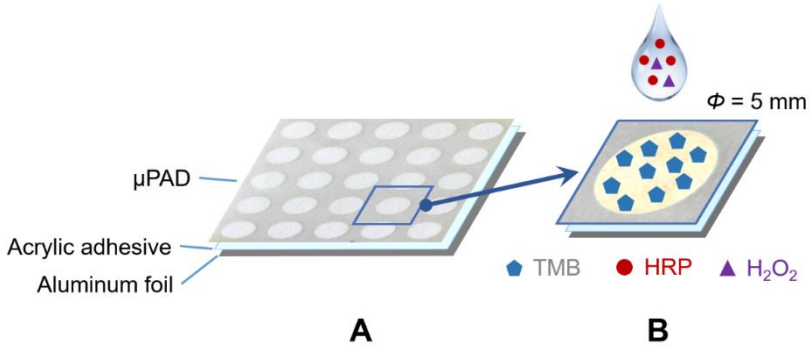

Figure 2-3 Schematic illustrations of the (A) μPAD for the (B) HRP assay.

2.2.5 Optimization of HRP Assay System

Certain parameters were optimized before HRP measurement. The drop volume sufficient to immobilize reagents onto a 5-mm diameter test region (Figure 2-3) was investigated using 0.50 to 2.50 μL of 2.0 mM methyl orange (Sigma-Aldrich, USA). Different types of blocking and washing reagents were investigated as well to determine which reagents gave the optimum results. Blockers BSA-PBS and casein-PBS were investigated in combination with PBST (pH 7.5) as the washing solution, and blockers BSA-TBS and casein-TBS were investigated in combination with TBST (pH 7.5) as the washing solution.

The optimum TMB and H_2O_2 compositions were simultaneously determined for the range of 0.05 to 30.0 mM TMB using a 100 ng mL^{-1} of HRP standard with H_2O_2 concentrations from 0.0001 to 0.50 % (v/v).

2.2.6 HRP Determination

After getting the optimum conditions for the HRP assay system, a determination of HRP was made. Similar to the procedure described above, the μPADs with the 5 mm diameter test region were first immobilized with 10 mM of TMB solution, blocked with BSA-PBS, washed three times with PBST (pH 7.5), and then air-dried for 20 min. After that, 5 μL solutions with concentrations of HRP in PBST ranging from 0 to 1000 ng mL^{-1} containing 0.001% (v/v) each of H_2O_2 were dropped onto the test regions. Figure 2-3B illustrates the HRP assay. Color images were captured using a digital camera and then analyzed using ImageJ software.

2.2.7 TMB Oxidation on Photolithography-fabricated vs. Wax-printed μPADs

Then, the effect of the photoresist and solvent exposure of the hydrophilic areas of the photolithography-fabricated paper-based analytical devices (P-μPADs) to the detection signals produced was investigated as opposed to the un-exposed hydrophilic areas that were fabricated via wax-printing (W-μPADs). The W-μPADs were fabricated via wax-printing as described previously [38] with slight modification. In brief, the patterns were first designed using Inkscape software, printed on the chromatography paper using wax-printer (Tektronix Phaser 850), and then melted the wax into the paper at 100^{o}C for 2 min using an oven (Yamato Drying-oven DX-38) to form the hydrophobic barriers.

Using both a P-μPAD and a W-μPAD, a simple HRP assay via spot test method was simultaneously performed. Figure 2-4 shows the schematic illustration of the assay procedure. Firstly, 1.4 μL of 35.7 mM TMB solution (equivalent to 50 nmol of TMB) was added onto each test zones of the paper-based arrays. After at least 2 min of drying, 10 μL of blocker BSA-PBS was next added onto each test zone. After 20 min of incubation, the test zones were washed three times with 7.5 μL each of PBST. After 15 min of air drying

at ambient temperature, 5 µL of the HRP standard solutions (0 – 1000 ng mL–1) containing 0.001% (v/v) hydrogen peroxide in PBST were added into respective test zones. The images of the PADs were recorded using a digital camera (EOS Kiss X6i Canon) and analyzed using ImageJ software (NIH) as described previously.

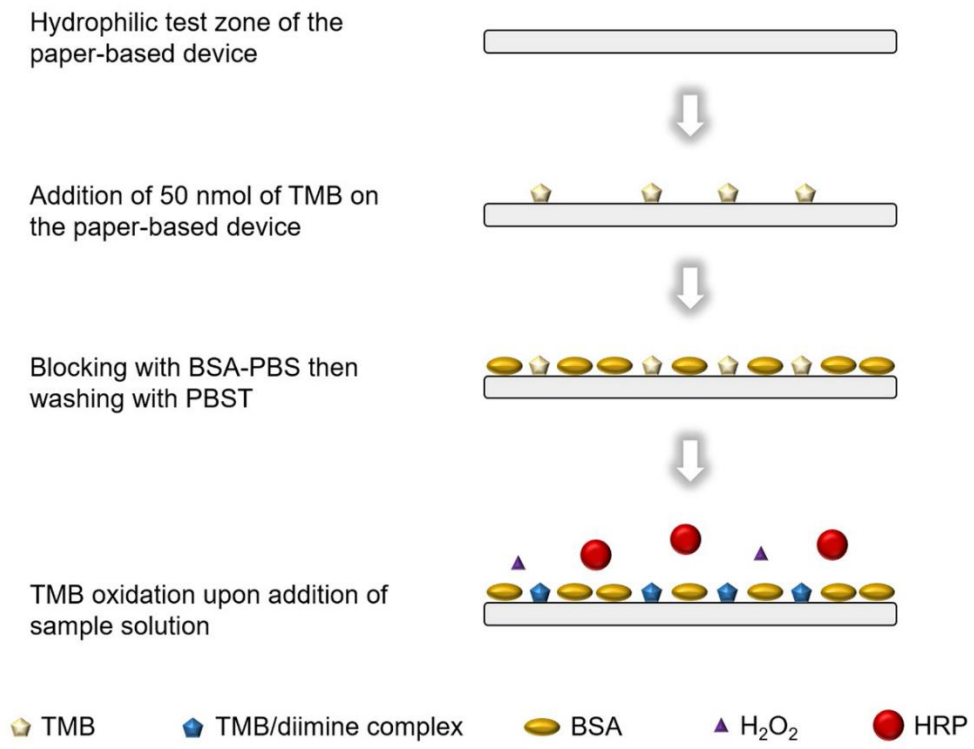

Figure 2-4 Schematic illustration of the colorimetric assay procedure involving the catalytic oxidation of TMB by hydrogen peroxide on PADs.

2.3 Results and Discussion

2.3.1 SEM Observation and Wicking Rate Evaluation of the Substrates and µPADs

The paper substrates were investigated to determine which one would be the most suitable for fabricating the µPADs. Each µPAD and each untreated paper substrate were observed by SEM. Figures 4A and C show the SEM images for two µPADs, using a cellulose membrane-based paper substrate, Whatman filter paper grade 41 (FP41), and the

NC membrane-based substrate (FF120HP), respectively, and Figures 4B and D show the SEM images for their respective paper substrates before photolithography. All of the μPADs fabricated using cellulose-based paper substrates had similar SEM images, suggesting that each is capable of forming well-defined hydrophobic regions after photolithography (Figure 2-5A is one example; see also Figure 2-13 in Section 2.5); additionally, the hydrophilic regions showed no particular structural changes compared to their original untreated counterparts. However, the cellulose nitrate matrix of FF120HP (Figure 2-5D) was completely destroyed after the photolithography (Figure 2-5C). When the NC membrane was impregnated with SU-8 developer, the NC matrix was immediately damaged; and after the membrane was exposed to UV radiation and developed using the SU-8 developer, the damage became even more (see also Figure 2-14). The NC membrane was unstable to the SU-8 photoresist, which is mainly composed of cyclopentanone and epoxy resin, and to the SU-8 developer, which consists of propylene glycol monomethyl ether acetate (PGMEA). These instabilities led to the complete destruction of the membrane after photolithography (Figure 2-5C). Therefore, the NC-based substrate was eliminated as a choice for the μPAD fabrication.

In a microfluidic paper-based assay, the wicking rate of the μPAD is an essential property to influence rapid flow detection. In a spot test method, the wicking rate is directly related to the rate of spreading of the fluids within the hydrophilic test regions during assay. Therefore, the μPAD wicking properties of the cellulose-based paper substrates were investigated. Although FP541 has the fastest wicking rate before photolithography (1.8 ± 0.1 s mm^{-1}, Table 2-1), FP41 μPAD showed the fastest wicking rate, 2.8 ± 0.1 s mm^{-1}. This is attributed to the different properties of the cellulose substrates, including the particle retention (pore size), nominal basis weight and the typical thickness of each (Please refer to Table 2-2 in Section 2.5 for more details). The different properties of the paper substrates

suggest that the degree of compactness of the cellulose fibers in the fiber network composition of the paper substrates possibly affects the capabilities of the paper substrates to liberate the unpolymerized SU-8 photoresist during the washing procedure, therefore, resulting to the reduced wicking rates of the µPADs.

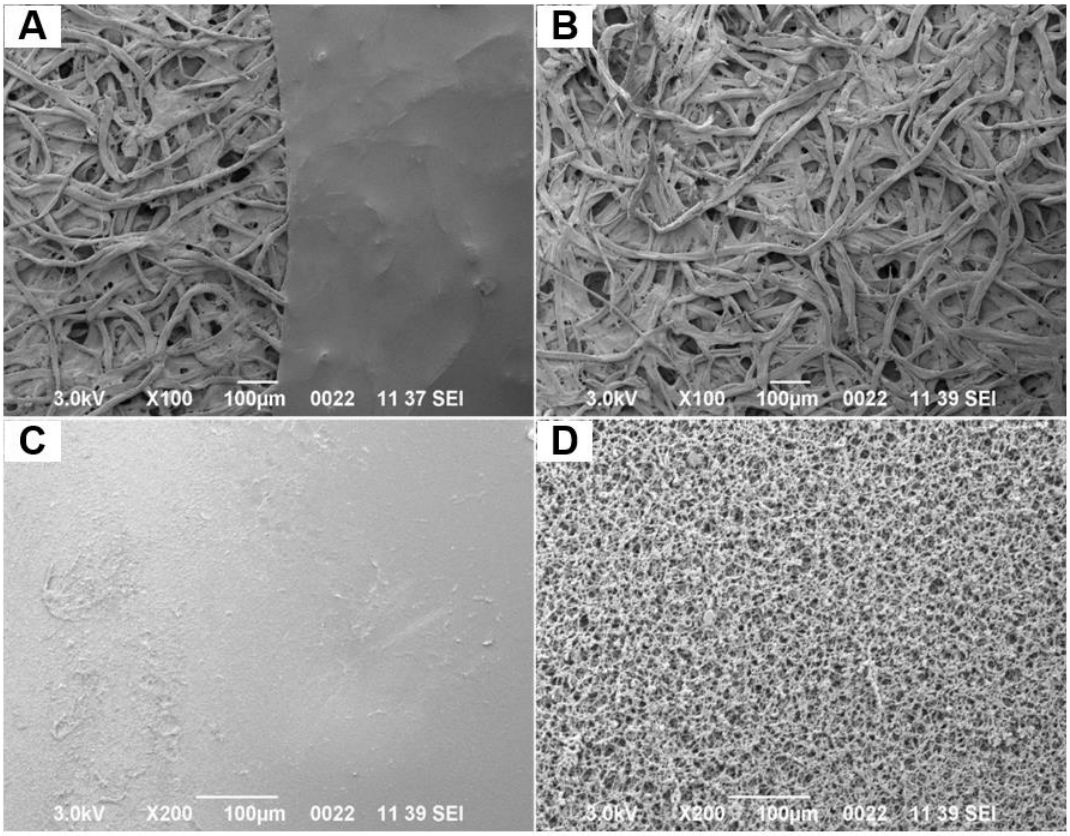

Figure 2-5 SEM images of (A, C) µPADs and (B, D) plain Whatman filter paper grade 41 and Whatman nitrocellulose membrane FF120HP, respectively.

2.3.2 Simple HRP Reaction on the µPADs

To determine which paper substrate would be most suitable for the µPAD fabrication, a TMB reaction with H_2O_2 in the presence of HRP was done to observe how the devices responded to the assay. Figure 2-6 compares the cyan intensities obtained by the µPADs under uniform reaction conditions. Figure 2-6A shows that µPADs using CP1, FP4, and

FP41 produced the highest intensities and there was little difference between the three. However, FP41 showed the fastest wicking rate, 2.8 ± 0.1 s mm^{-1}.

Although NC membrane paper substrate is commonly used for μPAD fabrication, specifically for lateral flow assays [39,40], it was unstable to photolithography as shown here. Hence, for the HRP assay system, FP41 was chosen as the most suitable cellulose-based paper substrate for the μPADs.

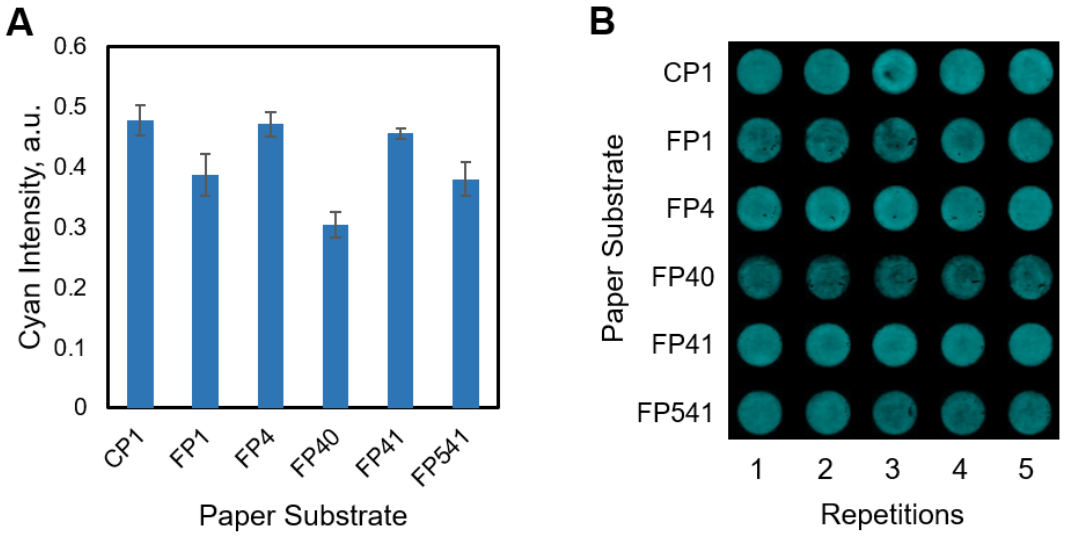

Figure 2-6 (A) A comparison of cyan intensities obtained by the μPADs for the HRP reaction with TMB under uniform conditions (*n*=2). (B) An image of the μPADs showing the cyan intensities separated through ImageJ analysis after the HRP reaction with TMB. [Conditions: 10 mM TMB, 100 ng mL^{-1} HRP in PBST with 0.001% (v/v) H_2O_2]

2.3.3 Optimization of HRP Assay System

Prior to HRP detection, parameters including drop volume were investigated. The drop volume is the amount of reagent needed to spread onto the entire test region. Figure 2-7 shows the FP41 μPADs for the drop volume optimization obtained after a few seconds of

incubation using 2 mM methyl orange solution. The first trial (T1) showed that the optimum drop volume should be from 1.25 to 1.5 µL. The second trial narrowed the optimum drop volume to 1.4 µL. This volume was then used to introduce reagents for immobilization of the TMB.

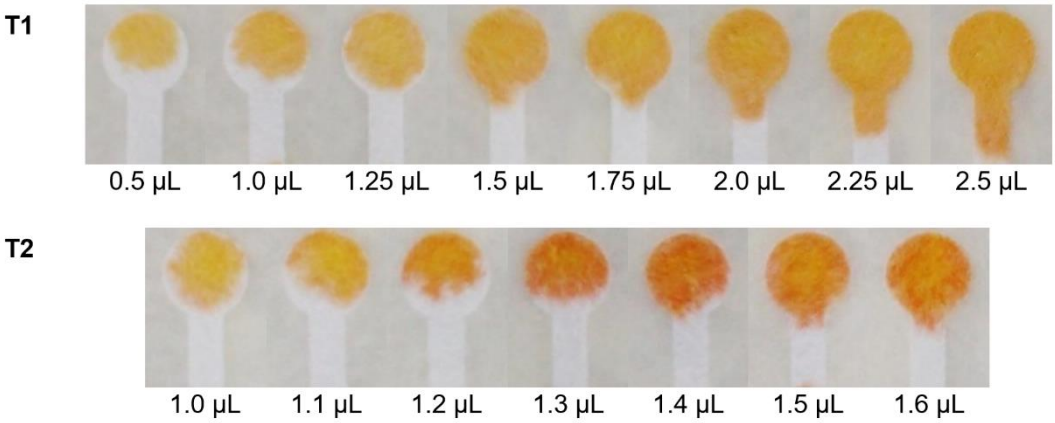

Figure 2-7 Photographs of the optimum drop volume investigation results using 2 mM of methyl orange with FP41 µPADs of 5 mm diameter test regions.

Though the HRP assay system presented here involves a spot test method, a suitable blocking condition is essential when the system is considered for practical application to a microfluidic paper-based system involving flow-based detection. The most suitable blocking condition was therefore determined. Blocking in bioassays allows specific binding of target molecules and eliminates unwanted side reactions due to nonspecific adsorption on possible remaining unblocked active sites [41]. Moreover, the blocking step in an assay is necessary to improve sensitivity by reducing background interference. In figure 2-8A, the signal intensity for BSA-PBS as blocking solution was more than twice as high as the other three, and hence it was chosen for the subsequent blocking procedures. Washing, on the other hand, is necessary to eliminate excess reagents. The blocking

solution showing optimum washing results was BSA in PBST solution. Hence, PBST (pH, 7.5) was used for all succeeding measurements.

Investigating the optimum amount of TMB for immobilization also showed that visible blue color intensities increased with increasing TMB concentration, as shown in Figure 2-8B. TMB was oxidized to a blue TMB diimine product by H_2O_2 in the presence of HRP, forming water as another byproduct (Figure 2-9) [14,42]. The blue color intensity produced after TMB oxidization depended on the amount of HRP present during the reaction (see also Figure 2-16). However, higher TMB concentrations than 10 mM gave almost uniform intensities as illustrated in Figure 2-8B (see also Figure 2-17). Hence, the concentration used for TMB for the rest of the study was 10 mM.

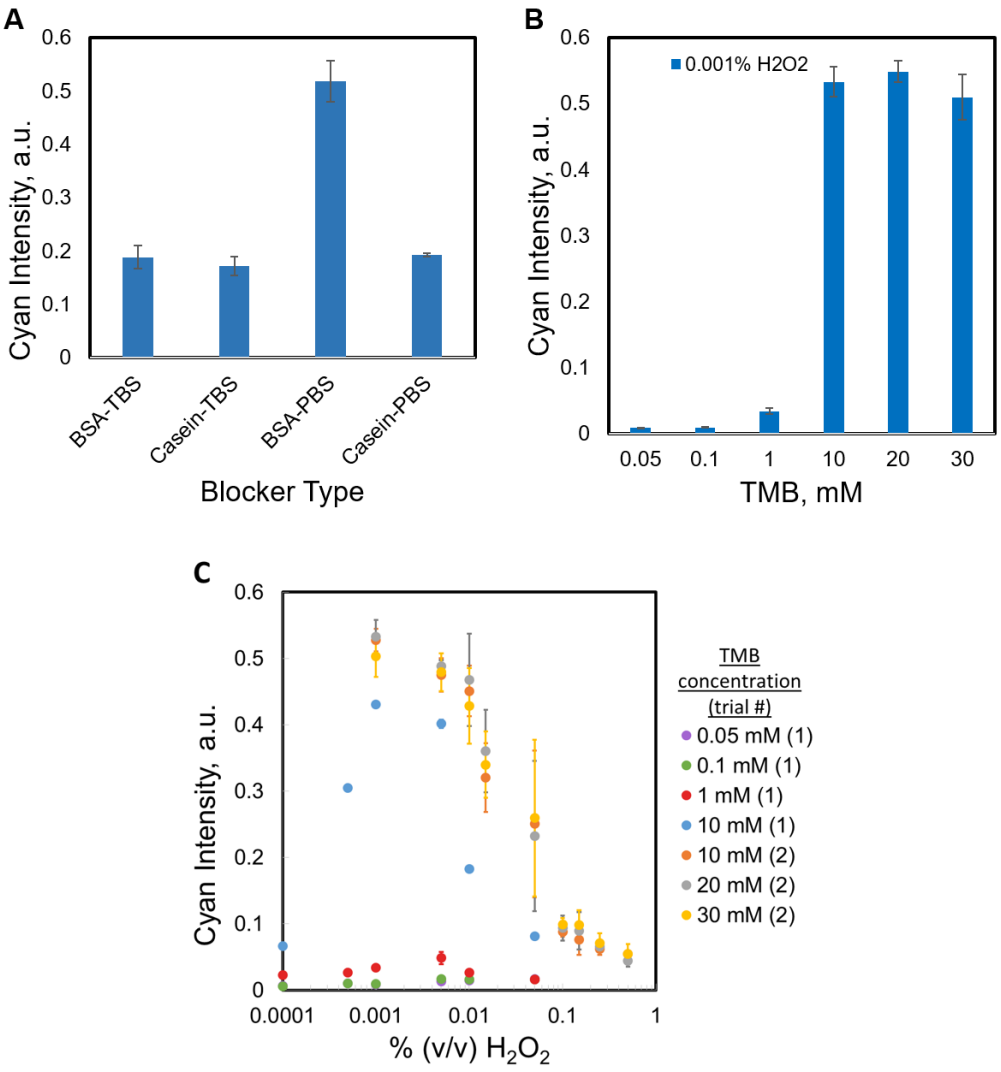

Figure 2-8 (A) Comparison of intensities produced during the HRP-TMB reaction using different blocking conditions (n=2). (B) Signal intensities for TMB analysis with the optimum intensity at TMB concentration of 10 mM (n=2 for 0.05 to 1 mM of TMB concentrations, and n=4 for 10 to 30 mM of TMB concentrations). (C) Signal intensities for 100 ng mL^{-1} of HRP in PBST containing an increasing amount of H_2O_2 upon reaction with different concentrations of TMB: (1) from 0.05 to 10 mM of TMB (n=2); and (2) from 10 to 30 mM of TMB (n=4). The measured cyan intensity at 10 mM of TMB in trial (1) was slightly different from the cyan intensity at 10 mM of TMB

in trial (2) due to the difference in the brightness of the background as the images were captured separately and later measured by ImageJ analysis. [Conditions: 10 mM TMB, 100 ng mL^{-1} HRP with 0.001% (v/v) H_2O_2 in PBST and TBST, respectively]

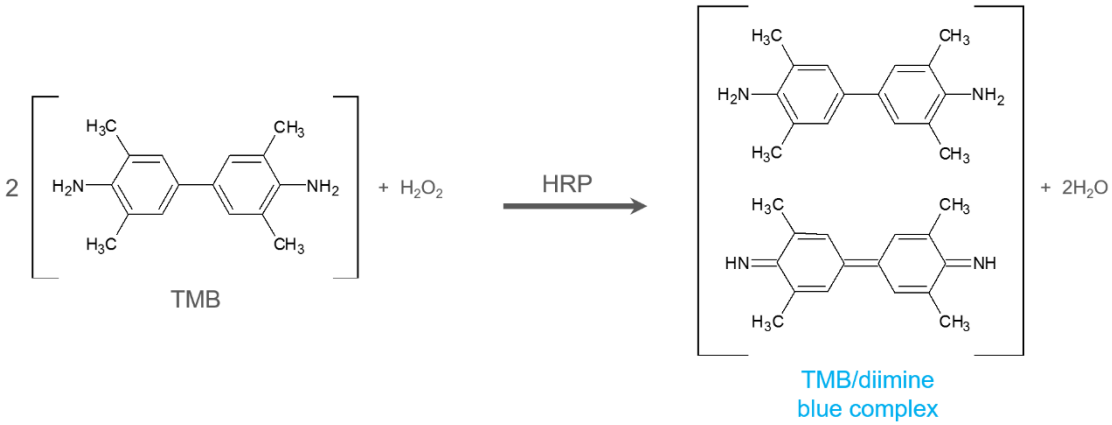

Figure 2-9 TMB oxidation by H_2O_2 in the presence of HRP produced a blue TMB diimine product and water [41].

The optimum amount of H_2O_2 needed to obtain maximum intensity upon TMB oxidation was determined to be 0.001% (v/v), as shown in Figure 2-8C. Although Josephy, et al. [43] showed that 1 mole of H_2O_2 requires 2 moles of TMB for its oxidation to produce the maximum blue color intensity in a solution reaction, the present results showed that about 30 times less H_2O_2 was enough to produce the maximum intensity using µPADs. With 50 nmol of TMB immobilized on the µPAD, only 1.66 nmol of H_2O_2 was necessary to obtain the optimum cyan intensity in the presence of HRP. This was assumed to be due to the shorter diffusion length for TMB to undergo catalytic oxidation within the pores of the paper substrate, therefore, allowing faster reaction with much less H_2O_2 within the cellulose fiber networks than in bulk solution. However, for higher amounts of H_2O_2, lower to no intensities were obtained. This might be attributed to the possibility that the HRP

activity was impeded at high H_2O_2 concentration, and hence, the oxidation of TMB was hindered. Another possibility was that at high H_2O_2 concentration, the excess H_2O_2 attacked the oxidized blue colored diimine product of the TMB, leading to lower or no intensities. As reported by Josephy et al. [43], the blue product was formed and then subsequently destroyed with more H_2O_2. This indicated that the blue product was a one-electron oxidation product of TMB. Hence, 0.001% (v/v) of H_2O_2 was added to the HRP solution for reaction with immobilized TMB.

2.3.4 HRP Determination

Figure 2-10 shows the μPAD calibration plot, an actual image and the cyan profile obtained using ImageJ analysis for the HRP determination. At the optimum working conditions, the concentration detection range was 3 to 1000 ng mL^{-1}. Since the expected curve for most HRP-involved assays is sigmoidal in shape [44,45], a 4-parameter logistic (4PL) nonlinear regression was done and the calibration curve was obtained as following the equation:

$$y = d + \frac{a - d}{1 + \left(\frac{x}{c}\right)^b}$$

where, *y* is the cyan intensity, *x* is log [HRP], *a* is the minimum asymptote, which can be thought of as the response intensity at blank concentration, *b* is the Hill slope, which refers to the steepness of the curve, *c* is the inflection point where the curvature changes in direction or sign, and *d* is the maximum asymptote, which can be thought of as the response intensity at infinite concentration [46,47]. Using Ngraph software, the 4PL equation for the HRP-TMB system was determined as:

$$y = 0.471 + \frac{0.019 - 0.471}{1 + \left(\frac{x}{1.461}\right)^{3.869}}.$$

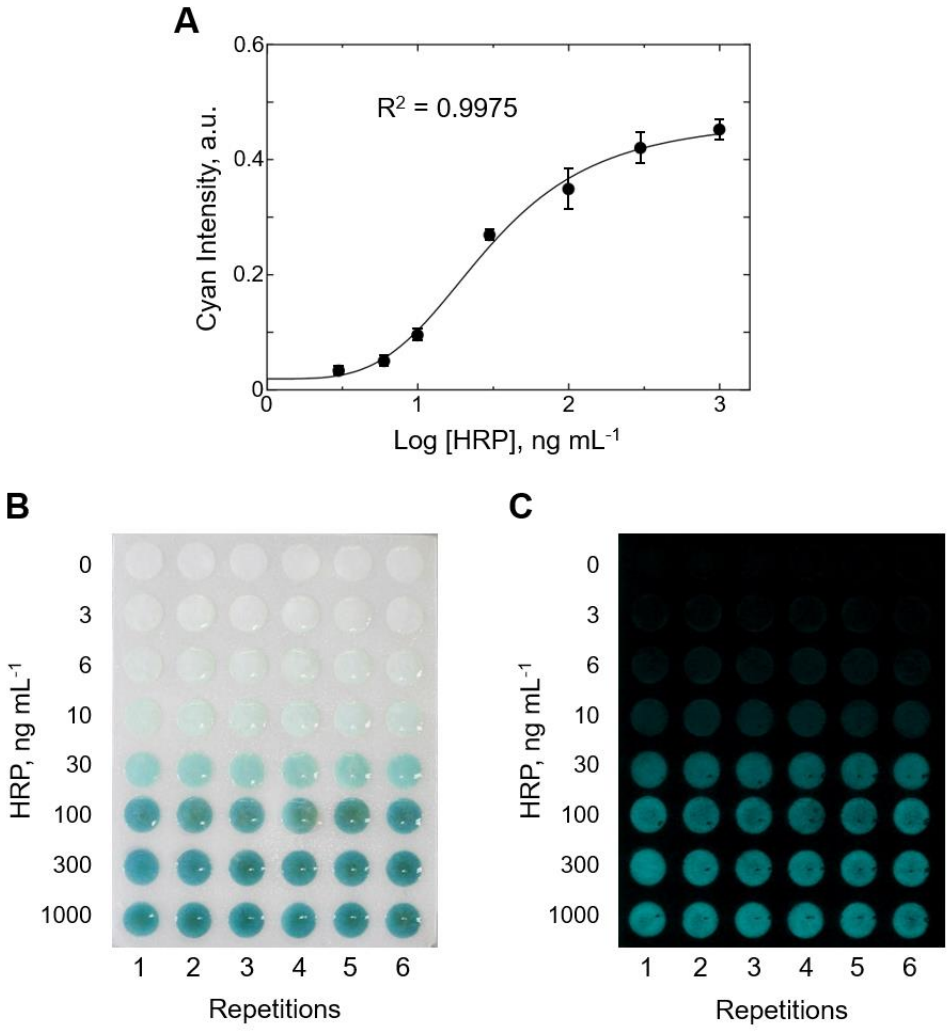

Figure 2-10 (A) HRP measurements at optimum conditions (*n*=6). (B) An image of the μPAD used to measure increasing concentrations of HRP in PBST in ng mL^{-1} unit. (C) The cyan profile separated from the captured image in (B) using ImageJ analysis.

The inflection point, or the concentration where the curve changes direction, as computed from the above equation is at 28.9 ng mL^{-1} HRP. The limit of detection (LOD), determined experimentally as the lowest HRP concentration that gives a cyan intensity equal to the sum of the cyan intensity of the blank and three times its standard deviation, was 5.58 ng mL^{-1} (or 0.69 fmol) HRP. Simple lateral-flow assays for HRP and peroxidase-conjugated

antibody have been successfully demonstrated on μPADs (see Figures 2-18 and 2-19 in Section 2.5.4 for additional information). A further application of the established HRP assay system to demonstrate the HRP-mediated quantification of a specific target in real samples is kept as a scope for future work.

2.3.5 Effect of Photoresist and Solvent Exposure of the μPADs on TMB Oxidation

The catalytic oxidation of TMB by hydrogen peroxide on μPADs produces blue colored products that can be easily detected by the naked eye. As described previously by Josephy et al. [43], the blue color production is caused by the one-electron oxidation of TMB in solution producing a blue charge-transfer complex of the parent compound and its imine oxidation product in equilibrium with its cation free-radical in the presence of less than equimolar hydrogen peroxide (see Figure 2-11A for structures). However, μPADs that are fabricated via photolithography have hydrophilic areas that are exposed to polymers and solvents, specifically to the SU-8 photoresist, a strong electron-donor consisting of 8 epoxy groups (Figure 2-11B), which causes the production of detection signals from the possible formation of a charge-transfer complex with TMB. As observed experimentally, even prior to the addition of the sample solution consisting of HRP and hydrogen peroxide, the simple addition of TMB on the hydrophilic test zones of the PADs produce a slight blue color intensity. This observation may be attributed to the unavoidable incomplete elimination of the photoresist during fabrication.

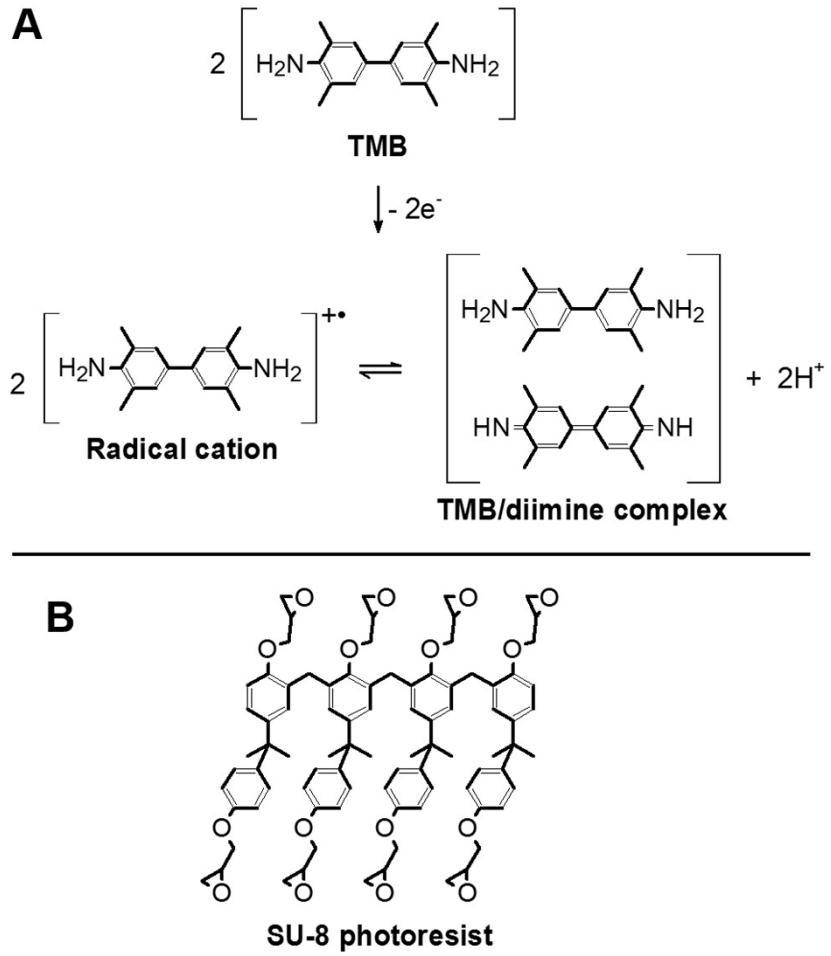

Figure 2-11 (A) Catalytic oxidation of TMB by hydrogen peroxide producing the blue colored TMB/diimine complex [43]. (B) Chemical structure of SU-8 photoresist.

We further confirmed such observation by comparing experimental results using μPADs that were fabricated via photolithography, in parallel with μPADs that were fabricated via wax-printing. As described previously, photolithography has the disadvantage of exposing the hydrophilic areas of the μPADs to polymers and solvents, which greatly reduces the hydrophilicity and wicking ability of the PADs after fabrication. Therefore, although this work presents a spot test method of detection, the need for blocking was necessary to increase the hydrophilicity of the chromatography paper after being subjected to photolithography. The blocking also enables the 5-μL volume of sample

solution to spread throughout the 5-mm diameter test zones. As the HRP assay was further performed on both the P-PAD and W-PAD, we have observed notable differences on the signal intensities produced at similar HRP concentration range. Figure 2-12 shows the comparison of detection signals observed using the two µPADs. At very low HRP concentrations including the blank, the P-µPAD produced light blue detection signals. Analyzing the images at the blank concentration using ImageJ software shows higher cyan intensity using the P-µPAD (Figure 2-12B) compared to that using the W-µPAD (Figure 2-12C). This may be attributed to the photoresist residues on the P-µPAD that possibly formed a charge-transfer complex with TMB, therefore producing the faint blue false detection signal. Another possibility could be that the amine groups of TMB may have interacted with the epoxy groups of the photoresist, facilitating the early deprotonation of the amine groups upon the addition of TMB to the P-µPAD (Figure 2-11). Then, the early formation of the deprotonated TMB could have formed charge-transfer complex with the free TMB, resulting to the formation of higher background signal (i.e., detection signal at blank concentration). However, as the HRP concentration increased, detection signals also increased but the magnitude of intensities are reversed showing higher intensities with the polymer-free test zones of the W-µPAD from 10 – 1000 ng mL^{-1} HRP concentration than with those of P-µPAD. This may be due to a decrease in the available TMB concentration for the reaction to proceed at the hydrophilic test zone of the P-µPAD, owing it to the possible binding of the TMB molecules to the photoresist, hence, the production of lower signal intensity. Yet, computing for the detection limits (LODs) of HRP (blank intensity plus 3 times the standard deviation) on both µPADs via 4-parameter logistic (4PL) nonlinear regression using OriginPro software (OriginLab Corporation) show a lower value for the P-µPAD (0.33 ng mL^{-1} or 0.038 fmol) compared to that of W-µPAD (1.08 ng mL^{-1} or 0.12 fmol). The lower LOD for the P-µPAD may be attributed to the sigmoidal shape

of the 4PL calibration curve with determined inflection point of 5.47 ng mL^{-1} HRP and Hill slope (referring to the steepness of the curve) of 1.32 ng^{-1} mL, which are lower values compared to those of W-PAD (7.33 ng mL^{-1} HRP and 1.46 ng^{-1} mL, respectively). Nevertheless, visual analysis reveal that colorimetric detection for HRP using the TMB-H_2O_2 assay system on W-µPAD present more reliable readouts using the naked eye than on P-µPAD.

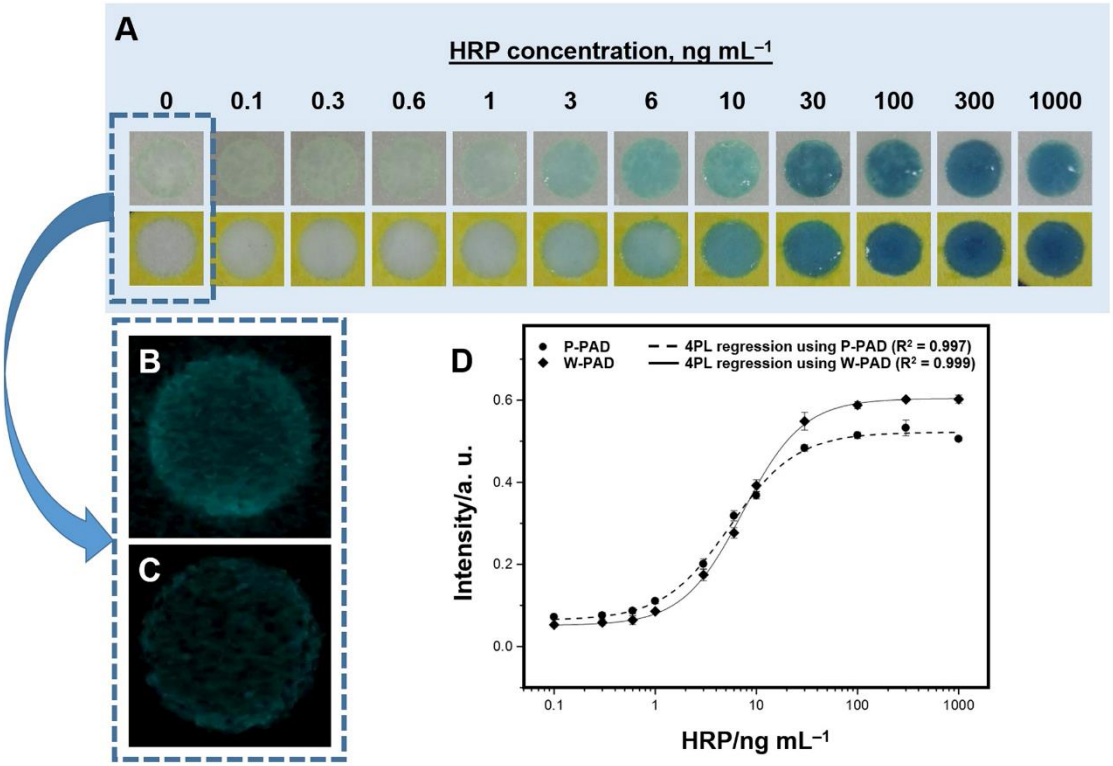

Figure 2-12 (A) Representative images of the spot tests performed on P-µPAD (top images) and W-µPAD (bottom images) at increasing HRP concentration. (B) And (C) Respective cyan profiles of the images of the fabricated devices at blank HRP concentration. The cyan profiles were enhanced by adjusting the contrast and brightness to –20% and +40%, respectively. (D) 4-Parameter logistics nonlinear regression for HRP determination. Error bars represent 4 replicate measurements.

2.4 Conclusion

A highly sensitive HRP assay system implemented on a microfluidic paper-based analytical device (μPAD) using Whatman filter paper grade 41 (FP41) has been developed where HRP can be visually detected by the naked eye using blue color intensity for a minimum concentration of about 6 ng mL^{-1} (0.75 fmol) within a 15-minute reaction time. The detection signals were comparably higher for the FP41 μPAD using the HRP-TMB-H_2O_2 reaction than for μPADs using other paper substrates. These results suggest that the developed FP41 μPAD can be utilized for the measurement of specific target substances by appropriately designing the assay system for HRP-conjugated molecules. A journal article regarding these findings has been published in *Sensors and Actuators B: Chemical* (2016).

Moreover, the colorimetric oxidation of 3,3',5,5'-tetramethylbenzidine by hydrogen peroxide in the presence of horseradish peroxidase using photolithography-fabricated and wax-printed paper-based analytical devices has been investigated. The production of faint detection signal even at blank intensity suggest the possible formation of a blue colored complex of TMB and the photoresist residues on P-μPAD. However, at higher HRP concentration more intense detection signals are produced using W-μPAD at concentrations from 10 to 1000 ng mL^{-1}, which may be attributed to the possible binding of the TMB molecules to the photoresist residues on the P-μPAD, hence, reducing the available TMB concentration for reaction, and producing less intense detection signals. The findings therefore demonstrate that the use of W-μPADs for the TMB-H_2O_2 assay system in the presence of HRP offer more reliable visual readouts for practical applications involving HRP-labeled molecules in clinical and bioanalytical fields of research. Another journal article regarding these findings has been published in *Analytical Sciences* (2016).

2.5 Additional Information

2.5.1 Preparation of Buffer and Blocking Solutions

During the optimization of blocking conditions, two buffer solutions were used depending on the type of blocking solutions used. Phosphate-buffered saline Tween®-20 (PBST), pH 7.5 (Product # 28352, Thermo Fisher Scientific Inc., IL, USA) and Tris-buffered saline Tween®-20 (TBST), pH 7.5 (Thermo Fisher Scientific Inc.) were both diluted 20x with deionized water (Millipore, France) to obtain 1x working buffer solutions, respectively. The 1x diluted concentration of PBST contains 10 mM sodium phosphate, 0.15 M sodium chloride and 0.05 % Tween®-20. pH 7.5. The 1x diluted concentration of TBST on the other hand contains 25 mM Tris, 0.15 M sodium chloride and 0.05 % Tween®-20, pH 7.5. The blocker stock solutions including bovine serum albumin in phosphate-buffered saline (BSA-PBS, Product # 37525), casein in PBS (casein-PBS, Product # 37582), BSA in Tris-buffered saline (BSA-TBS, Product # 37520) and casein in TBS (casein-TBS, Product # 37583) were obtained from Thermo Fisher Scientific Inc. The working solutions of BSA-PBS and BSA-TBS were diluted 10x with PBST and TBST, respectively. The washing buffer used for BSA-PBS (containing 1 % (w/v) BSA) and casein-PBS (containing 1 % (w/v) casein) was PBST, while that for BSA-TBS (containing 1 % (w/v) BSA) and casein-TBS (containing 1 % (w/v) casein) was TBST.

2.5.2 Image Processing using ImageJ Software

The blue color intensities produced during the HRP-TMB-H_2O_2 assay were captured using a digital camera (EOS Kiss X6i Canon, Japan) equipped with a standard 18-55 mm objective lens. The photos were taken using the ISO AUTO Close-up Mode with an exposure time of 1/40 s, aperture of F/4, ISO of 125, focal distance of 27 mm, and color

representation in standard RGB (sRGB). The camera was hand held by the researcher and was positioned above the μPAD during image acquisition.

The JPG file formats of the images were analyzed using ImageJ software (NIH, Bethesda, MD). During ImageJ analysis, the RGB images were first split to obtain the CMYK (cyan-magenta-yellow-key) profiles. Using the cyan profile of each image, a circular region of interest (ROI) was drawn around each test region of the μPAD for quantitative determinations. The histogram of each of these ROI delivered a mean cyan value that was used for quantitative determinations and construction of calibration plots.

2.5.3 Wicking Rate Evaluation of the μPADs

The wicking rates of the different paper substrates and their μPADs have been evaluated. Before photolithography, the untreated paper substrates showed wicking rates that were comparable to each other and were correlated to their filtration speed (in Herzberg) as well. However, after photolithographic fabrication of the μPADs, the paper substrates (excluding the NC membrane) revealed highly reduced wicking rates, except for FP41 μPAD which showed the fastest wicking rate of 2.8 ± 0.1 s mm^{-1}.

Excluding the NC (FF120HP) membrane, all the other paper substrates are composed of cellulose fibers. Despite the similarity in composition, each paper substrate differ in properties as shown in Table 2-2. For instance, FP41 has a typical particle retention (pore size) of 20-25 μm similar to FP4, but the nominal basis weights of FP41 and FP4 are 85 g m^{-2} and 92 g m^{-2}, respectively. The typical thickness of FP41 and FP4 are 220 μm and 205 μm, respectively. Considering the properties of the two paper substrates, FP4 would have a more compact cellulose fiber structure than FP41 since it is less thick but has more nominal basis weight. Therefore, although the wicking rates of both before photolithography are comparable (2.5 ± 0.1 s mm^{-1} and 2.4 ± 0.1 s mm^{-1} for FP41 and FP4,

respectively), the obtained experimental result for FP41 μPAD having the faster wicking rate compared to FP4 μPAD agrees well when taking into account the individual properties of the paper substrates.

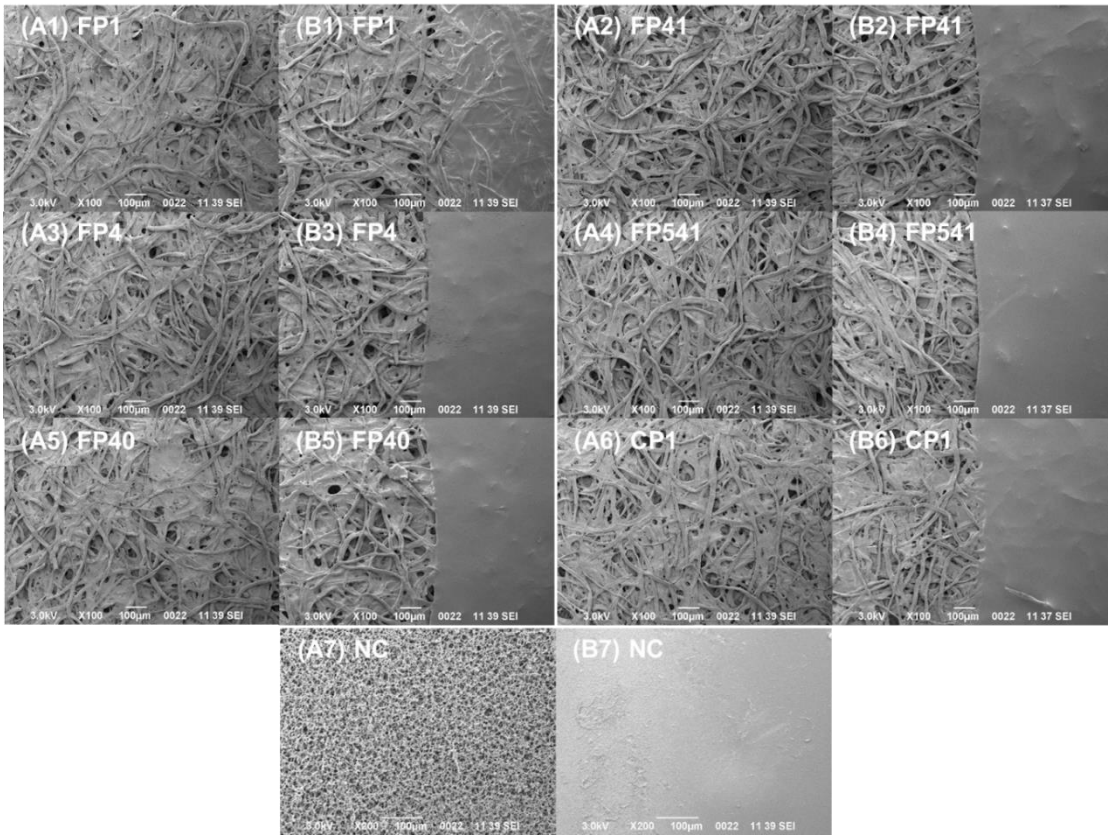

Figure 2-13 (A1 – A7) SEM images of different plain hydrophilic paper substrates and (B) their corresponding SEM images after μPAD fabrication by photolithography showing the respective boundaries that were formed separating the hydrophilic (left) and hydrophobic (right) regions for the cellulose-based papers (B1 – B6). The NC nitrocellulose membrane was completely destroyed after photolithography (B7).

Table 2-2 Relevant properties and evaluated wicking rates of the paper substrates and the evaluated wicking rates of their μPADs.

Paper type*[a]	**Typical particle retention in liquid*[b] (pore size) (μm)**	**Nominal basis weight*[b] (g m^{-2})**	**Typical thickness*[b] (μm)**	**Filtration speed*[b] (Herzberg) (s per 100 mL)**	**Wicking rate before photolithography (s mm^{-1})*[c]**	**Wicking rate after photolithography (s mm^{-1})*[c]**
FP41	20-25	85	220	54	2.5 ± 0.1	2.8 ± 0.1
FP4	20-25	92	205	ca. 37	2.4 ± 0.1	21 ± 23
FP541	22	78	155	34	1.8 ± 0.1	40 ± 9
CP1	---	88	180	---	5.9 ± 0.1	86 ± 8
FP40	8	95	210	340	4.0 ± 0.2	120 ± 16
FP1	11	87	180	ca. 150	6.2 ± 0.2	183 ± 60
NC	---	---	200*[d]	---	2.4 ± 0.1	N/A

*[a] FP – filter paper; CP – chromatography paper; NC – Nitrocellulose membrane (FF120HP)

*[b] Data obtained from GE Healthcare Life Sciences

*[c] 4 mm × 20 mm (n=3)

*[d] 200 μm including 100 μm backing

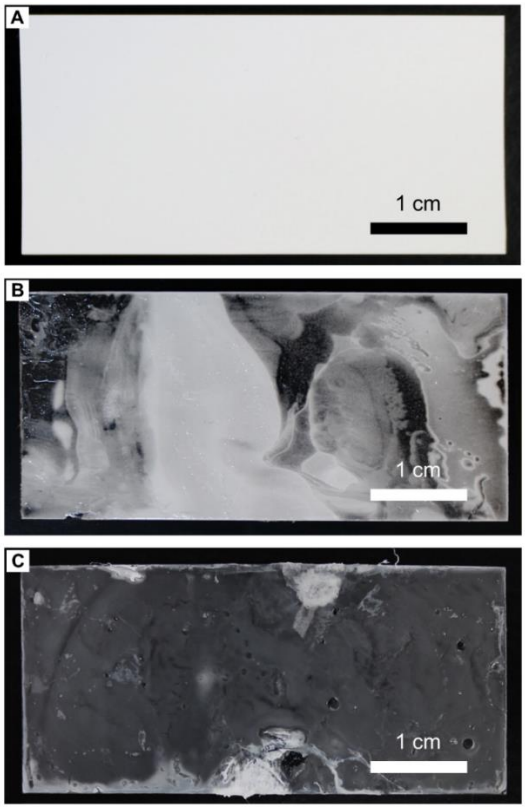

Figure 2-14 Photographs of the NC membrane (FF120HP) (A) before photolithography, (B) after impregnating with photoresist, and (C) after the development step.

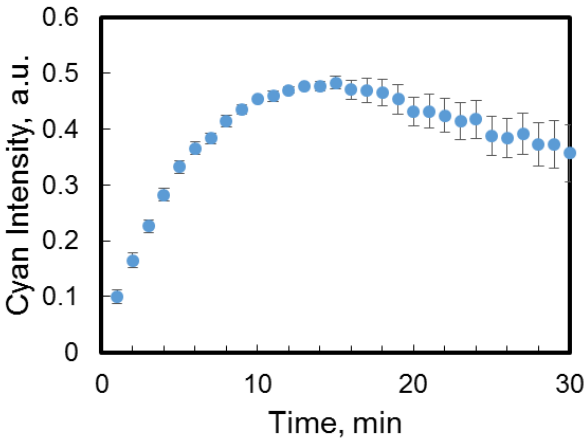

Figure 2-15 Color development profile of the oxidation of TMB during HRP-TMB-H_2O_2 assay in duplicate measurements. [Conditions: 10 mM TMB; 100 ng mL^{-1} HRP standard with 0.001 % (v/v) H_2O_2 in PBST; blocking with BSA-PBS, washing with PBST, pH 7.5.]

The color development during TMB oxidation was observed to determine the necessary incubation time during HRP-TMB-H_2O_2 assay. As shown in Figure 2-15, the cyan intensity during color development is maximum at 15 min incubation time. However, as observed in the color development profile, the intensities not only diminish but also the error bars widen with further incubation as the μPADs gradually dry. Therefore, the intensities were measured after 15 min of reaction in all experiments.

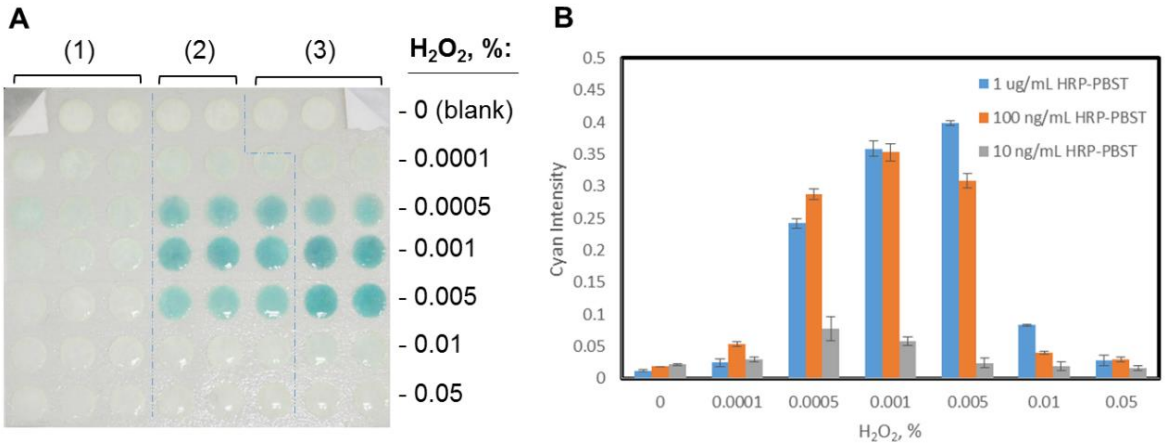

Figure 2-16 (A) The captured image of the μPAD during the optimum H_2O_2 investigation with different HRP concentrations of (1) 10, (2) 100, and (3) 1000 ng mL^{-1}. (B) The bar graph of the analyzed data in (A) (triplicate measurements for 10 and 100 ng mL^{-1} HRP concentrations; and, duplicate measurements for 1000 ng mL^{-1} HRP). [Conditions: 10 mM TMB; blocking with BSA-PBS; washing with PBST, pH 7.5.]

It was observed in Figure 2-16, however, that as the concentration of HRP was increased, the H_2O_2 composition necessary to produce a more intense signal also increased. This observation was somehow expected because the amount of HRP affects the rate of TMB oxidation, although not the concentration of the final product, as discussed previously by Josephy, et al. (1982) [43]. In other words, it takes longer time to achieve the same blue

color intensity of the oxidized product with lower HRP concentration. Hence, since we were interested in working within the concentration range of 100 ng mL^{-1} and 15 min reaction time, a H_2O_2 composition of 0.001% was then specifically chosen for the study.

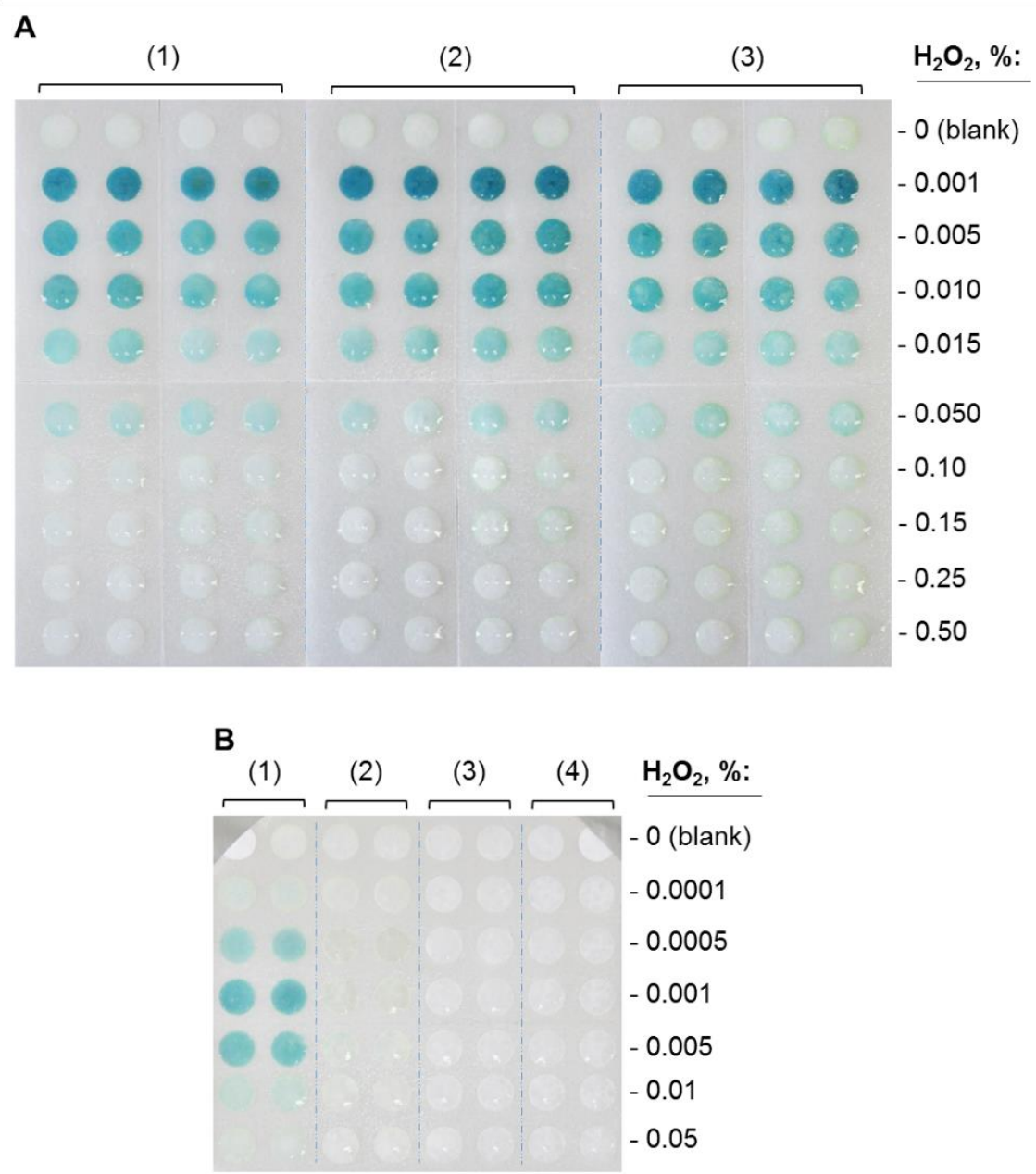

Figure 2-17 Digitally captured images of the μPADs used for simultaneous investigation of optimum TMB and H_2O_2 compositions. (A) The μPAD image showing intensities with TMB concentrations of (1) 10, (2) 20, and (3) 30 mM. (B)

The μPAD image with different TMB concentrations of (1) 10, (2) 1, (3) 0.1, and (4) 0.05 mM. [Conditions: blocking with BSA-PBS; washing with PBST, pH 7.5; 100 ng mL^{-1} HRP standard.]

2.5.4 Comparison of Results With and Without Blocking in the Assay Procedure

2.5.4.1 Microfluidic Paper-based Assay of HRP

Blocking is an essential step during protein transport in immunoassay procedures to prevent nonspecific binding of the protein during the transport, which often results to lower detection signal. Hence, in order to demonstrate the applicability of the developed method in this work to a μPAD detection, a simple HRP assay was performed on a microfluidic paper-based platform while comparing the results of an assay with a blocking procedure to that without BSA-PBS blocking. The μPADs were fabrication similarly via photolithography as described in the main article and consist of a test zone with 5 mm diameter, where TMB-H_2O_2 reaction in the presence of HRP takes place, and a sample region with 7.75 mm diameter, where the sample solution is introduced. 1.4 μL of 35.7 mM TMB equivalent to 50 nmol TMB was first added onto the test regions of the μPADs. After drying for at least 2 min, the μPADs were blocked with 35 μL of BSA-PBS for 20 min. On the other hand, 35 μL PBST was introduced to the other μPADs and incubated similarly for 20 min. After incubation, the μPADs were washed three times with PBST, pH 7.5. After air-drying for at least 5 min, 12.5 μL of 100 ng mL^{-1} HRP containing 0.001 % H_2O_2 in PBST, pH 7.5, was added onto the sample region for HRP detection. The generated cyan intensities the μPADs were compared by computing the percent difference, % difference, of the intensities with and without the blocking procedures. The % difference was determined by dividing the difference of the generated cyan intensities with blocking, X_b,

and without blocking, X_{b0}, to half the sum of both the intensities as shown in the following equation:

$$\%\ \boldsymbol{difference} = \frac{(\boldsymbol{X_b} - \boldsymbol{X_{b0}})}{(\boldsymbol{X_b} + \boldsymbol{X_{b0}})/\boldsymbol{2}} \times \boldsymbol{100}\%$$

It was then determined that the cyan intensity produced when a blocking procedure is performed was 11.5 % higher than the cyan intensity produced without blocking (Figure 2-18).

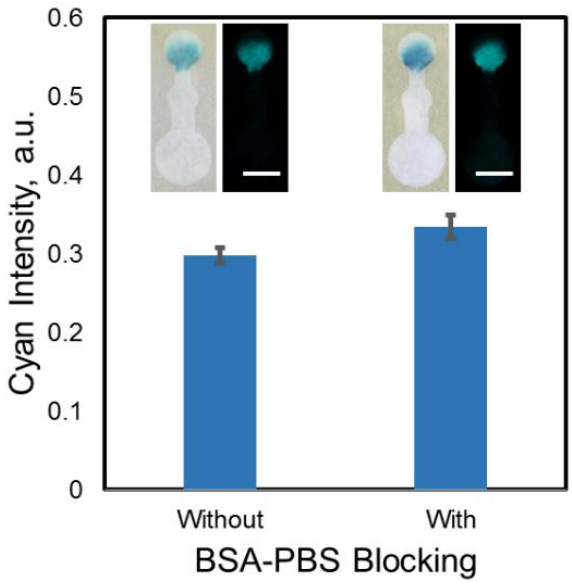

Figure 2-18 A comparison of signal intensities produced in a microfluidic paper-based assay of HRP with and without the blocking procedure at triplicate measurements. Inset: Representative images and their respective cyan profiles of the μPADs used for the HRP assay with a scale bar of 5 mm. [Conditions: 50 nmol TMB; blocking with BSA-PBS; washing with PBST, pH 7.5; 12.5 μL of 100 ng mL^{-1} HRP containing 0.001 % H_2O_2 in PBST, pH 7.5, solution.]

2.5.4.2 Microfluidic Paper-based Assay of Anti-biotin IgG-peroxidase

To evaluate further the applicability of the proposed method for μPAD detection using HRP-conjugated proteins, anti-biotin IgG-peroxidase was measured as a model compound in a similar fashion as described above for the HRP assay while comparing the generated signal intensities with and without the blocking procedures during the assay. 50 nmol TMB was first added onto the test regions of the μPADs and allowed to dry for at least 2 min. After drying, the μPADs were blocked with BSA-PBS and incubated for 20 min, while the other set were simply incubated with PBST, pH 7.5, for 20 min. After incubation, the μPADs were washed three times with PBST, pH 7.5, and allowed to dry for at least 5 min. After drying, the sample solution consisting of 0.26 μg mL^{-1} of the peroxidase-conjugated biotin antibody and 0.001 % H_2O_2 in PBST, pH 7.5, was introduced in the sample region. The generated cyan intensities were then measured and compared in Figure 2-19. At 15 min incubation time, the % difference were determined to be 17.6 %, with results obtained via μPAD assay with blocking procedure more intense than that obtained for the μPAD assay without blocking. This result then demonstrates that nonspecific binding of the proteins during protein transport is highly more likely in the absence of a blocking step during assay. With this observation, a longer μPAD compared to the 2.05-cm long μPAD used in this work would then be expected to generate signal intensity with a larger % difference due to more nonspecific binding that is expected to occur during protein transport before reaching the detection zone.

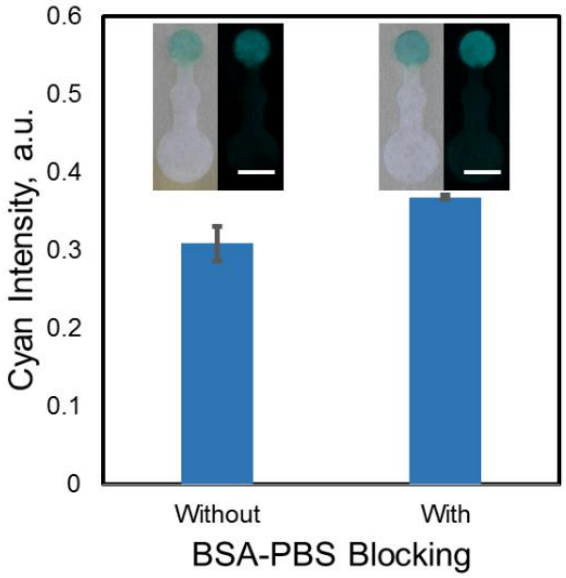

Figure 2-19 A comparison of signal intensities produced during the microfluidic paper-based assay of peroxidase-conjugated biotin antibody with and without the blocking procedure at triplicate measurements. Inset: Representative images and their respective cyan profiles of the μPADs used for the HRP assay with a scale bar of 5 mm. [Conditions: 50 nmol TMB; blocking with BSA-PBS; washing with PBST, pH 7.5; 25 μL of 0.26 μg mL^{-1} anti-biotin IgG-peroxidase containing 0.001 % H_2O_2 in PBST, pH 7.5, solution.]

References

[1] S. J. Vella, P. Beattie, R. Cademartiri, A. Laromaine, A. W. Martinez, S. T. Phillips, K. A. Mirica and G. M. Whitesides, Measuring markers of liver function using a micropatterned paper device designed for blood from a fingerstick, *Anal. Chem.*, 2012, **84**, 2883–2891.

[2] E. Fu, T. Liang, P. Spicar-Mihalic, J. Houghtaling, S. Ramachandran and P. Yager, Two-dimensional paper network format that enables simple multistep assays for use in low-resource settings in the context of malaria antigen detection, *Anal. Chem.*, 2012, **84**, 4574–4579.

[3] W.-J. Zhu, D.-Q. Feng, M. Chen, Z.-D. Chen, R. Zhu, H.-L. Fang and W. Wang, Bienzyme colorimetric detection of glucose with self-calibration based on tree-shaped paper strip, *Sensors Actuators B Chem.*, 2014, **190**, 414–418.

[4] G. Demirel and E. Babur, Vapor-phase deposition of polymers as a simple and versatile technique to generate paper-based microfluidic platforms for bioassay applications, *Analyst*, 2014, **139**, 2326–2331.

[5] S. M. Z. Hossain and J. D. Brennan, β-Galactosidase-based colorimetric paper sensor for determination of heavy metals, *Anal. Chem.*, 2011, **83**, 8772–8778.

[6] Z. Nie, C. A. Nijhuis, J. Gong, X. Chen, A. Kumachev, A. W. Martinez, M. Narovlyansky and G. M. Whitesides, Electrochemical sensing in paper-based microfluidic devices, *Lab Chip*, 2010, **10**, 477–483.

[7] Z. Gu, M. Zhao, Y. Sheng, L. A. Bentolila and Y. Tang, Detection of mercury ion by infrared fluorescence protein and its hydrogel-based paper assay, *Anal. Chem.*, 2011, **83**, 2324–2329.

[8] C. H. Lee, L. Tian and S. Singamaneni, Paper-based SERS swab for rapid trace detection on real-world surfaces, *ACS Appl. Mater. Interfaces*, 2010, **2**, 3429–3435.

[9] S. Burnham, J. Hu, H. Anany, L. Brovko, F. Deiss, R. Derda and M. W. Griffiths, Towards rapid on-site phage-mediated detection of generic *Escherichia coli* in water using luminescent and visual readout, *Anal. Bioanal. Chem.*, 2014, **406**, 5685–5693.

[10] J. C. Jokerst, J. A. Adkins, B. Bisha, M. M. Mentele, L. D. Goodridge and C. S. Henry, Development of a paper-based analytical device for colorimetric detection of select foodborne pathogens, *Anal. Chem.*, 2012, **84**, 2900–2907.

[11] J. Shi, F. Tang, H. Xing, H. Zheng, B. Lianhua and W. Wei, Electrochemical detection of Pb and Cd in paper-based microfluidic devices, *J. Braz. Chem. Soc.*, 2012, **23**, 1124–1130.

[12] W. Liu, J. Kou, H. Xing and B. Li, Paper-based chromatographic chemiluminescence chip for the detection of dichlorvos in vegetables, *Biosens. Bioelectron.*, 2014, **52**, 76–81.

[13] S. Mohammadi, M. Maeki, R. M. Mohamadi, A. Ishida, H. Tani and M. Tokeshi, An instrument-free, screen-printed paper microfluidic device that enables bio and chemical sensing, *Analyst*, 2015, **140**, 6493–6499.

[14] Y. Zhang, C. Zhou, J. Nie, S. Le, Q. Qin, F. Liu, Y. Li and J. Li, Equipment-free quantitative measurement for microfluidic paper-based analytical devices fabricated using the principles of movable-type printing, *Anal. Chem.*, 2014, **86**, 2005–2012.

[15] W. Dungchai, O. Chailapakul and C. S. Henry, A low-cost, simple, and rapid fabrication method for paper-based microfluidics using wax screen-printing, *Analyst*, 2011, **136**, 77–82.

[16] D. M. Cate, J. A. Adkins, J. Mettakoonpitak and C. S. Henry, Recent developments in paper-based microfluidic devices, *Anal. Chem.*, 2015, **87**, 19–41.

[17] M. M. Mentele, J. Cunningham, K. Koehler, J. Volckens and C. S. Henry, Microfluidic paper-based analytical device for particulate metals, *Anal. Chem.*, 2012, **84**, 4474–4480.

[18] N. M. Myers, E. N. Kernisan and M. Lieberman, Automatic paper chromatography, *Anal. Chem.*, 2015, **87**, 3764–3770.

[19] N. K. Thom, G. G. Lewis, K. Yeung and S. T. Phillips, Quantitative fluorescence assays using a self-powered paper-based microfluidic device and a camera-equipped cellular phone, *RSC Adv.*, 2014, **4**, 1334–1340.

[20] A. Zhang and Y. Zha, Fabrication of paper-based microfluidic device using printed circuit technology, *AIP Adv.*, 2012, **2**, 022171.

[21] W. Dungchai, O. Chailapakul and C. S. Henry, Use of multiple colorimetric indicators for paper-based microfluidic devices, *Anal. Chim. Acta*, 2010, **674**, 227–233.

[22] S. Ge, L. Ge, M. Yan, X. Song, J. Yu and J. Huang, A disposable paper-based electrochemical sensor with an addressable electrode array for cancer screening, *Chem. Commun. (Camb).*, 2012, **48**, 9397–9399.

[23] J. Davy, On a gaseous compound of carbonic oxide and chlorine *Philos. Trans. R. Soc. London*, 1812, **102**, 144–151.

[24] A. W. Martinez, S. T. Phillips, M. J. Butte and G. M. Whitesides, Patterned paper as a platform for inexpensive, low-volume, portable bioassays, *Angew. Chemie - Int. Ed.*, 2007, **46**, 1318–1320.

[25] W. Dungchai, O. Chailapakul and C. S. Henry, Electrochemical detection for paper-based microfluidics, *Anal. Chem.*, 2009, **81**, 5821–5826.

[26] A. W. Martinez, S. T. Phillips, B. J. Wiley, M. Gupta and G. M. Whitesides, FLASH: a rapid method for prototyping paper-based microfluidic devices, *Lab Chip*, 2008, **8**, 2146–2150.

[27] D. Tang and J. Ren, In-situ amplified electrochemical immunoassay for carcinoembryonic antigen using horseradish peroxidase-encapsulated nanogold hollow microspheres as labels, *Anal. Chem.*, 2008, **80**, 8064–8070.

[28] Y. P. Chau and K. S. Lu, Investigation of the blood-ganglion barrier properties in rat sympathetic ganglia by using lanthanum ion and horseradish peroxidase as tracers, *Cells Tissues Organs*, 1995, **153**, 135–144.

[29] D. Tang, R. Yuan and Y. Chai, Ultrasensitive electrochemical immunosensor for clinical immunoassay using thionine-doped magnetic gold nanospheres as labels and horseradish peroxidase as enhancer, *Anal. Chem.*, 2008, **80**, 1582–1588.

[30] W.-W. Zhao, Z.-Y. Ma, P.-P. Yu, X.-Y. Dong, J.-J. Xu and H.-Y. Chen, Highly sensitive photoelectrochemical immunoassay with enhanced amplification using horseradish peroxidase induced biocatalytic precipitation on a CdS quantum dots multilayer electrode, *Anal. Chem.*, 2012, **84**, 917–923.

[31] Y. Wu, P. Xue, K. M. Hui and Y. Kang, A paper-based microfluidic electrochemical immunodevice integrated with amplification-by-polymerization for the ultrasensitive multiplex detection of cancer biomarkers, *Biosens. Bioelectron.*, 2014, **52**, 180–187.

[32] M. N. Bobrow, T. D. Harris, K. J. Shaughnessy and G. J. Litt, Catalyzed reporter deposition, a novel method of signal amplification. Application to immunoassays, *J. Immunol. Methods*, 1989, **125**, 279–285.

[33] Y. Bai, C. G. Koh, M. Boreman, Y.-J. Juang, I.-C. Tang, L. J. Lee and S.-T. Yang, Surface modification for enhancing antibody binding on polymer-based microfluidic device for enzyme-linked immunosorbent assay, *Langmuir*, 2006, **22**, 9458–9467.

[34] Y. Lu, W. Shi, L. Jiang, J. Qin and B. Lin, Rapid prototyping of paper-based microfluidics with wax for low-cost, portable bioassay, *Electrophoresis*, 2009, **30**, 1497–1500.

[35] K.-K. Fung, C. P.-Y. Chan and R. Renneberg, Development of enzyme-based bar code-style lateral-flow assay for hydrogen peroxidase determination, *Anal. Chim. Acta*, 2009, **634**, 89–95.

[36] L. Zhan, S. J. Zhen, X. Y. Wan, P. F. Gao and C. Z. Huang, A sensitive surface-enhanced Raman scattering enzyme-catalyzed immunoassay of respiratory syncytial virus, *Talanta*, 2016, **148**, 308–312.

[37] L. Zhan, W. B. Wu, X. X. Yang and C. Z. Huang, Gold nanoparticle-based enhanced ELISA for respiratory syncytial virus, *New J. Chem.*, 2014, **38**, 2935–2940.

[38] S. Wang, C. Zhang, J. Wang and Y. Zhang, Development of colloidal gold-based flow-through and lateral-flow immunoassays for the rapid detection of the insecticide carbaryl, *Anal. Chim. Acta*, 2005, **546**, 161–166.

[39] E. Carrilho, A. W. Martinez and G. M. Whitesides, Understanding wax printing: A simple micropatterning process for paper-based microfluidics, *Anal. Chem.*, 2009, **81**, 7091–7095.

[40] E. M. Fenton, M. R. Mascarenas, G. P. López and S. S. Sibbett, Multiplex lateral-flow test strips fabricated by two-dimensional shaping, *ACS Appl. Mater. Interfaces*, 2009, **1**, 124–129.

[41] D. Zang, L. Ge, M. Yan, X. Song and J. Yu, Electrochemical immunoassay on a 3D microfluidic paper-based device, *Chem. Commun. (Camb).*, 2012, **48**, 4683–4685.

[42] S. Ramachandran, E. Fu, B. Lutz and P. Yager, Long-term dry storage of an enzyme-based reagent system for ELISA in point-of-care devices, *Analyst*, 2014, **139**, 1456–1462.

[43] P. D. Josephy, T. Eling and R. P. Mason, The horseradish peroxidase-catalyzed oxidation of 3,5,3',5',-tetramethylbenzidine. Free radical and charge-transfer complex intermediates, *J. Biol. Chem.*, 1982, **257**, 3669–3675.

[44] J. W. A. Findlay and R. F. Dillard, Appropriate calibration curve fitting in ligand binding assays, *AAPS J.*, 2007, **9**, E260–E267.

[45] K. Kloth, M. Rye-Johnsen, A. Didier, R. Dietrich, E. Märtlbauer, R. Niessner and M. Seidel, A regenerable immunochip for the rapid determination of 13 different antibiotics in raw milk, *Analyst*, 2009, **134**, 1433–1439.

[46] P. G. Gottschalk and J. R. Dunn, The five-parameter logistic: a characterization and comparison with the four-parameter logistic, *Anal. Biochem.*, 2005, **343**, 54–65.

[47] C. A. Holstein, M. Griffin, J. Hong and P. D. Sampson, Statistical method for determining and comparing limits of detection of bioassay, *Anal. Chem.*, 2015, **87**, 9795–9801.

CHAPTER 3 Competitive Immunoassay System for Microfluidic Paper-based Analytical Detection

3.1 Introduction

Several detection methods have been incorporated in microfluidic paper-based analytical devices (μPADs) for target detection including colorimetric [1–5], electrochemical [6–10], fluorescence [11–13], chemiluminescence [14–17], and electrochemiluminescence [18] methods. Among these methods, colorimetric method offers the simplest means to display detection results without the use of additional read-out devices since a simple production of or change in color intensity as a result of the presence or absence of a target compound is easily obtained. Such colorimetric methods include immunoassays [19–21], which involve the recognition and binding of antibodies to specific molecules in what might be a complex mixture of molecules, providing high specificity for target detection. Moreover, another key feature that immunoassays have is the means to produce measureable detection signal as a result of the antibody-antigen binding.

The conventional method for competitive immunoassay such as the enzyme-linked immunosorbent assay (ELISA) involves the use of microtiter plates and a photometer to measure the absorbance or optical density of the solution being measured. This conventional method, however, has the disadvantage of not only requiring such device readers making it impractical for onsite monitoring of target substances, but also requires larger volumes of reagents as well as the need of an expert to perform the measurement. Therefore, the application of μPADs for onsite screening and monitoring of target substances provide a low-cost, easy-to-perform and rapid analysis, requiring only small amounts of reagents, as well as sample solution, and little to no external supporting

equipment or power, and that may not require trained personnel to perform the measurement.

In the previous chapter, we have demonstrated a simple colorimetric assay system of horseradish peroxidase (HRP) on μPADs. The color production reaction was based on the oxidation of the chromogen 3,3'5,5'-tetramethylbenzidine (TMB) by hydrogen peroxide, H_2O_2, in the presence of the HRP enzyme. Similar assay system has been developed in the present work. Here, however, an antigen-antibody interaction is involved, the antigen being of a small molecular weight molecule, hence, a competitive immunoassay system using μPADs was designed as the platform. The μPADs have been fabricated first via photolithography, and then further prepared by depositing and immobilizing reagents on the μPADs. The μPADs consist of control and test regions, where the TMB chromogen were deposited, a capture region, where the capture reagent was immobilized, and sample introduction zone, where the sample solution was introduced into the device. The developed competitive immunoassay system was successfully demonstrated using biotin as a model compound and aflatoxin B_1 for practical application of the system on μPADs.

3.2 Research Methodology

3.2.1 Chemicals

All reagents were of analytical grade. 35.7 mM of 3,3',5,5'-tetramethylbenzidine chromogen reagent (Dojindo Laboratories, Kumamoto, Japan) was prepared with acetonitrile (Wako Pure Chemical Industries, Ltd., Japan). The 1x blocker bovine serum albumin in phosphate-buffered saline (BSA-PBS) (Thermo Fisher Scientific Inc) was diluted with 1x phosphate-buffered saline Tween® 20 (PBST), pH 7.5 (Thermo Fisher Scientific Inc., IL, USA), which was also used as the washing solution during immunoassay. For the biotin immunoassay, 200 μg mL^{-1} biotin stock solution (Sigma-Aldrich, Inc.) and

10 mg mL^{-1} biotin-BSA conjugate (Sigma-Aldrich, Inc.) were prepared by dissolving the solids separately in PBST. For the AFB_1 immunoassay, 1 mg Aflatoxin B_1 (AFB_1) powder (Sigma-Aldrich, Inc., MO, USA) was dissolved in 1 mL acetonitrile, and 1 mg mL^{-1} AFB_1-BSA conjugate (Sigma-Aldrich, Inc.) was prepared in PBST.

3.2.2 Fabrication of µPADs

The µPADs were fabricated by photolithography as described in our previous work[1], with slight modification of the first reported method [22]. The fabrication procedure includes the following steps: (1) soaking of Whatman filter paper grade 41 (GE Healthcare Life Sciences, UK) or Alhstrom grade 319 (Ahlstrom Corporation, Helsinki, Finland) in SU-8 2010 photoresist (Microchem, MA, USA) for about 30 s; (2) spinning for 5 s at 500 rpm then for 30 s at 2000 rpm to remove excess photoresist using a spin coater (Mikasa MS-A100, Japan); (3) prebaking for 5 min at 95^{o}C; (4) aligning under a photomask (designed using AutoCAD 2015 (Autodesk, Inc., USA), and then ordered from Unno Giken Co., Ltd. (Tokyo, Japan) for printing with a resolution of 12700 dpi) using a mask aligner (Mikasa M-1S, Japan) after cooling to room temperature for 30 s and before being exposed to UV radiation for 18 s; (5) post-baking for another 5 min at 95^{o}C; and, (6) developing (SU-8 developer, Microchem) for 6 min then washing 3 times with 2-propanol (Wako Pure Chemical Industries, Ltd.). The fabricated µPADs were dried with high pressured air and then stored in a sealed plastic bag until the time of use.

3.2.3 Preparation of µPADs for Competitive Immunoassay

Before using for immunoassay, one side of the fabricated µPADs was bonded to an acrylic double adhesive tape without removing the rayon of the other side of the tape to limit the reagents on the hydrophilic regions and avoid leakage (Figure 3-1). The capture zone was then chitosan-activated as described in a previous report before immobilizing the

capture reagents [23]. In brief, 0.25 mg mL^{-1} of chitosan (Wako Pure Chemical Industries, Ltd.) solution was prepared by dissolving the flakes in hot (80 – 90^{o}C) aqueous solution of 0.05 M HCl (Wako Pure Chemical Industries, Ltd.), and then adjusting the pH to 3.5~5.0 with sodium hydroxide solution (Wako Pure Chemical Industries, Ltd.) after cooling to room temperature. 0.6 μL of the chitosan solution was added to the capture zone and allowed to dry for at least 5 min. Then, chitosan was activated with 2.5% glutaraldehyde (Wako Pure Chemical Industries, Ltd.) in PBST and incubated for 1 hr at room temperature. After incubation, the capture zone with glutaraldehyde-activated chitosan was washed three times with PBST and then sequentially wiped by simply pressing a cellulose absorbent sheet on top of the μPADs with the washing solution and then allowed to dry for at least 5 min. For the biotin immunoassay, a total of 3.0 μL of 10 mg mL^{-1} of biotin-BSA conjugate was added 5 times at 0.6 μL volume each onto the capture zone for immobilization. For the AFB_1 immunoassay, a total of 10 μL of 1.0 mg mL^{-1} capture AFB_1-BSA was added 10 times at 1 μL volume each onto the capture zone for immobilization. After allowing to dry for at least 5 min, the capture zone was similarly washed three times with PBST and then sequentially wiped. Then, 1.4 μL of 35.7 mM TMB solution (50 nmol TMB) was added onto the test and control zones of the μPADs and were allowed to air-dry for at least 2 min each before blocking with 100 μL of BSA-PBS solution for 20 min. After blocking, the μPADs were washed three times with 75 μL each of PBST washing solution, sequentially wiped with cellulose absorbent sheet, and then allowed to air-dry at room temperature.

3.2.4 Competitive Immunoassay of Biotin on μPADs

For the biotin immunoassay, the biotin standard solutions composed of increasing concentration of the standard (0 – 10 μg mL^{-1}), 1:7,000 dilution of anti-biotin IgG-peroxidase (Sigma-Aldrich, Inc), and 0.001% hydrogen peroxide solution (Wako Pure

Chemical Industries, Ltd.). 50 µL each of the biotin standard solutions were introduced separately on the µPADs for colorimetric detection. The images of the µPADs were captured using a digital camera (EOS Kiss X6i Canon, Japan), and then analyzed using ImageJ software.

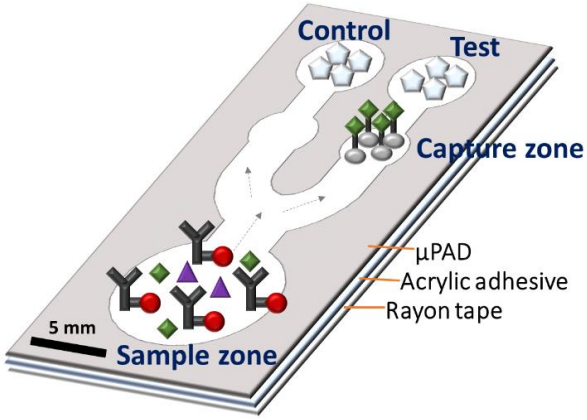

Figure 3-1 Schematic illustration of the competitive immunoassay system on µPAD. [Legend: ⬠ – TMB; 🧍 – biotin-BSA or AFB_1-BSA; ▲ – H_2O_2; ◆ – biotin or AFB_1; 🧍 – anti-biotin IgG-peroxidase or anti-AFB_1 IgG-peroxidase]

3.2.5 Competitive Immunoassay of Aflatoxin B_1 on µPADs

For the AFB_1 immunoassay, the standard solutions composed of increasing concentration of the AFB_1 standard (0 – 25 ng mL^{-1}), 1:25,000 dilution of anti-AFB_1 IgG-peroxidase, and 0.001% hydrogen peroxide solution. 50 µL each of the AFB_1 standard solutions were introduced separately on the µPADs for colorimetric detection. The images were captured using digital camera and analyzed using ImageJ software.

3.2.6 Image Analysis for Colorimetric Measurements

The blue color intensities produced during the competitive immunoassay were captured using a digital camera (EOS Kiss X6i Canon, Japan) equipped with a standard 18-

55 mm objective lens. For the biotin measurements, the photos were taken using the ISO AUTO Close-up Mode with an exposure time of 1/125 s, aperture of F/5, ISO of 100, focal distance of 44 mm, and color representation in standard RGB (sRGB). The μPADs were placed in a light box made of acrylic and painted black with two LED lights positioned parallel to each other on top of the box (Figure 3-2). The light box has a cover with a hole that exactly fits the camera lens where the camera is positioned above the μPAD during image acquisition. For the AFB_1 measurements, the photos were taken using the ISO AUTO Close-up Mode with an exposure time of 1/60 s, aperture of F/4.5, ISO of 1250, focal distance of 36 mm, and color representation in standard RGB (sRGB). The camera was hand held by the researcher and was positioned above the μPAD during image acquisition.

The RAW file formats of the images were processed with Digital Photo Professional (Canon, Japan) and stored as a 16-bit color TIF file (Figure 3-4A). The RGB file was then split to obtain the CMYK (cyan-magenta-yellow-key) profiles (Figures 3-4B to 3-4E) using ImageJ software (NIH, MD, USA). Using the cyan profile of each image, a circular region of interest (ROI) was drawn around each test and control zones of the μPAD for quantitative determinations. The histogram of each of these ROI delivered a mean cyan intensity value that was used for quantitative determinations and construction of calibration plots.

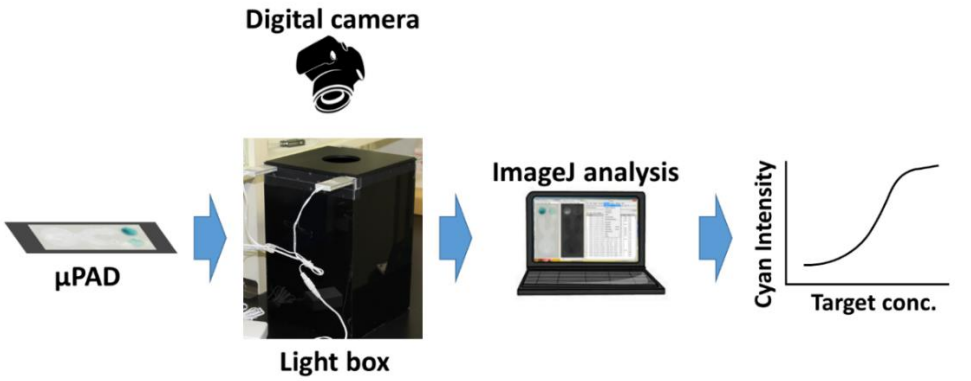

Figure 3-2 Process of data acquisition using digital camera and data quantification using ImageJ software.

3.3 Results and Discussion

3.3.1 Competitive Immunoassay on μPADs

The μPAD detection system presented in this work demonstrates a competitive type of immunoassay. The μPAD composed of a sample introduction zone located on one end of the μPAD, a control zone and a test zone that branch out from the sample introduction zone and are located on the other end of the μPAD opposite to the sample zone, and a capture zone located between the test zone and the sample introduction zone where competitive immunoassay takes place. Upon mixing of the components of the sample solutions, the peroxidase-conjugated antibody binds to the free antigen in the solution. As the sample solution is introduced in the sample zone of the μPAD, all the components flow via capillary action to the capture zone, where, unbound peroxidase-conjugated antibody are captured and allowed to bind to the immobilized BSA-conjugated antigen. The previously antigen-bound peroxidase-conjugated antibody however flows past the capture zone and reaches the TMB-immobilized test zone as illustrated in Figure 3-3. A blue-colored TMB diimine product is then formed at the test zone for quantitative measurement. Hence, competition happens at the capture zone of the μPAD immunoassay system. With

increasing antigen concentration in the sample solution, more antigen-bound peroxidase-conjugated antibody component flows past the capture and to the test zone which result to an increasing blue colored product intensity as well. At the control zone however, all antigen-bound peroxidase-conjugated antibodies flow completely to the TMB-immobilized control zone, hence producing a constant blue color intensity. Quantification is then performed by measuring the relative intensity, I_R, which is computed by simply dividing the test intensity, I_t, with the control intensity, I_c, with the following equation:

$$I_R = \frac{I_t}{I_c}.$$

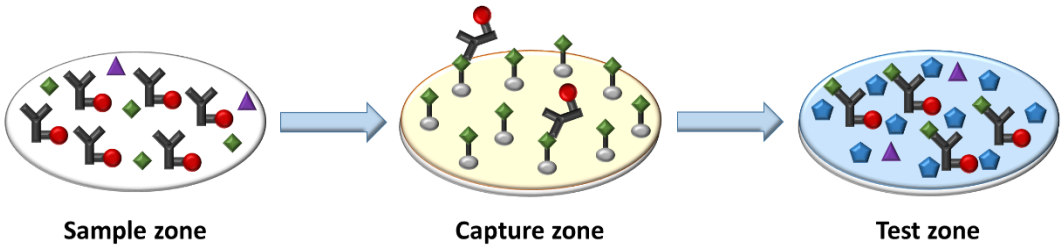

Figure 3-3 Schematic illustration of the competitive immunoassay on µPAD. [Legend: ▲ – H_2O_2; ◆ – biotin or AFB_1; – anti-biotin IgG-peroxidase or anti-AFB_1 IgG-BSA; – biotin-BSA or AFB_1-BSA; – biotin-BSA-captured anti-biotin IgG-peroxidase or AFB_1-BSA-captured anti-AFB_1 IgG-peroxidase; ⬟ – TMB diimine]

3.3.2 Data Evaluation for Colorimetric Measurements

The competitive immunoassay system demonstrated a colorimetric detection of the target on a µPAD using the common enzymatically catalyzed TMB-H_2O_2 system. Upon enzymatic oxidation of TMB by hydrogen peroxide in the presence of peroxidase, a blue TMB diimine product is produced with water as byproduct. The blue intensity of the TMB

diimine product depends on the amount of peroxidase that catalyzes the reaction of TMB and H_2O_2 as demonstrated in our previous work.[3] The intensities were captured using a digital camera, and then image-processed using Digital Photo Professional (Canon, Japan) and analyzed using ImageJ software (NIH, MD, USA).

During image processing, the RGB images were first split to CMYK (cyan-magenta-yellow-key) profiles to determine which profile would best provide quantitative results during analysis. Figure 3-4 shows the split CMYK profiles of a representative detection μPAD. Based on the different profiles, since the immunoassay produces a blue colored product after target detection with different concentration producing varying intensities, we find that the cyan profile would provide the best quantitation for target measurement. Therefore, the TMB-H_2O_2 immunoassay system was quantitatively measured via cyan profiles of each μPAD used for immunoassay.

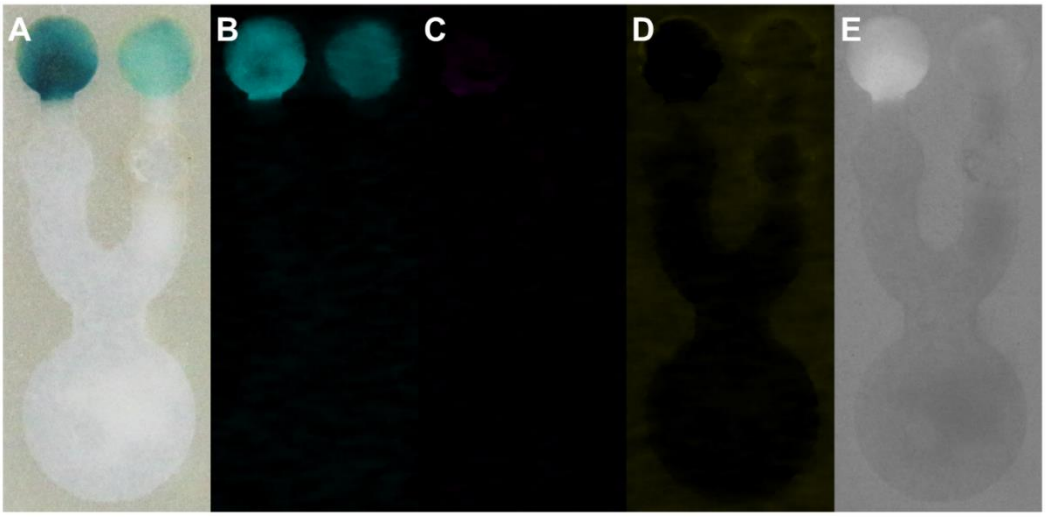

Figure 3-4 (A) The RGB image and its (B) cyan, (C) magenta, (D) yellow, and (E) key split profiles of a FP41 μPAD after image-processing with ImageJ.

3.3.3 Method Application for Specific Target Detection

3.3.3.1 Biotin Immunoassay

The proposed competitive immunoassay system on μPAD was tested using biotin as the first model compound. To determine the time it takes for the reaction to produce the maximum relative intensity, the development profile of the biotin immunoassay was plotted. As shown in Figure 3-5, although the cyan test intensity increases with time (Figure 3-5A), the relative intensity is constant at any time from 5 min up to 30 min incubation time (Figure 3-5B). However, to allow enough time for color development, the calibration plot for the biotin measurement was constructed after analyzing the color intensities of each μPAD obtained after 20 min of incubation time. Figure 3-6 shows the calibration plot for the biotin measurements after analyzing the cyan intensities produced during biotin μPAD immunoassay. The limit of detection (LOD), determined experimentally as the lowest biotin concentration that gives a cyan intensity equal to the sum of the cyan intensity of the blank and three times its standard deviation, was 0.10 μg mL^{-1} biotin.

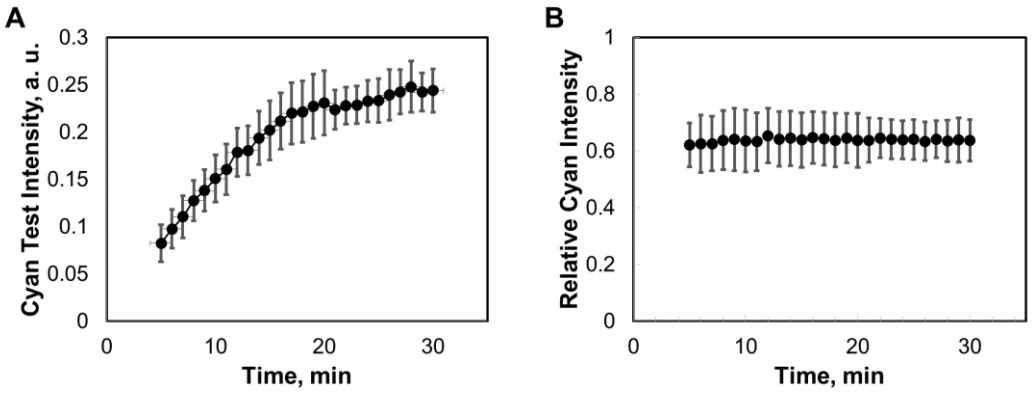

Figure 3-5 Color development profile showing (A) the cyan test intensity , and (B) the relative cyan intensity of biotin immunoassay on FP41 μPAD (n=3). [Conditions: 10 μg mL^{-1} biotin with 1:7,000 dilution of anti-biotin IgG-

peroxidase conjugate and 0.001% H_2O_2; BSA-PBS blocking; PBST washing; 0.050 μmol TMB]

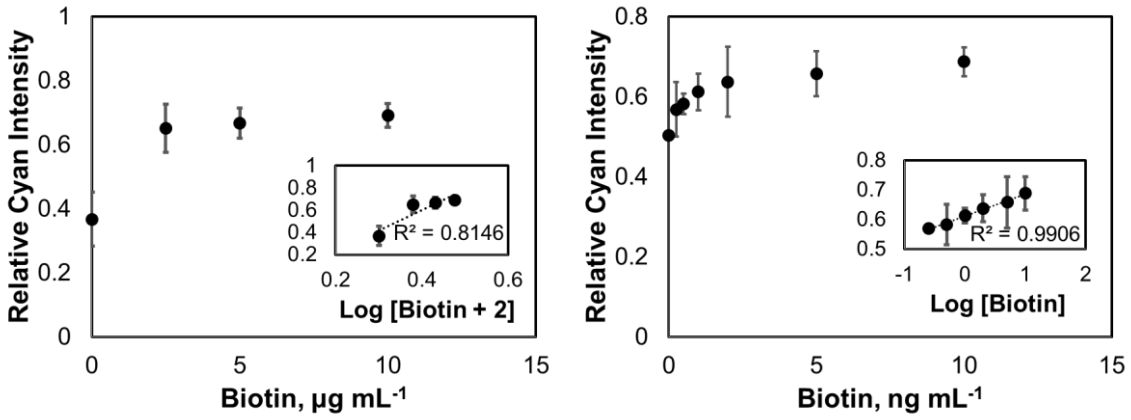

Figure 3-6 Biotin immunoassay on FP41 μPAD.

3.3.3.2 Aflatoxin B_1 Immunoassay

To demonstrate the versatility of the proposed competitive immunoassay system for detecting target compounds on μPAD for practical applications, a highly toxic foodborne substance in the form of aflatoxin B_1 (AFB_1) was detected as well along with the comparison of AFB_1 immunoassay results using two different paper substrates – Whatman filter paper grade 41 (FP41) as previously reported[1], and a commonly used absorbent pad Ahlstrom grade 319 (A319). Although the previous demonstrations of HRP-catalyzed TMB-H_2O_2 assay on different cellulose-based μPADs showed constant tint of blue color in the oxidized TMB product, TMB oxidation using A319 μPAD during AFB_1 immunoassay revealed a bluish yellow-green color of product as shown in Figure 3-7A. Since similar competitive immunoassay system of identical target compound was being evaluated using the two μPADs, the measured relative cyan intensities are similar as well (Figure 3-7B). However, with the different tint of product being measured with the A319 μPAD, the standard deviations represented by the error bars for the A319 μPAD measurements are

significantly higher than the results using FP41. Moreover, visual analysis is more reliably performed using FP41 μPADs with its more intense blue colored product after immunoassay. Hence, the quantitative measurements of AFB_1 on FP41 μPADs are plotted in Figure 3-8, showing a detection limit of 1.31 ng mL^{-1} at the highest test intensities produced between 6 to 9 min of incubation.

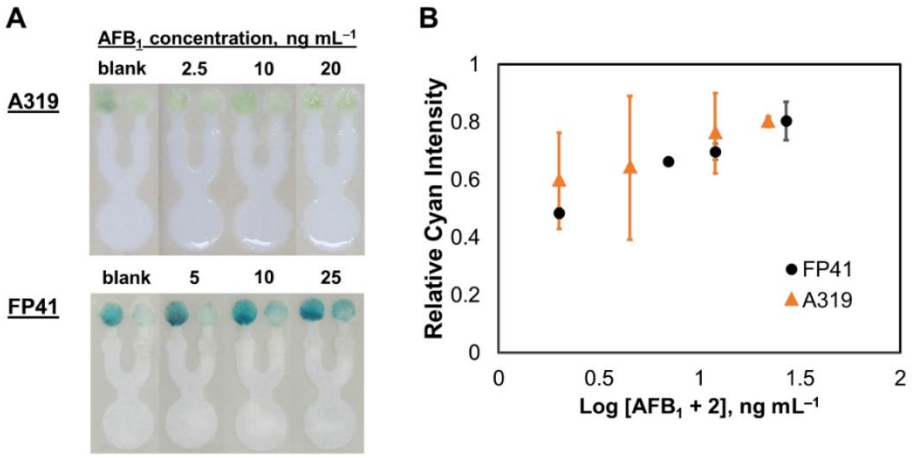

Figure 3-7 (A) Images of the A319 and FP41 μPADs, and (B) the comparative results of AFB_1 immunoassay on the μPADs.

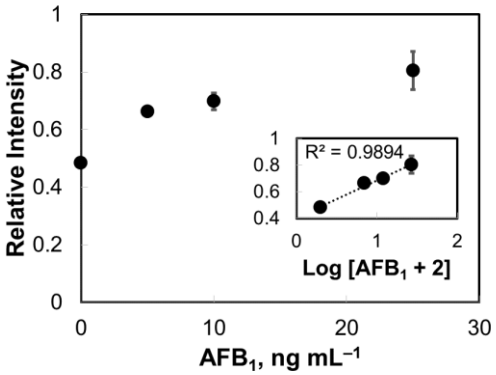

Figure 3-8 Competitive immunoassay of AFB_1 on FP41 μPAD.

3.4 Conclusion

A novel competitive immunoassay system on a microfluidic paper-based device has been demonstrated. The μPAD consisted of three main elements: (1) test and control zones; (2) a sample introduction zone; and (3) a capture zone. Competition happens in the capture zone, where antigen-free peroxidase-conjugated antibodies are captured before it reaches the test zone, inhibiting the production of blue colored TMB diimine product due to the limited peroxidase molecules reaching the test zone, which in turn implies the absence or the limited presence of antigen in the sample solution. The proposed competitive immunoassay system was demonstrated on μPADs with biotin as a model compound and with aflatoxin B_1 for analytical testing as a practical application for food monitoring, with limits of 0.10 μg mL^{-1} for biotin and 1.31 ng mL^{-1} for AFB_1. This simple competitive immunoassay system introduces the basic fundamental principle of competitive ELISA on microfluidic paper-based devices, verifying its promising applications on a broad range of analytical testing, not only in food monitoring, but also in environmental as well as clinical applications. A journal article regarding this chapter has been submitted for consideration in *Analyst* and is now currently under revision

References

[1] J. C. Jokerst, J. A. Adkins, B. Bisha, M. M. Mentele, L. D. Goodridge and C. S. Henry, Development of a paper-based analytical device for colorimetric detection of select foodborne pathogens, *Anal. Chem.*, 2012, **84**, 2900–2907.

[2] C. Sicard, C. Glen, B. Aubie, D. Wallace, S. Jahanshahi-Anbuhi, K. Pennings, G. T. Daigger, R. Pelton, J. D. Brennan and C. D. M. Filipe, Tools for water quality monitoring and mapping using paper-based sensors and cell phones, *Water Res.*, 2015, **70**, 360–369.

[3] T. M. G. Cardoso, P. T. Garcia and W. K. T. Coltro, Colorimetric determination of nitrite in clinical, food and environmental samples using microfluidic devices stamped in paper platform, *Anal. Methods*, 2015, **7**, 7311–7317.

[4] S. M. Z. Hossain and J. D. Brennan, β-Galactosidase-based colorimetric paper sensor for determination of heavy metals, *Anal. Chem.*, 2011, **83**, 8772–8778.

[5] N. M. Myers, E. N. Kernisan and M. Lieberman, Lab on Paper: Iodometric titration on a printed card, *Anal. Chem.*, 2015, **87**, 3764–3770.

[6] J. A. Adkins and C. S. Henry, Electrochemical detection in paper-based analytical devices using microwire electrodes, *Anal. Chim. Acta*, 2015, **891**, 247–254.

[7] J. Shi, F. Tang, H. Xing, H. Zheng, B. Lianhua and W. Wei, Electrochemical detection of Pb and Cd in paper-based microfluidic devices, *J. Braz. Chem. Soc.*, 2012, **23**, 1124–1130.

[8] M. Cuartero, G. A. Crespo and E. Bakker, Paper-based thin-layer coulometric sensor for halide determination, *Anal. Chem.*, 2015, **87**, 1981–1990.

[9] S. Ge, W. Liu, L. Ge, M. Yan, J. Yan, J. Huang and J. Yu, In-situ assembly of porous Au-paper electrode and functionalization of magnetic silica nanoparticles with HRP

via click chemistry for microcystin-LR immunoassay, *Biosens. Bioelectron.*, 2013, **49**, 111–117.

[10] Z. Nie, F. Deiss, X. Liu, O. Akbulut and G. M. Whitesides, Integration of paper-based microfluidic devices with commercial electrochemical readers, *Lab Chip*, 2010, **10**, 3163–3169.

[11] P. Zuo, X. Li, D. C. Dominguez and B.-C. Ye, A PDMS/paper/glass hybrid microfluidic biochip integrated with aptamer-functionalized graphene oxide nano-biosensors for one-step multiplexed pathogen detection, *Lab Chip*, 2013, **13**, 3921–3928.

[12] Y. Su, S. Ma, K. Jiang and X. Han, CdTe-paper based visual sensor for detecting methy viologen, *Chinese J. Chem.*, 2015, **33**, 446–450.

[13] Y. Zhang, P. Zuo and B.-C. Ye, A low-cost and simple paper-based microfluidic device for simultaneous multiplex determination of different types of chemical contaminants in food, *Biosens. Bioelectron.*, 2015, **68**, 14–19.

[14] S. Wang, L. Ge, L. Li, M. Yan, S. Ge and J. Yu, Molecularly imprinted polymer grafted paper-based multi-disk micro-disk plate for chemiluminescence detection of pesticide, *Biosens. Bioelectron.*, 2013, **50**, 262–268.

[15] S.-Q. Jin, S.-M. Guo, P. Zuo and B.-C. Ye, A cost-effective Z-folding controlled liquid handling microfluidic paper analysis device for pathogen detection via ATP quantification, *Biosens. Bioelectron.*, 2014, **63**, 379–383.

[16] W. Liu, J. Kou, H. Xing and B. Li, Paper-based chromatographic chemiluminescence chip for the detection of dichlorvos in vegetables, *Biosens. Bioelectron.*, 2014, **52**, 76–81.

[17] W. Liu, Y. Guo, J. Luo, J. Kou, H. Zheng, B. Li and Z. Zhang, A molecularly imprinted polymer based a lab-on-paper chemiluminescence device for the detection of dichlorvos, *Spectrochim. Acta. A. Mol. Biomol. Spectrosc.*, 2015, **141**, 51–57.

[18] V. Mani, K. Kadimisetty, S. Malla, A. A. Joshi and J. F. Rusling, Paper-based electrochemiluminescent screening for genotoxic activity in the environment, *Environ. Sci. Technol.*, 2013, **47**, 1937–1944.

[19] Y. Kasahara and Y. Ashihara, Simple devices and their possible application in clinical laboratory downsizing, *Clin. Chim. Acta*, 1997, **267**, 87–102.

[20] G. A. Posthuma-Trumpie, J. Korf and A. van Amerongen, Lateral flow (immuno)assay: its strengths, weaknesses, opportunities and threats. A literature survey, *Anal. Bioanal. Chem.*, 2009, **393**, 569–582.

[21] S. Rattle, O. Hofmann, C. P. Price and L. J. Kricka, *The Immunoassay Handbook*, Elsevier, 2013.

[22] A. W. Martinez, S. T. Phillips, M. J. Butte and G. M. Whitesides, Patterned paper as a platform for inexpensive, low-volume, portable bioassays, *Angew. Chem. Int. Ed. Engl.*, 2007, **46**, 1318–20.

[23] D. Zang, L. Ge, M. Yan, X. Song and J. Yu, Electrochemical immunoassay on a 3D microfluidic paper-based device, *Chem. Commun. (Camb).*, 2012, **48**, 4683–5.

Chapter 4 Microfluidic Paper-based Analytical Devices for Aflatoxin B_1 Immunoassay in Food

4.1 Introduction

Aflatoxin B1 (AFB1), is a highly toxic and carcinogenic substance that is produced by *Aspergillus* fungi and is found in food and agricultural products such as corn and peanuts, among others. Being the most predominant and most toxic kind of mycotoxin, AFB_1 has been classified by the International Agency for Research in Cancer (IARC, 2002) as a group 1 carcinogen in humans as well as in animals [1]. Since its discovery in 1960s, many conventional methods based on chromatographic principles have been developed for the quantification of AFB_1 [2–8]. However, these methods are costly, time-consuming, laborious, unsuitable for on-site detection, and require trained personnel in performing the measurement [9]. Microfluidic paper-based analytical devices (μPADs), on the other hand, are constantly being developed in various fields of analytical research mainly due to the inexpensive materials and cost-effective manufacturing processes required [10-15]. Additional advantages of such devices include simplicity, portability, and rapid with highly-multiplexed analysis when fully developed, therefore making it an inexpensive alternative method to more advances methodologies and equipment already being used to date. Moreover, μPADs have the characteristic advantage of being highly suitable for onsite detection without requiring trained personnel when performing the analysis, hence, making it an attractive method for use in less industrialized countries.

In the present work, μPADs, which were first fabricated through photolithography – a fabrication technique that offers high resolution with regards to the construction of microfluidic channels with sharp barriers [10] – have been proposed for the determination of AFB_1 via colorimetric immunoassay technique. The μPADs consisted of a sample

introduction zone, a capture zone immobilized with a capture reagent, and a reaction zone deposited with 3,3',5,5'-tetramethylbenzidine (TMB) chromogen substrate. Since AFB_1 has a small molecular weight compared to proteins and other macromolecules, two competitive immunoassay (CI) systems have been developed using μPAD platform for AFB_1 detection. The first CI system (CI-S1) was designed to allow competition of the target AFB_1 with the immobilized capture AFB_1-BSA at the capture zone, allowing only the target AFB_1-bound anti-AFB_1 IgG-peroxidase to be transported past the capture zone via capillary action and oxidize the deposited TMB into a blue colored TMB diimine product at the reaction zone by H_2O_2 in the presence of the peroxidase-conjugate. The second CI system (CI-S2), on the other hand, was designed to allow competition prior to sample introduction. As the sample solution was introduced into the μPAD, the sample components travel through the capture zone via capillary action, wherein, an anti-BSA IgG capture reagent was immobilized. At the capture zone, the AFB_1-BSA-bound anti-AFB_1 IgG-peroxidase is captured, allowing only the target AFB_1-bound anti-AFB_1 IgG-peroxidase to be transported past the capture zone and similarly oxidize the deposited TMB at the reaction zone by H_2O_2 in the presence of the peroxidase-conjugate. For both CI systems, signal intensities were expected to increase with increasing target AFB_1 concentration. Then, AFB_1 was measured using the proposed CI systems and the results obtained are discussed for each system.

4.2 Research Methodology

4.2.1 Chemicals

All reagents were of analytical grade. 35.7 mM of 3,3',5,5'-tetramethylbenzidine chromogen reagent (Dojindo Laboratories, Kumamoto, Japan) was prepared with acetonitrile (Wako Pure Chemical Industries, Ltd., Japan). The blocking solution composed of 1x blocker bovine serum albumin in phosphate-buffered saline (BSA-PBS) (Thermo

Fisher Scientific Inc) was diluted with 1x phosphate-buffered saline Tween® 20 (PBST), pH 7.5 (Thermo Fisher Scientific Inc., IL, USA), which was also used as the washing solution during immunoassay. 1.0 mg mL^{-1} Aflatoxin B_1 (AFB_1) (Sigma-Aldrich, Inc., MO, USA) stock solution prepared by dissolving 1.0 mg of the powder in 1.0 mL acetonitrile, from which different concentration of standard solutions (0 – 25 ng mL^{-1}) were prepared. 1.0 mg mL^{-1} AFB_1-BSA conjugate (Sigma-Aldrich, Inc.) and 2.2 mg mL^{-1} anti-BSA IgG (Sigma-Aldrich, Inc.) solutions were prepared separately with PBST, pH 7.5.

4.2.2 Preparation of µPADs

The µPADs were fabricated by photolithography as described in Chapter 2, with slight modification of the first reported method.[1] Before using for immunoassay, one side of the fabricated µPADs was bonded to an acrylic double adhesive tape without removing the rayon of the other side of the tape to limit the reagents on the hydrophilic regions and avoid leakage (Figure 4-1).

4.2.2.1 µPADs for AFB_1 Measurements via Competitive Immunoassay System 1 (CI-S1)

The capture zone was first chitosan-activated as described in a previous report before immobilizing the capture reagents.[2] 0.6 µL of the chitosan solution was added to the capture zone and allowed to dry for at least 5 min. Then, chitosan was activated with 2.5% glutaraldehyde (Wako Pure Chemical Industries, Ltd.) in PBST and incubated for 1 hr at room temperature. After incubation, the capture zone with glutaraldehyde-activated chitosan was washed three times with PBST and then sequentially wiped by simply pressing a cellulose absorbent sheet on top of the µPADs with the washing solution and then allowed to dry for at least 5 min. 1.0 µL of 1.0 mg mL^{-1} capture AFB_1-BSA was added onto the capture zone for immobilization. After incubating for 20 min, the capture zone

was similarly washed three times with PBST and then sequentially wiped. Then, 1.4 μL of 35.7 mM TMB solution (0.050 μmol TMB) was added onto the test and control zones of the μPADs and were allowed to air-dry for at least 2 min each before blocking with 35 μL of BSA-PBS solution for at least 5 min. After blocking, the μPADs were washed three times with 35 μL each of PBST washing solution, sequentially wiped with cellulose absorbent sheet, and then allowed to air-dry at room temperature. For the AFB_1 immunoassay via competitive immunoassay system 1 (CI-S1), the standard solutions composed of increasing concentration of the AFB_1 standard (0 – 20 ng mL^{-1}), 1:25,000 dilution of anti-AFB_1 IgG-peroxidase, and 0.001% hydrogen peroxide solution. 12.5 μL each of the AFB_1 standard solutions were introduced separately on the μPADs for colorimetric detection. The images were captured using digital camera (EOS Kiss X6i Canon, Japan), processed using Digital Photo Professional (Canon, Japan), and analyzed using ImageJ software (NIH, MD, USA) as described in Chapter 3 of this manuscript.

4.2.2.2 μPADs for AFB_1 Measurements via Competitive Immunoassay System 2 (CI-S2)

Similarly, the capture zone was first chitosan-activated before immobilizing the capture reagents. After chitosan activation, 1.0 μL of 2.2 mg mL^{-1} capture anti-BSA IgG solution was added onto the capture zone for immobilization. After incubating for 20 min, the capture zone was similarly washed three times with PBST and then sequentially wiped. Then, 1.4 μL of 35.7 mM TMB solution (0.050 μmol TMB) was added onto the test and control zones of the μPADs and were allowed to air-dry for at least 2 min each before blocking with 35 μL of BSA-PBS solution for at least 5 min. After blocking, the μPADs were washed three times with 35 μL each of PBST washing solution, sequentially wiped with cellulose absorbent sheet, and then allowed to air-dry at room temperature. For the

AFB_1 immunoassay via competitive immunoassay system 2 (CI-S2), the standard solutions composed of increasing concentration of the AFB_1 standard (0 – 50 ng mL^{-1}), 0.32 μg mL^{-1} AFB_1-BSA conjugate, 1:25,000 dilution of anti-AFB_1 IgG-peroxidase, and 0.001% hydrogen peroxide solution. 12.5 μL each of the AFB_1 standard solutions were introduced separately on the μPADs for colorimetric detection. Then, the images were captured using digital camera, processed using Digital Photo Professional, and analyzed using ImageJ software.

4.2.3 AFB_1 Detection using ELISA kit

The conventional method of detection for AFB_1 via ELISA was performed using a commercial Aflatoxin B_1 ELISA kit (5121AFB, EuroProxima, Netherlands). The kit composed of a ready-to-use microtiter plate coated with antibodies directed against mouse-IgG.

4.3 Results and Discussion

4.3.1 Competitive Immunoassay Systems on μPADs

Two competitive immunoassay (CI) systems for the detection of AFB_1 on μPADs have been proposed in this work. Though both consist of 3 similar elements – a sample introduction zone located at one end of the μPAD, a reaction zone located at the other end of the μPAD opposite to the sample introduction zone, and a capture zone located between the reaction zone and the sample introduction zone, – the chemical components of CI systems differ. For CI-S1, the capture zone was composed of AFB_1-BSA, while that of the CI-S2 composed of anti-BSA IgG as illustrated in Figure 4-1. Moreover, for CI-S1, the sample solution was composed of the AFB_1 antigen, anti-AFB_1 IgG-peroxidase conjugate, and hydrogen peroxide solution. On the other hand, the sample solution for CI-S2

composed of the AFB_1 antigen, AFB_1-BSA conjugate, anti-AFB_1 IgG-peroxidase conjugate, and hydrogen peroxide solution. Hence, competition occurs at the capture zone for CI-S1, while competition occurs at the sample zone or even before sample introduction for CI-S2.

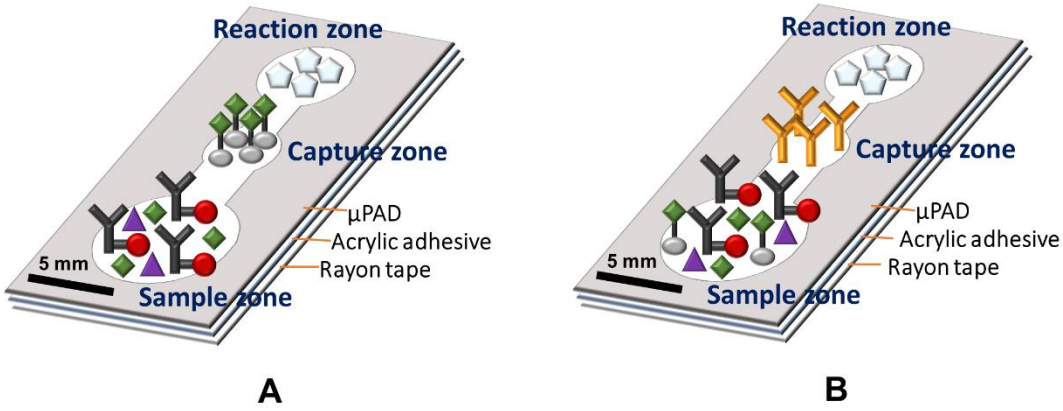

Figure 4-1 Schematic illustration of the competitive immunoassay systems (A) CI-S1 and (B) CI-S2 on µPADs. [Legend: ◆ – AFB_1; ▲ – H_2O_2; – anti-AFB_1 IgG-peroxidase; – AFB_1-BSA; – anti-BSA IgG; – TMB]

4.3.1.1 AFB_1 Competitive Immunoassay System 1 (CI-S1)

In CI-S1, the anti-AFB_1 IgG-peroxidase conjugate binds to the free AFB_1 upon mixing of the components in the sample solution. As the sample solution is introduced in the sample zone of the µPAD, all the components flow via capillary action to the capture zone, wherein, unbound anti-AFB_1 IgG-peroxidase conjugates are captured and allowed to bind to the immobilized AFB_1-BSA. The previously bound AFB_1–anti-AFB_1 IgG-peroxidase, however, flows past the capture zone and reaches the TMB-immobilized test zone as illustrated in Figure 4-2. A blue-colored TMB diimine product is then formed at the test zone for quantitative measurement. Hence, competition happens at the capture zone of the µPAD immunoassay system. With increasing AFB_1 concentration in the sample solution,

more AFB_1–anti-AFB_1 IgG-peroxidase form and flow past the capture zone all the way to the test zone which result to an increasing blue colored product intensity as well. Quantification is then performed and the AFB_1 measurements via CI-S1 are plotted in Figure 4-3A and the image of the μPAD is shown in Figure 4-3B.

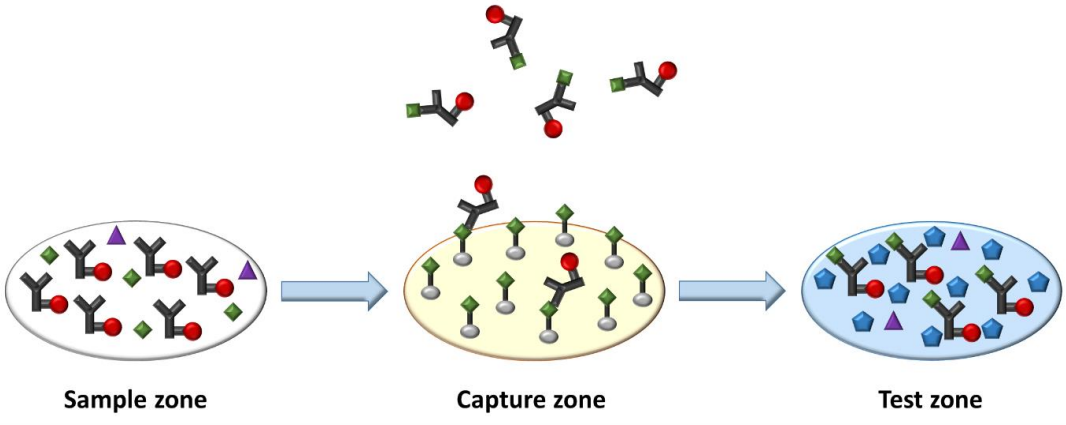

Figure 4-2 Schematic illustration of the competitive immunoassay on μPAD. [Legend: ▲ – H_2O_2; ◆ – AFB_1; – anti-AFB_1 IgG-BSA; – AFB_1-BSA; – AFB_1-BSA-captured anti-AFB_1 IgG-peroxidase; – AFB_1-bonded anti-AFB_1 IgG-peroxidase; ⬟ – TMB diimine]

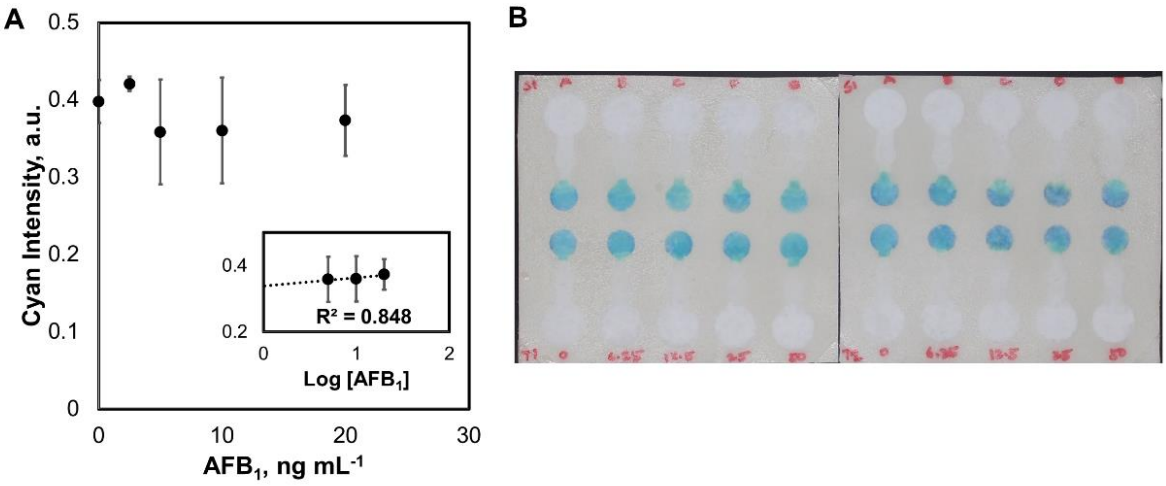

Figure 4-3 Competitive immunoassay of AFB_1 on μPAD via CI-S1 at pH 7.5.

4.3.1.2 AFB_1 Competitive Immunoassay System 2 (CI-S2)

As described earlier for CI-S2, competition occurs prior to sample introduction. The anti-AFB_1 IgG-peroxidase conjugates bind to either the AFB_1 target or the AFB_1-BSA conjugate present in the solution. The components in the sample solution then flow through the capture zone via capillary action after sample introduction. At the capture zone, the AFB_1-BSA-bound anti-AFB_1 IgG-peroxidase is captured by another antibody that has been previously immobilized and is specific to BSA. Hence, only the target AFB_1-bound anti-AFB_1 IgG-peroxidase flows past the capture zone and reaches the reaction zone as illustrated in Figure 4-4. At the reaction zone, colorimetric reaction occurs producing blue colored TMB diimine product after TMB oxidation by H_2O_2 in the presence of the peroxidase conjugate. The produced blue color intensity depends on the amount of peroxidase-conjugated AFB_1 antibody present at the reaction zone, which indirectly indicates the amount of AFB_1 target present in the sample. Similarly then, quantification is performed and the AFB_1 measurements via CI-S2 are plotted in Figure 4-5A and the image of the μPAD is shown in Figure 4-5B.

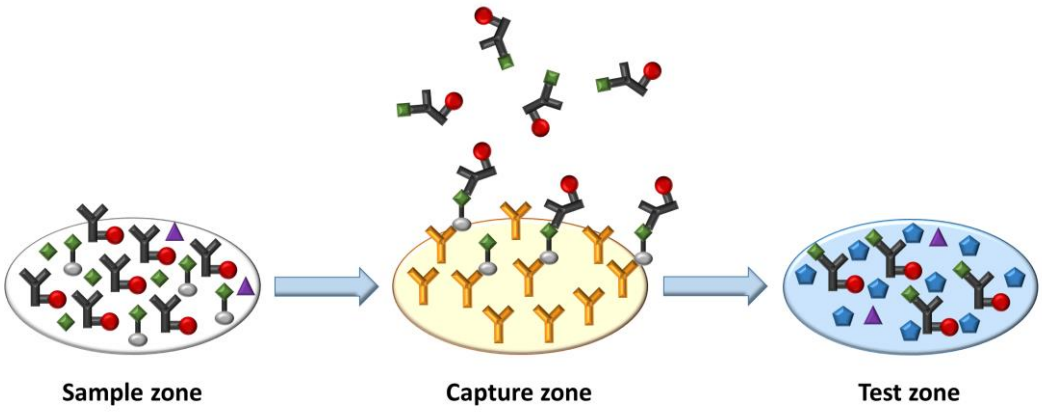

Figure 4-4 Schematic illustration of the competitive immunoassay on μPAD. [Legend: ▲ – H_2O_2; ◆ – AFB_1; – anti-AFB_1 IgG-BSA; – AFB_1-BSA; – anti-

BSA IgG; – anti-BSA IgG-capture AFB_1-BSA; – AFB_1-BSA-bonded anti-AFB_1 IgG-peroxidase captured by anti-BSA IgG; – AFB_1-bonded anti-AFB_1 IgG-peroxidase; – TMB diimine]

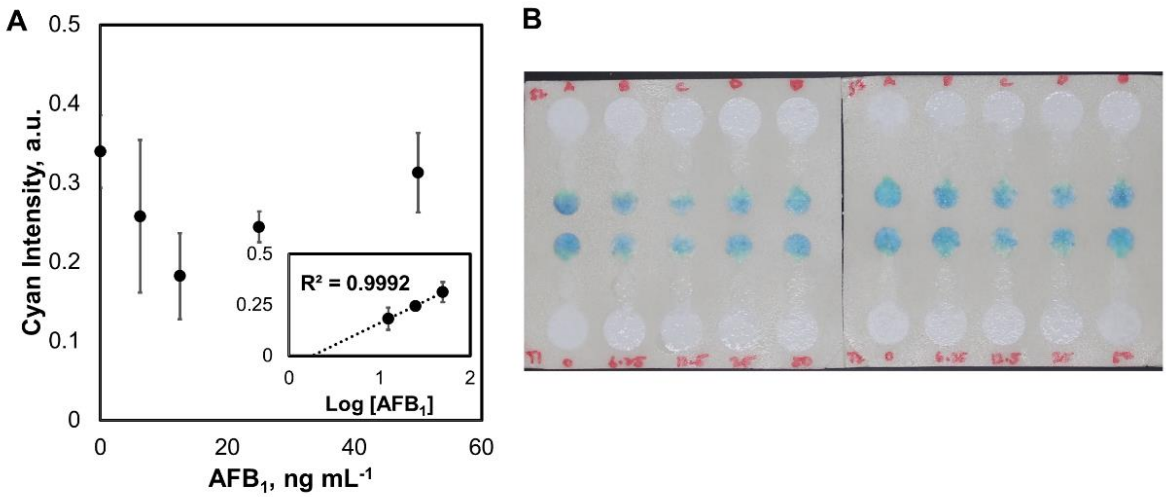

Figure 4-5 Competitive immunoassay of AFB_1 on μPAD via CI-S2 at pH 7.5.

4.3.2 Comparison of the μPAD CI Methods with the Conventional Method for AFB_1 Detection

The conventional method for AFB_1 detection via enzyme linked immunosorbent assay (ELISA) on microtiter plate was performed for method comparison. The assay protocol for the AFB_1 ELISA on microtiter plate is illustrated in Figure 4-6. In step 1 of the assay, the target AFB_1 was added in the cell, which was pre-coated with antibodies directed to mouse IgG, followed by the peroxidase-labeled AFB_1. Then the anti-AFB_1 IgG was added and competition took place. The mixture was incubated for 1 hour to allow competitive binding of the target AFB_1-bound or peroxidase conjugated AFB_1-bound anti-AFB_1 IgG to the anti-mouse IgG coating on the cell. Finally, after washing off the free antigen and peroxidase-conjugated antigen, the TMB chromogen solution was added allow TMB oxidation by

hydrogen peroxide in the presence of peroxidase enzyme. The absorbance values were then measured at 450 nm wavelength and the calibration curve obtained is shown in Figure 4-7. Performing a 4-parameter logistic regression delivered a limit of detection of 0.030 ng mL^{-1} for the AFB_1 ELISA kit.

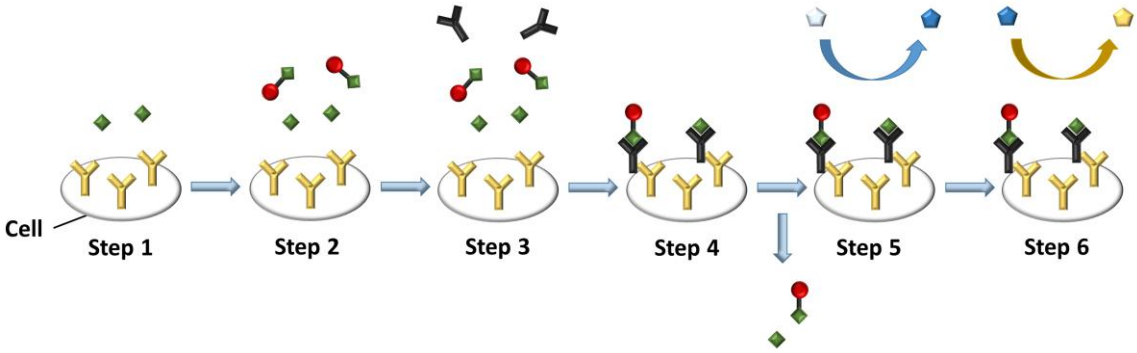

Figure 4-6 Schematic illustration of the competitive immunoassay procedure using the Aflatoxin ELISA kit. [Legend: ◆ – AFB_1; Y – anti-mouse IgG; – AFB_1-peroxidase; Y – anti-AFB_1 IgG; ⬠ – TMB; ⬟ – oxidized TMB (TMB diimine)]

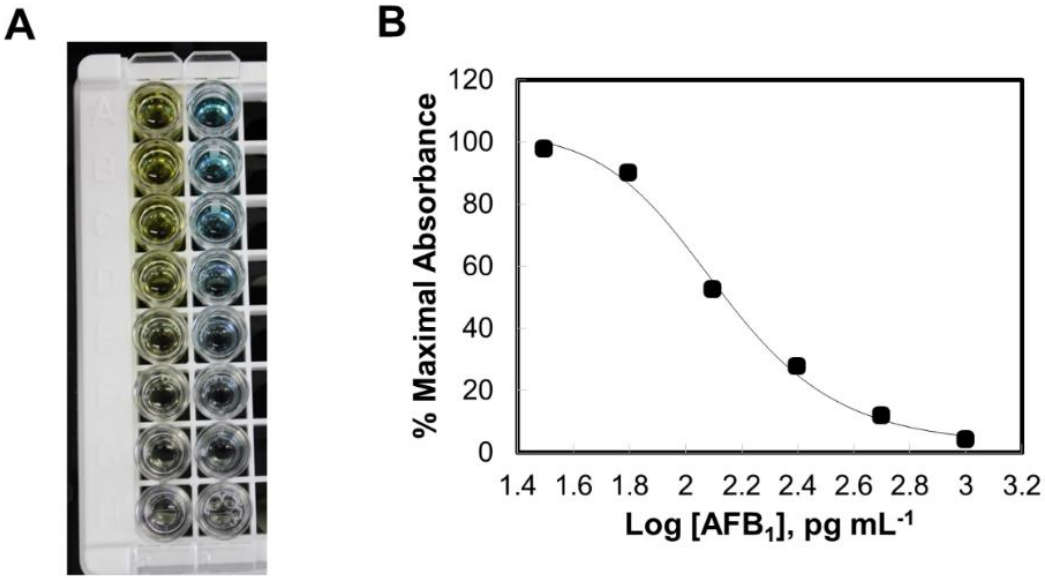

Figure 4-7 (A) Image of the portion of the microtiter plate during (B) AFB_1 ELISA detection.

4.3.3 pH Evaluation on µPAD CI systems

Due to the fact that the working pH used in the AFB_1 ELISA kit was pH 6.5, the effect of this pH was also evaluated in this work. Figure 4-8 shows the cyan intensities obtained via spot test of a simple TMB-H_2O_2 reaction catalyzed by HRP. As observed in the figure, TMB oxidation produces a 29.1% higher intensity with pH 6.5 than with pH 7.5 at 14 min of incubation, after which, the cyan intensities decreased with pH 6.5. The percent difference was calculated by dividing the difference of the intensities at pH 6.5 and pH 7.5 ($X_{pH6.5}$ and $X_{pH7.5}$, respectively) from the half the sum of both the intensities, as shown in the equation below:

$$\%\ difference = \frac{(X_{pH6.5} - X_{pH7.5})}{(X_{pH6.5} + X_{pH7.5})/2} \times 100\%$$

Hence, AFB_1 was further measured via CI-S1 at pH 6.5 with results shown in Figure 4-9.

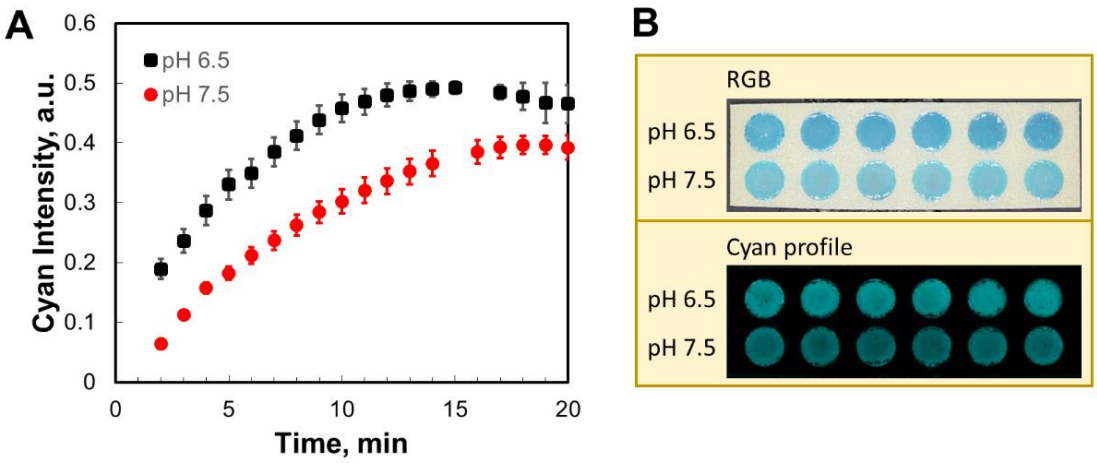

Figure 4-8 (A) Color development profile of HRP during assay at pH 6.5 and pH 7.5. (B) RGB image and the corresponding cyan profile of the paper-device. [Conditions: 50 nmol TMB; blocking with BSA-PBS; washing with PBST, pH 7.5; 5 µL of 100 ng mL^{-1} HRP containing 0.001 % H_2O_2 in PBST, pH 6.5 or pH 7.5, solution.]

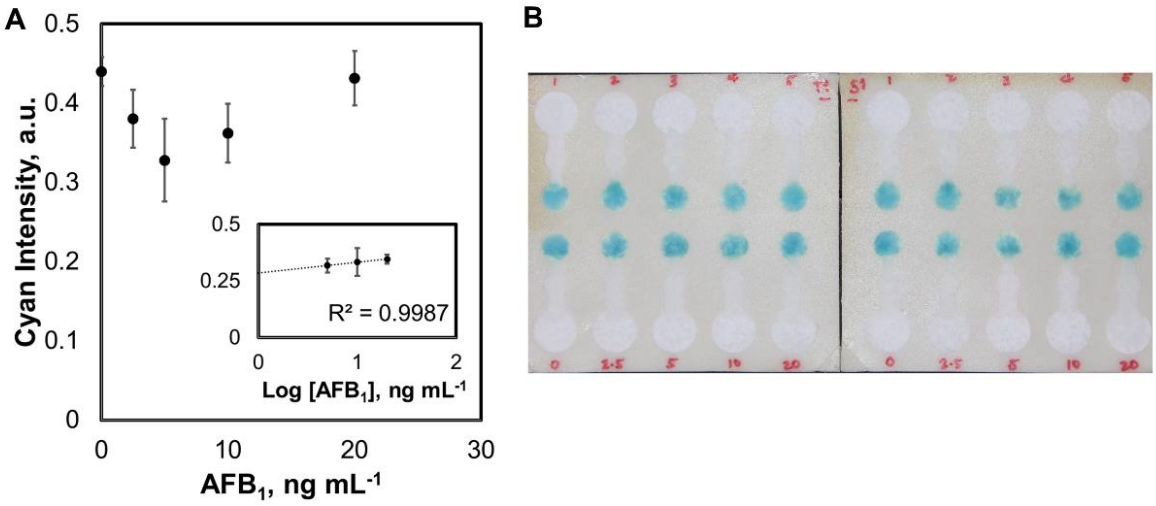

Figure 4-9 Competitive immunoassay of AFB_1 on μPAD via CI-S1 at pH 6.5.

4.4 Conclusion

Two different competitive immunoassay systems for microfluidic paper-based detection have been proposed in this study. The first system (CI-S1) was a μPAD detection of aflatoxin B_1 demonstrating a competitive immunoassay with target competition occurring at the capture zone, while the second system (CI-S2) demonstrated target competition for the immunoassay prior to μPAD sample introduction. Although current results were not quite excellent, we have realized that the problem lies at the protein immobilization step at the capture zone, and hence we intend to simply correct this part of the experiment in order to obtain better results for later journal submission and publication. We have further realized that a working pH of 6.5 produces higher cyan intensities, which might possibly lead to a lower detection limit, and therefore, the next experiments shall be done at this working pH.

In the conventional competitive ELISA, the substrate used is the microtiter plate that is usually made of polymers such as polystyrene, which is more costly than the use of paper as substrate in μPADs. Moreover, a secondary antibody is necessary in the conventional

competitive ELISA to allow the capture of the competitively bound target antigen and peroxidase-conjugated antigen for detection, as opposed to the developed μPAD CI-S1 system, which only needed one type of antibody specific to the target substance. Hence, the developed μPAD immunoassay systems provide promising applications for analytical as well as clinical testing, more specifically for on-site target monitoring.

References

[24] IARC. *IARC Monographs on the Evaluation of Carcinogenic Risks to Humans*; IARC Press: Lyon, France, 2002; Volume 82.

[25] I. Balzer, C. Bogdanić and S. Pepeljnjak, Rapid thin layer chromatographic method for determining aflatoxin B1, ochratoxin A, and zearalenone in corn, *J. Assoc. Off. Anal. Chem.*, 1978, **61**, 584–5.

[26] D. L. Park, S. Nesheim, M. W. Trucksess, M. E. Stack and R. F. Newell, Liquid chromatographic method for determination of aflatoxins B1, B2, and G2 in corn and peanut products: collaborative study, *J. Assoc. Off. Anal. Chem.*, 1990, **73**, 260–266.

[27] M. Nakajima, H. Tsubouchi, M. Miyabe and Y. Ueno, Survey of aflatoxin B1 and ochratoxin A in commercial green coffee beans by high-performance liquid chromatography linked with immunoaffinity chromatography, *Food Agric. Immunol.*, 1997, **9**, 77–83.

[28] M. Ventura, A. Gómez, I. Anaya, J. Díaz, F. Broto, M. Agut and L. Comellas, Determination of aflatoxins B1, G1, B2 and G2 in medicinal herbs by liquid chromatography-tandem mass spectrometry, *J. Chromatogr. A*, 2004, **1048**, 25–29.

[29] C. Baltacı, H. İlyasoğlu and F. Yüksel, Single-laboratory validation for the determination of aflatoxin B_1, B_2, G_1, and G_2, in foods based on immunoaffinity column and liquid chromatography with postcolumn derivatization and fluorescence detection, *Food Anal. Methods*, 2012, **6**, 36–44.

[30] L. Wang, Z. Wang, W. Gao, J. Chen, M. Yang, Y. Kuang, L. Huang and S. Chen, Simultaneous determination of aflatoxin B(1) and orchratoxin A in licorice roots and fritillary bulbs by solid-phase extraction coupled with high-performance liquid chromatography-tandem mass spectrometry, *Food Chem.*, 2013, **138**, 1048–1054.

[31] Y. Li, S. Wen, Z. Chen, Z. Xiao and M. Ma, Ultra-high performance liquid chromatography tandem mass spectrometry for simultaneous analysis of aflatoxin B1, G1, B2, G2, zearalenone and its metabolites in eggs using a QuEChERS-based extraction procedure, *Anal. Methods*, 2015, **7**, 4145–4151.

[32] Shim, W.-B.; Yang, Z.-Y.; Kim, J.-S.; Kang, S.-J.; Woo, G.-J.; Chung, Y.-C.; Eremin, S. A.; Chung, D.-H. Development of immunochromatography strip-test using nanocolloidal gold-antibody probe for the rapid detection of aflatoxin B1 in grain and feed samples, *J. Microbiol. Biotechnol.* 2007, **17**, 1629-1637.

[33] A. W. Martinez, S. T. Phillips, M. J. Butte and G. M. Whitesides, Patterned paper as a platform for inexpensive, low-volume, portable bioassays, *Angew. Chem. Int. Ed. Engl.*, 2007, **46**, 1318–1320.

[34] D. Zang, L. Ge, M. Yan, X. Song and J. Yu, Electrochemical immunoassay on a 3D microfluidic paper-based device, *Chem. Commun. (Camb).*, 2012, **48**, 4683–5.

CHAPTER 5 Conclusion and Future Prospects

5.1 Conclusive Remarks in the Present Research

In the present research, microfluidic paper-based analytical immunoassay systems for the rapid onsite measurement of aflatoxin B_1 in food have been developed. First, the incorporation of a colorimetric detection via enzyme-catalyzed TMB-H_2O_2 reaction on μPADs for rapid measurements was investigated and described in chapter 2. The properties of different paper substrates were first investigated to determine which type of paper would be the most suitable for the fabrication of the μPADs. Simultaneous detection of horseradish peroxidase (HRP) utilizing a 5-μL sample analytical volume was demonstrated using a single μPAD. Hydrophilic test regions were separated by hydrophobic barriers, which were fabricated through photolithography. These test regions were immobilized with 10 mM of 3,3',5,5'-tetramethylbenzidine for HRP assay. The detection range obtained with the proposed system covered HRP concentrations from 0.37 to 124 fmol (or 3 to 1000 ng mL^{-1}). The detection limit (blank + 3σ) for HRP was calculated to be 0.69 fmol (or 5.58 ng mL^{-1}) through a 4-parameter logistic nonlinear regression using results obtained within a 15 min assay time. The findings obtained using the developed system suggest that μPAD assay systems for simple but highly sensitive measurements can be designed to give on-site determinations of target compounds using peroxidase-conjugated molecules.

In chapter 3, a competitive immunoassay system on a μPAD platform has been developed. The photolithographically fabricated μPAD consisted of three elements – (1) a sample introduction zone located at one end of the μPAD, (2) control and test zones located at the other end of the μPAD opposite to the sample introduction zone, and (3) a capture zone, wherein, a capture reagent was immobilized allowing competition during immunoassay. The colorimetric detection similarly involved TMB-H_2O_2 reaction to

produce the blue colored TMB dimiine product in the presence of peroxidase enzyme conjugated to antibody. Biotin was first used as the model compound to test the developed competitive immunoassay system using μPADs. The capture reagent composed of biotin-BSA, which captured the free peroxidase-conjugated biotin antibody in the absence (or in the presence of a limited amount) of the target biotin. In the presence of biotin in the sample solution, the anti-biotin IgG-peroxidase conjugate bonded to the target biotin. The biotin-bonded anti-biotin IgG-peroxidase then flowed past the capture zone and then into the test zone, wherein, TMB was oxidized by the hydrogen peroxide in the presence of the peroxidase conjugate, producing the blue colored TMB diimine product. Hence, color intensity at the test zone increased with increasing biotin concentration that were introduced at the sample zone, but remained constant at the control zone. In the present work, the detection limit for the competitive immunoassay of biotin utilizing 50-μL sample volume introduced onto the μPAD was 0.10 μg mL^{-1}. To demonstrate further the versatility of the developed competitive immunoassay system for the detection of target compounds on μPADs for practical applications, AFB_1 has been detected as well. With a similar detection procedure as with the biotin, the detection limit obtained for AFB_1 using the developed μPAD detection system was 1.31 ng mL^{-1}.

In chapter 4, two competitive immunoassay (CI) systems have been developed for the detection of AFB_1. Using a different μPAD platform, the μPAD assay system similarly consisted of three elements – (1) a reaction zone, (2) a sample introduction zone, and (3) a capture zone. In both CI systems, the reaction zone was immobilized with 50 nmol of TMB. However, in the first CI system (CI-S1), the capture zone was immobilized with AFB_1-BSA, and the sample solution consisted of the target AFB_1, anti-AFB_1 IgG-peroxidase conjugate, and hydrogen peroxide in phosphate-buffered saline Tween® 20 (PBST), pH 6.5. With this kind of μPAD immunoassay system, competition occurred at the capture zone

and signal intensities at the reaction zone increased with increasing target AFB_1 concentration. In CI system 2 (CI-S2), on the other hand, the capture zone was immobilized with anti-BSA IgG, and the sample solution was composed of the target AFB_1, AFB_1-BSA, anti-AFB_1 IgG-peroxidase conjugate, and hydrogen peroxide in PBST, pH 6.5. In this μPAD immunoassay system, competition took place prior to sample introduction. The BSA-conjugated AFB_1 bonded to the anti-AFB_1 IgG-peroxidase were captured by the anti-BSA IgG at the capture zone, allowing only the target-AFB_1 bonded anti-AFB_1 IgG-peroxidase to pass through and reach the reaction zone, wherein, TMB was oxidized by hydrogen peroxide to blue TMB diimine product in the presence of peroxidase conjugate. Hence, similarly, signal intensity increased with increasing target AFB_1 concentration. The novel competitive immunoassay systems described in this research are believed to be the first to have been reported on μPADs so far. In all sections of the manuscript, images of the μPADs were captured and colorimetrically analyzed through ImageJ software for quantification.

5.2 Future Prospects

Some of the key features of microfluidic paper-based analytical devices for specific target detection is its applicability for a low-cost and reliable point-of-need testing without the necessity of highly expensive and sophisticated instrumentation as well as trained personnel to perform the testing, especially in extreme point-of-need settings such as in the developing countries. Food and water contamination are always of safety and health concern, making the quest for a reliable, low-cost, and accessible devices for target detection in food and water incessant.

5.2.1 Innovation of Novel Microfluidic Paper-based Analytical Detection Methods for Food and Water Monitoring

There shall be several topics to be considered regarding the development of microfluidic paper-based analytical detection methods for future research on food and water monitoring. One is to design a multiplexed detection system that may be utilized to simultaneously detect target species using a single μPAD. One possible application of such kind of μPAD system would be the simultaneous detection of fumonisin and trichothecene mycotoxins as well as the *Fusarium* fungi that produce the mycotoxins and cause fungal disease in food crops [1]. Such mycotoxins are toxic and carcinogenic to humans [2,3]. Exposure to these toxins are often observed from intake of foods including cereal grains.

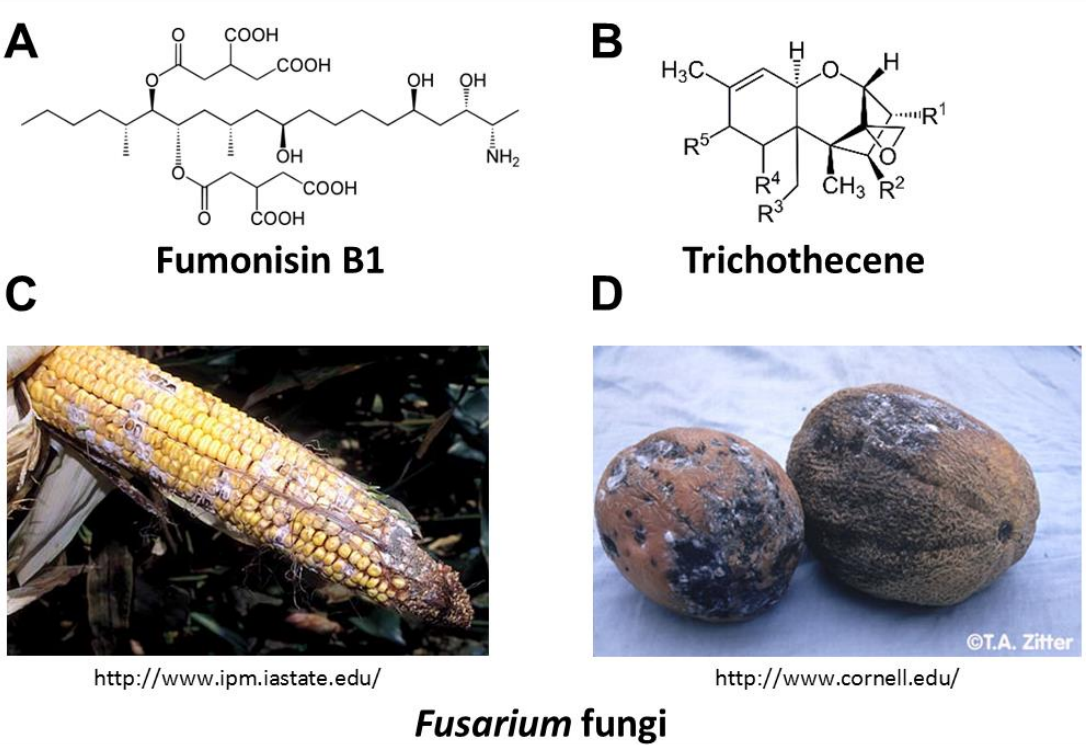

Figure 5-1 The chemical structures of (A) fumonisin B1 and (B) trichothecene, which are mycotoxins produced by *Fusarium* fungi found in rotting food crops such as in (C) corn and (D) melon.

A colorimetric approach would be highly appropriate for such multiplexed detection system, with the capability to provide a “yes/no” result depending on the generation of a certain colored product or a change in color of the detection species upon multiplexed assay. Such multiplexed μPAD colorimetric system would be suitable for on-site monitoring of agricultural plantations without requiring expensive equipment and trained personnel to perform the monitoring.

5.2.2 μPAD Analysis of Target Analytes in Food and Water via Enhanced Detection Methods

Another prospect is to incorporate other detection methods such as fluorescence, chemiluminescence and electrochemical methods on μPADs to obtain improved sensitivity and selectivity of the detection system. In many other food toxins, very low maximum permissible levels of the substance are allowed to be present in food to guaranty food and health safety. An example of which is aflatoxin M_1, a metabolite of aflatoxin B_1 that is excreted in milk [4,5], wherein, the maximum permissible level is 0.50 μg kg^{-1} in milk and milk products according to the United States Food and Drug Administration (US-FDA) [6]. A more strict regulation set by the European Union was a maximum permissible level of 0.05 μg kg^{-1} [7]. Hence, the goal to devise a μPAD detection system that offers the advantages of simplicity and reliability of a μPAD for affordable target monitoring but without sacrificing the quality of the device to perform sensitive detection.

References

[1] S. Zeilinger, J.-F. Martín and C. García-Estrada, Eds., *Biosynthesis and Molecular Genetics of Fungal Secondary Metabolites, Volume 2*, Springer New York, New York, NY, 2015.

[2] C. M. Placinta, J. P. D'Mello, and A. M. C. Macdonald, A review of worldwide contamination of cereal grains and animal feed with *Fusarium* mycotoxins, *Anim. Feed Sci. Technol.*, 1999, **78**, 21–37.

[3] P. C. Turner, P. Nikiema, and C. P. Wild, Fumonisin contamination of food: progress in development of biomarkers to better assess human health risks, *Mutat. Res. Toxicol. Environ. Mutagen.*, 1999, **443**, 81–93.

[4] M. M. Vdovenko, C.-C. Lu, F.-Y. Yu and I. Y. Sakharov, Development of ultrasensitive direct chemiluminescence enzyme immunoassay for determination of aflatoxin M1 in milk, *Food Chem.*, 2014, **158**, 310–314.

[5] M. Sabino, A. Purchio and T. V. Milanez, Aflatoxin B_1, M_1 and aflatoxicol in tissues and urine of calves receiving aflatoxin, *Food Addit. Contam.*, 1995, **12**, 467–472.

[6] L. Stoloff, H. P. van Egmond and D. L. Park, Rationales for the establishment of limits and regulations for mycotoxins, *Food Addit. Contam.*, 1991, **8**, 213–221.

[7] European Commission, Commission regulation (EC) No 683/2004 of 13 April 2004 amending regulation (EC) No 466/2001 as regards aflatoxins and orchratoxin A in foods for infants and young children, *Off. J. Eur. Union*, 2004, **L106**, 3–5.

Curriculum Vitae

LORI SHAYNE ALAMO BUSA

PERSONAL INFORMATION

Citizenship : Filipino (Philippines)

Current Address : Higashinaebo 1-Jo 2-Chome, 6-3-28, Higashi-ku, Sapporo-shi 007-0801 Japan

Email : lorishayne_busa@eis.hokudai.ac.jp / aeris84ph@gmail.com

Date of Birth : 1984 November 20

EDUCATION AND ACHIEVEMENTS

2013 – 2016 **Doctor of Philosophy** (*Chemical Sciences and Engineering*), September 26, 2016

HOKKAIDO UNIVERSITY, Sapporo, Japan

• Japanese Government (MONBUKAGAKUSHO) Scholarship

2007 – 2009 **Master of Science** (*Applied Chemistry*), December 15, 2009

MAEJO UNIVERSITY, Chiang Mai, Thailand

• International Graduate Scholarship under MOU (Maejo University – Nueva Vizcaya State University)

2001 – 2005 **Bachelor of Science** (*Chemistry*), April 24, 2005

UNIVERSITY OF THE PHILIPPINES, Diliman, Quezon City, Philippines

• Department of Sciences and Technology Undergraduate Scholarship Project 5801 (Program B), 2001-2005

WORK EXPERIENCE

January 2012 – Present	**Assistant Professor**, Physical Sciences Department, College of Arts and Sciences, NUEVA VIZCAYA STATE UNIVERSITY, Bayombong, Nueva Vizcaya, Philippines
July 2006 – December 2011	**Instructor**, Physical Sciences Department, College of Arts and Sciences, NUEVA VIZCAYA STATE UNIVERSITY, Bayombong, Nueva Vizcaya, Philippines

RESEARCH WORKS AND AWARDS

**** Theses***

2013 – 2016	**Development of Microfluidic Paper-based Analytical Devices for Food Analysis** • Dissertation (Doctoral degree)
2007 – 2009	**Novel Flow-Injection Methods for the Determination of Sulfite and Glucose in Food Samples** • Graduate Thesis (Master's degree)
2004 – 2005	**Synthesis and Characterization of Dipeptides Glycylalanine and Alanylvaline Using Solution Phase Chemistry** •Undergraduate Thesis (Bachelor's degree)

**** Publications***

Original Papers

(1) Lori Shayne Alamo Busa, Masatoshi Maeki, Akihiko Ishida, Hirofumi Tani, Manabu Tokeshi : "Competitive immunoassay system for microfluidic paper-based detection", **Analyst**, *Submitted manuscript, Under review* (2016)

(2) Lori Shayne Alamo Busa, Saeed Mohammadi, Masatoshi Maeki, Akihiko Ishida, Hirofumi Tani, Manabu Tokeshi : "3,3',5,5'-Tetramethylbenzidine oxidation on paper devices for horseradish peroxidase-based assays", **Analytical Sciences**, Vol. 32, No. 8, pp. 815-818 (2016) doi: 10.2116/analsci.32.815

(3) Lori Shayne Alamo Busa, Masatoshi Maeki, Akihiko Ishida, Hirofumi Tani, Manabu Tokeshi : "Simple and sensitive colorimetric assay system for horseradish peroxidase using microfluidic paper-based devices", **Sensors and Actuators B: Chemical**, Vol. 236, pp. 433-441 (2016) doi: 10.1016/j.snb.2016.06.013

(4) Lori Shayne T. Alamo, Tanin Tangkuaram, Sakchai Satienperakul : "Determination of sulfite by pervaporation-flow injection with amperometric detection using copper hexacyanoferrate-carbon nanotube modified carbon paste electrode", **Talanta**, Vol. 81, Nos. 4-5, pp. 1793-1799 (2010) doi: 10.1016/j.talanta.2010.03.043

Review and Co-authored Papers

(1) Lori Shayne Alamo Busa, Saeed Mohammadi, Masatoshi Maeki, Akihiko Ishida, Hirofumi Tani, Manabu Tokeshi : "Advances in microfluidic paper-based analytical devices for food and water analysis", **Micromachines**, Vol. 7, No. 5 (86), (2016) doi:10.3390/mi7050086.

(2) Takeshi Komatsu, Saeed Mohammadi, Lori Shayne Alamo Busa, Masatoshi Maeki, Akihiko Ishida, Hirofumi Tani, Manabu Tokeshi : "Image analysis for microfluidic paper-based analytical device using the CIE L*a*b* color system", **Analyst**, *Submitted manuscript, Under review* (2016)

(3) Saeed Mohammadi, Lori Shayne Alamo Busa, Masatoshi Maeki, Reza M. Mohamadi, Akihiko Ishida, Hirofumi Tani, Manabu Tokeshi : "Novel concept of washing for microfluidic paper-based analytical devices based on capillary force of paper substrates", **Analytical and Bioanalytical Chemistry**, *In press, Accepted manuscript* (2016) Published online: 20 August 2016. doi: 10.1007/s00216-016-9853-9

(4) Saeed Mohammadi, Lori Shayne Alamo Busa, Masatoshi Maeki, Reza M. Mohamadi, Akihiko Ishida, Hirofumi Tani, Manabu Tokeshi : "Rapid detection

of cat cystatin C (cCys-C) using immuno-pillar chips", **Analytical Sciences**, Vol. 32, *In press, Accepted manuscript* (2016)

(5) Watcharin Seeramad, Lori Shayne T. Alamo, Tanin Tangkuaram, Sakchai Satienperakul : "Design and optimization of enzymatic glucose assay in mesofluidic chemiluminescence device with glucose oxidase immobilized on pencil lead", **Maejo International Journal of Science and Technology**, Vol. 10, No. 01, pp. 66-78 (2016) doi: 10.14456/mijst.2016.6

**** Oral Presentations***

(1) Lori Shayne Alamo Busa, Masatoshi Maeki, Akihiko Ishida, Hirofumi Tani, Manabu Tokeshi : "Development of paper-based devices for food analysis: Aflatoxin B_1 immunoassay", *Hokkaido University International Graduate Program, Training Program for Global Leaders in Life Science,* **3rd International Life-Science Symposium for Young Scientists**, (2015 November 26., Sapporo, Japan)

(2) Lori Shayne T. Alamo, Tanin Tangkuaram, Sakchai Satienperakul : "Pervaporation-flow injection amperometry for sulfite determination using a copper hexacyanoferrate-carbon nanotube-modified carbon paste electrode", *Science Society of Thailand,* **35th Congress on Science and Technology of Thailand**, (2009 October 15-17, Chonburi, Thailand)

(3) Lori Shayne T. Alamo, Tanin Tangkuaram, Sakchai Satienperakul : "Copper hexacyanoferrate-carbon nanotube modified carbon paste electrode: Application to amperometric determination of sulfite", *Chaing Mai Flow-based Research Group,* **Research for Better Life Quality: Symposium on Flow Based Analysis 2009**, (2009 April 24-25, Chiang Mai, Thailand)

**** Poster Presentations***

(1) Lori Shayne Alamo Busa, Masatoshi Maeki, Akihiko Ishida, Hirofumi Tani, Manabu Tokeshi : "Competitive immunoassay approach for aflatoxin B_1 detection on microfluidic paper devices", *Hokkaido University Frontier Chemistry Center*,

The 4th Frontier Chemistry Center International Symposium, (2016 February 23-24, Sapporo, Japan)

(2) Lori Shayne Alamo Busa, Masatoshi Maeki, Akihiko Ishida, Hirofumi Tani, Manabu Tokeshi : "Microfluidic paper-based devices for aflatoxin B_1 analysis", *American Chemical Society*, **International Chemical Congress of Pacific Basin Societies**, (2015 December 15-20, Honolulu, Hawaii, USA)

(3) Lori Shayne Alamo Busa, Masatoshi Maeki, Akihiko Ishida, Hirofumi Tani, Manabu Tokeshi : "Aflatoxin B_1 Immunoassay Using Microfluidic Paper-based Analytical Devices", *AOAC International*, **129th AOAC Annual Meeting & Exposition**, (2015 September 27-30, Los Angeles, California, USA)

(4) Lori Shayne Alamo Busa, Masatoshi Maeki, Akihiko Ishida, Hirofumi Tani, Manabu Tokeshi : "Fabrication of Paper-Based Device for Aflatoxin B_1 Immunoassay", *Society for Chemistry and Micro-Nano Systems*, **30th CHEMINAS**, (2014 October 2-3, Sapporo, Japan)

(5) Lori Shayne T. Alamo, Tanin Tangkuaram, Sakchai Satienperakul : "Copper hexacyanoferrate-carbon nanotube modified carbon paste electrode: Application to amperometric determination of sulfite", *Chiang Mai Flow-based Analysis Research Group*, **Research for Better Life Quality: Symposium on Flow Based Analysis 2009** (2009 April 24-25, Chiang Mai, Thailand)

(6) Lori Shayne T. Alamo, Tanin Tangkuaram, Sakchai Satienperakul : "Chemically modified carbon paste working electrode for the amperometric determination of sulfite", *Science Society of Thailand*, **34th Congress on Science and Technology of Thailand** (2008 October 31-November 2, Bangkok, Thailand)

(7) Lori Shayne T. Alamo, Tanin Tangkuaram, Sakchai Satienperakul : "A carbon nanotubes-copper hexacyanoferrate composite electrode and its application for the determination of sulphite by pervaporation flow injection amperometry", *Japanese Association of Flow Injection Analysis*, **15th International Conference on Flow Injection Analysis – ICFIA 2008** (2008 September 28-October 3, Nagoya, Japan)

Acknowledgement

Getting to this point of my life and career would have been impossible without the many important persons who have helped me and inspired me to keep going and to pursue my PhD degree for my own personal career growth.

First, I would like to express my sincerest respect and gratitude to my supervisor, Professor Manabu Tokeshi of the Division of Applied Chemistry, Faculty of Engineering, Hokkaido University for his wisdom and guidance, continuous support, meaningful advices and encouragements as I take on the challenges of pursuing my PhD degree from Hokkaido University. I am especially grateful for his kind support and concern for the well-being of every one of us under his supervision in the Bioanalytical Chemistry Laboratory (Tokeshi Lab). Likewise, to Associate Professor Hirofumi Tani, Assistant Professor Akihiko Ishida, and Assistant Professor Masatoshi Maeki of Tokeshi Lab for all the assistance, advices and valuable discussions.

I would like to acknowledge the Ministry of Education, Culture and Sports, Science and Technology of the Government of Japan for the PhD MEXT scholarship.

I would also like to thank my labmates Ryoko Kurishiba and Nanako Nishiwaki – who both picked me up from the airport the first time I arrived in Sapporo, Japan and assisted me in what might have been an impossible task of working out my residence as a research student in Sapporo – Saeed Mohammadi, Yuusuke Nishitani, Keine Nishiyama, Taiga Ajiri, Wakao Osamu, Yuka Fujishima, Koto Aoki, Jun Sekiya, Sakai, Yamazaki, Nakamata, Kikuchi, Komatsu, Fujii, and Tani-san, who have been part of my life as a Ph.D. student and to whom I was able to share many experiences with. The completion of my present research would have not been made possible if not for the kind support of all the professors and lab mates in Tokeshi Lab.

To our brothers and sisters in Christ (most especially to Ka Gina Sasaki, Ka Minnie Tateda, and Ka Rosalie and their respective families, and Ka Mary Joy Labatino), and to our very good friends in Hokudai (Loida, Fatsy, Paul, Rachael, Fred, Kaye, Julius, Gian, Princess, and the rest of the members of HAFS…) Life away from home would never have been easier to live if not for the time and friendship you have shared with me and my family.

I dedicate this to Auntie Jean Alamo Santos. I have always been very grateful for all the sacrifices you and your family did for me to finish my undergraduate degree. I certainly wouldn't be here in the first place if not because of everything you and your family did for me and my family. With that, from the bottom of my heart, I am sincerely grateful.

To Professor Wilfredo Dumale, Jr., I wouldn't have been able to come to Japan and pursue my PhD if not because of your encouragement and support. You have been one of the very good mentors I have. I have always been very grateful for all the guidance and support you have given me. Thank you very much.

To our godparents Professor Loreta Vivian Galima and Professor Johnny Gilo, thank you for all the times I am able to seek advice and you are always ready to share your wisdom. I am always grateful for your concern and guidance.

To Professor Joan Hazel Tiongson, thank you for always being there for me. I sincerely apologize for being such a bother to you in so many ways, but I am truly grateful for all your patience and concern and for everything you have done for me especially during my study-leave from NVSU. Thank you for being such a very good friend.

To Ate Cathy Dela Cruz, Miss Dynamic Maye Balaw-ing, Miss Noela Palma, Ate Kath Ojano, Ma'am Lily Almanza, Ma'am Concepcion Asuncion, and to all my CAS and NVSU family who have encouraged me and wished me well during this journey of my life. Forgive

me for not being able to name you one by one but I know that you know who you all are and I thank you very much for the well wishes. I shall see you all again soon!

Most importantly, to my family. Through ups and downs, laughter and tears, success and failure… Thank you for always being there for me. To my father Rizal Raul Alamo, who have endured so much of my childish acts even at this age (haha!) I love you so much and thank you for the love and support. To Mama Noralyn and Papa Conrado, Noreen Joanne and Denise Lyndon, you have sacrificed a lot for us I know. I couldn't thank you enough for everything you have and still are doing for us. Thank you for always being there for us.

To my better half Eric Sam and my little angels Euone Samichi and Lylia Scarlet, this is all for you! This would mean nothing if not for you. I'd climb the highest mountains and swim the deepest oceans for you, my loves! I have stumbled so many times, but you were always ready to reach out your hands many times even before I hit the ground. I definitely couldn't have made it here without you, Daddy! I love you three to the moon and back!

And above all, I offer this You, Father. I praise You for all Your greatness. You have provided us well and never left our side. In sickness and in health, You have shown mercy upon us. May all these achievements bring glory to Your name. I can certainly do anything with You by my side. All glory are Yours forever.